National Library of Canada
Canadian Theses Service
Ottawa, Canada
K1A 0N4

Bibliothèque nationale du Canada
Service des thèses canadiennes

## NOTICE

The quality of this microform is heavily dependent upon the quality of the original thesis submitted for microfilming. Every effort has been made to ensure the highest quality of reproduction possible.

If pages are missing, contact the university which granted the degree.

Some pages may have indistinct print especially if the original pages were typed with a poor typewriter ribbon or if the university sent us an inferior photocopy.

Reproduction in full or in part of this microform is governed by the Canadian Copyright Act, R.S.C. 1970, c. C-30, and subsequent amendments.

## AVIS

La qualité de cette microforme dépend grandement de la qualité de la thèse soumise au microfilmage. Nous avons tout fait pour assurer une qualité supérieure de reproduction.

S'il manque des pages, veuillez communiquer avec l'université qui a conféré le grade.

La qualité d'impression de certaines pages peut laisser à désirer, surtout si les pages originales ont été dactylographiées à l'aide d'un ruban usé ou si l'université nous a fait parvenir une photocopie de qualité inférieure.

La reproduction, même partielle, de cette microforme est soumise à la Loi canadienne sur le droit d'auteur, SRC 1970, c. C-30, et ses amendements subséquents.

NL-339 (r. 88/04) c

Canada

UNIVERSITY OF ALBERTA

# A SOFT TISSUE TEST APPARATUS WITH APPLICATION TO THE KNEE JOINT MENISCUS

BY

**DARRELL JOHN GOERTZEN** ©

A thesis submitted to the Faculty of Graduate Studies and Research in partial fulfilment of the requirements for the degree of **MASTER OF SCIENCE**.

DEPARTMENT OF **MECHANICAL ENGINEERING**

Edmonton, Alberta
**Fall 1992**

National Library
of Canada

Bibliothèque nationale
du Canada

Canadian Theses Service

Service des thèses canadiennes

Ottawa, Canada
K1A 0N4

The author has granted an irrevocable non-exclusive licence allowing the National Library of Canada to reproduce, loan, distribute or sell copies of his/her thesis by any means and in any form or format, making this thesis available to interested persons.

The author retains ownership of the copyright in his/her thesis. Neither the thesis nor substantial extracts from it may be printed or otherwise reproduced without his/her permission.

L'auteur a accordé une licence irrévocable et non exclusive permettant à la Bibliothèque nationale du Canada de reproduire, prêter, distribuer ou vendre des copies de sa thèse de quelque manière et sous quelque forme que ce soit pour mettre des exemplaires de cette thèse à la disposition des personnes intéressées.

L'auteur conserve la propriété du droit d'auteur qui protège sa thèse. Ni la thèse ni des extraits substantiels de celle-ci ne doivent être imprimés ou autrement reproduits sans son autorisation.

ISBN 0-315-77064-3

Canadä

UNIVERSITY OF ALBERTA

RELEASE FORM

NAME OF AUTHOR: **Darrell John Goertzen**

TITLE OF THESIS: **A soft tissue test apparatus with application to the knee joint meniscus**

DEGREE: **Master of Science**

YEAR THIS DEGREE GRANTED: **1992**

Permission is hereby granted to the University of Alberta Library to reproduce single copies of this thesis and to lend or sell such copies for private, scholarly or scientific purposes only.

The author reserves all other publications and other rights in association with the copyright in the thesis and except as hereinbefore provided neither the thesis nor any substantial portion thereof may be printed or otherwise reproduced in any material form whatever without the author's prior written permission.

RR 2 Site 4 Box 17
Stony Plain, Alberta
T0E 2G0

Date: Aug 27/92

UNIVERSITY OF ALBERTA

FACULTY OF GRADUATE STUDIES AND RESEARCH

The undersigned certify that they have read and recommend to the Faculty of Graduate Studies and Research for acceptance, a thesis entitled **A SOFT TISSUE TEST APPARATUS WITH APPLICATION TO THE KNEE JOINT MENISCUS** submitted by **DARRELL JOHN GOERTZEN**, in partial fulfilment of the requirements for the degree of **MASTER OF SCIENCE**.

D. Steigmann
Dr. D Steigmann

Dr. D Budney

Garry Faulkner
Dr. G Faulkner

B. Andrews
Dr. B Andrews

Date: Aug 24 1992

# ABSTRACT

A testing apparatus has been developed for determining material properties of soft tissue specimens. The tensile machine has the ability to test small delicate samples and provide a humidified environment to prevent specimen moisture loss. A high resolution load cell and specimen alignment capabilities are also incorporated. Specimen deformation is measured on two sides of the specimen using a noncontact optical system employing two video cameras. Using an image capture board and accompanying software, the X-Y coordinates of surface markers are determined on two surfaces of the specimen. Two dimensional strain is determined for a region based on the relative positions of three markers. Shear strain is assessed as well as normal strains. Four markers placed on each surface allow calculation of strain in four separate regions on each surface thus assessing the homogeneity of the deformation.

The surface markers are 75 $\mu$m graphite particles which provide distinct points from which repeatable measurements are made while causing minimal specimen disturbance. Linearity of the camera as a displacement measuring device was confirmed using a micrometer calibrator. The captured image is represented by an array of 555 by 435 pixels. Repeatability in determining the coordinates of a single marker position was examined and successive measurements revealed a standard deviation of 0.5 pixel for both coordinates.

Prepared tensile specimens of knee joint meniscus were tested as an application of the test system. The solid phase of the meniscus was modeled as a linear transversely isotropic material. This model requires five material constants and it was shown that the material constants can be determined using tensile specimens with three collagen fiber bundle orientations relative to the direction of the applied tensile load; parallel, perpendicular and oblique or off axis. The off axis test determines the shear modulus along the collagen fiber direction, an important property of the meniscus. A single example of each of the three tests is presented. Further studies are recommended before quantitative results regarding material properties can be inferred. Important aspects for consideration are specimen size and width/thickness ratio and their effects on the resultant material properties.

# ACKNOWLEDGEMENTS

During this project, I have received help and encouragement from many people. I thank them as well as:

Dr. David Budney and Dr. David Stiegmann from the Mechanical Engineering Department for their help and support throughout this project.

Dr. John Cinats from the Department of Surgery for his help and support throughout the project.

the machinists: Max Schubert for his ideas and fine craftsmanship in the fabrication of the tensile test machine, Alan Muir for his ideas as well as Albert Yuen, Don Fuhr and Tony Van Straten for their contributions to the project.

the technical staff: Tom Villet, Brian Cielin, Ian Buttar, John Foy, Terry Nord, Bernie Faulkner, Tuula Hilvo for their contributions to the project.

Doug Hill and Jim Raso from the Glenrose Rehabilitation Hospital for their help with the optical measurement system.

Bill and Luc for being there (at the Power Plant on Friday afternoons) as well as all the other friends I have made during my studies.

and finally but not minimally I wish to thank my parents, Adaline and Henry, for their support which I have grown accustomed to in all the endeavours that I undertake.

# TABLE OF CONTENTS

CHAPTER 1 Page

## INTRODUCTION, ANATOMY AND LITERATURE REVIEW

1.1 Introduction . . . 1
1.2 Anatomy of the Knee Joint . . . 2
1.3 Description of the Menisci . . . 4
1.3 Composition and Fine Structure of the Meniscus . . . 5
1.4 Function of the Menisci . . . 6
1.5 How the Meniscus Transmits Load . . . 8
1.6 Injuries to the Meniscus . . . 9
1.7 Typical Stress-Strain Curve for a Parallel Fibered Collagenous Tissue . 10
1.8 Review of Literature on Material Properties of the Meniscus . . . 12
    1.8.1 Tensile Properties . . . 12
    1.8.2 Compressive Properties . . . 16
    1.8.3 Shear Properties . . . 16
    1.8.4 Discussion of Literature Review . . . 17
1.9 Objectives and Scope of Thesis . . . 17

CHAPTER 2

## THEORETICAL ANALYSIS: CONSTITUTIVE RELATION AND TESTS TO DETERMINE MATERIAL PROPERTIES

2.1 Introduction . . . 19
2.2 Constitutive Modelling . . . 19
2.3 Analysis of a Linear Elastic Isotropic Material . . . 20
    2.3.1 Determining Elastic Constants $\lambda$ and $\mu$ . . . 21
    2.3.2 Determining Engineering Moduli E and $\nu$ . . . 22
2.4 Analysis of a Linear Elastic Transversely Isotropic Material . . . 23
    2.4.1 Constitutive Relation . . . 23
    2.4.2 Determining Elastic Moduli $\lambda$, $\mu_T$, $\alpha$, $\mu_L$ and $\beta$ . . . 26
    2.4.3 Engineering Moduli for a Transversely Isotropic Material . . . 27
    2.4.4 Tests Required to Determine Engineering Parameters . . . 28
2.5 Chapter Summary . . . 32

CHAPTER 3

## TENSILE SPECIMEN PREPARATION AND FACTORS AFFECTING SOFT TISSUE PROPERTIES

3.1 Introduction . . . 33
3.2 Factors Affecting Material Properties . . . 33
    3.2.1 In Vivo Considerations . . . 34
        3.2.1.1 Species . . . 34
        3.2.1.1 Donor Age . . . 34
        3.2.1.3 Activity Level . . . 34
    3.2.2 In Vitro Considerations . . . 35

3.2.2.1 Storage ....35
3.2.2.2 Water content ....36
3.2.2.3 Temperature ....36
3.3 Preparation of Tensile Specimens ....37
3.3.1 Procurement of Menisci ....37
3.3.2 Sectioning ....38
3.3.3 Microtome Cutting ....38
3.3.4 Specimen Dimensions ....39
3.3.5 Cutting Die ....39
3.4 Chapter Summary ....42

**CHAPTER 4**
**TENSILE TEST APPARATUS**

4.1 Introduction ....43
4.2 Special Considerations for Soft Tissue Testing ....43
4.3 Review of Literature ....44
4.4 Tensile Test Machine Design and Construction ....44
4.4.1 Strain Rates and Electric Motor ....44
4.4.2 Load Cell ....46
4.4.3 Specimen Grips ....46
4.4.4 Measurement of Grip to Grip Displacement ....47
4.4.5 Test Specimen Environment ....48
4.5 Summary ....49

**CHAPTER 5**
**SOFT TISSUE DEFORMATION MEASUREMENT SYSTEM**

5.1 Introduction ....50
5.2 Considerations for Soft Tissue Deformation Measurement ....50
5.2.1 Grip Slippage ....50
5.2.2 Specimen Reinforcement and Damage ....51
5.3 Soft Tissue Strain/Deformation Measurement Techniques ....51
5.3.1 Grip to Grip Strain Measure ....51
5.3.2 Mercury Tube Strain Gauge ....52
5.3.3 Hall Effect Strain Measurement ....52
5.3.4 Hall Effect Thickness Reduction Measurement ....53
5.3.5 Extensometer Techniques ....54
5.3.6 Laser Method to Measure Lateral Contraction ....55
5.3.7 Non Contacting Optical Deformation Measurement ....55
5.3.7.1 One Dimensional Deformation Measurement from Discrete Photographs ....55
5.3.7.2 Video Dimension Analyzer ....56
5.3.7.3 Two Dimensional Deformation Measurement ....57

5.3.7.4 Three Dimensional Deformation Measurement . . . . . . . . . 58
5.3.8 Discussion of Measurement Techniques . . . . . . . . . . . . . . . . . . 58
5.4 Description of the Deformation Measurement System . . . . . . . . . . . . 60
5.4.1 Camera, Lens and Magnification . . . . . . . . . . . . . . . . . . . . . 60
5.4.2 Video Image Capture and Synchronization with Load Data . . . . 61
5.5 Specimen Markers . . . . . . . . . . . . . . . . . . . . . . . . . . . . . . . . . 64
5.6 Verification of Measurement System Performance . . . . . . . . . . . . . 66
5.6.1 Repeatability of Successive Measurements . . . . . . . . . . . . . 66
5.6.2 Lens Aberration . . . . . . . . . . . . . . . . . . . . . . . . . . . . . . . 67
5.6.3 Linearity and Calibration . . . . . . . . . . . . . . . . . . . . . . . . . 68
5.7 Chapter Summary . . . . . . . . . . . . . . . . . . . . . . . . . . . . . . . . 69

CHAPTER 6
CALCULATION OF STRESS AND STRAIN AND UNCERTAINTY ANALYSIS

6.1 Introduction . . . . . . . . . . . . . . . . . . . . . . . . . . . . . . . . . . . . 70
6.2 Stress Calculation . . . . . . . . . . . . . . . . . . . . . . . . . . . . . . . . . 70
6.2.1 Cross-Sectional Area Measurement . . . . . . . . . . . . . . . . . 70
6.3 Strain Calculation . . . . . . . . . . . . . . . . . . . . . . . . . . . . . . . . . 71
6.4 Uncertainty Analysis of Calculated Stress-Strain Values . . . . . . . . . . 75
6.4.1 Uncertainty in Stress Values . . . . . . . . . . . . . . . . . . . . . . 76
6.4.2 Uncertainty in Strain Calculation . . . . . . . . . . . . . . . . . . . . 78
6.4.3 Discussion of Uncertainty Analysis . . . . . . . . . . . . . . . . . . 82
6.5 Chapter Summary . . . . . . . . . . . . . . . . . . . . . . . . . . . . . . . . 83

CHAPTER 7
APPLICATION OF THE TEST SYSTEM TO MENISCUS SPECIMENS

7.1 Introduction . . . . . . . . . . . . . . . . . . . . . . . . . . . . . . . . . . . . 84
7.2 General Test Procedures . . . . . . . . . . . . . . . . . . . . . . . . . . . . . 84
7.3 Example of a Tensile Test for a Rubber Specimen . . . . . . . . . . . . . 85
7.4 Example of a Parallel Fiber Test for Meniscus Tissue . . . . . . . . . . . 89
7.5 Example of a Perpendicular Fiber Test for Meniscus Tissue . . . . . . . 93
7.6 Example of an Off-Axis Fiber Test for Meniscus Tissue . . . . . . . . . . 97
7.7 Discussion of Meniscus Test Results . . . . . . . . . . . . . . . . . . . . . 100
7.8 Chapter Summary . . . . . . . . . . . . . . . . . . . . . . . . . . . . . . . . 102

CHAPTER 8
RECOMMENDATIONS AND CONCLUSIONS . . . . . . . . . . . . . . . . . . 103

REFERENCES . . . . . . . . . . . . . . . . . . . . . . . . . . . . . . . . . . . . 106

**APPENDIX A** . . . . . . . . . . . . . . . . . . . . . . . . . . . . . . . . . . . . . . . 117
**Matrix Representation of Stiffness Tensor Components**

**APPENDIX B** . . . . . . . . . . . . . . . . . . . . . . . . . . . . . . . . . . . . . . . 118
**Transforming Elastic Constants**

**APPENDIX C** . . . . . . . . . . . . . . . . . . . . . . . . . . . . . . . . . . . . . . . 121
**Relationship Between Engineering Moduli $E_L$, $E_T$, $\nu_{LT}$ and $\nu_{LT}$**

**APPENDIX D** . . . . . . . . . . . . . . . . . . . . . . . . . . . . . . . . . . . . . . . 124
**Load Cell Design**

**APPENDIX E** . . . . . . . . . . . . . . . . . . . . . . . . . . . . . . . . . . . . . . . 126
**Camera Lens and Lens Extender Selection**

# LIST OF TABLES

**Table 1-1** Tensile results from Fithian et al (1989) . . . . . . . . . . . . . . . . . . 14

**Table 6-1** Sensitivity of relative uncertainty in strain measurement . . . . . . . . 81

## LIST OF FIGURES

**Figure 1-1** Major components in the knee joint . . . . . . . . . . . . . . . . . . . . 2

**Figure 1-2** Section through the lateral compartment of the knee . . . . . . . . . . . 3

**Figure 1-3** View of the tibial plateau . . . . . . . . . . . . . . . . . . . . . . . . . . 5

**Figure 1-4** Forces resisted by the meniscus . . . . . . . . . . . . . . . . . . . . . . . 8

**Figure 1-5** Types of tears occurring in the meniscus . . . . . . . . . . . . . . . . . 9

**Figure 1-6** Typical tensile stress-strain curve for a soft tissue specimen . . . . . 10

**Figure 1-7** Fiber orientations in tensile specimens and orientations of specimens within the meniscus . . . . . . . . . . . . . . . . . . . . . . . 13

**Figure 1-8** Radial tie fiber in a perpendicular fiber specimen . . . . . . . . . . . . 15

**Figure 2-1** Fiber orientation defined by vector a . . . . . . . . . . . . . . . . . . 25

**Figure 2-2** Parallel fiber test . . . . . . . . . . . . . . . . . . . . . . . . . . . . . 29

**Figure 2-3** Perpendicular fiber test . . . . . . . . . . . . . . . . . . . . . . . . . . 30

**Figure 2-4** Off-axis fiber test . . . . . . . . . . . . . . . . . . . . . . . . . . . . . 31

**Figure 3-1** Steps used to obtain a thin slab of meniscus tissue with a uniform fiber orientation. . . . . . . . . . . . . . . . . . . . . . . . . . . . 39

**Figure 3-2** Components of one side of the adjustable die used to obtain tensile specimens . . . . . . . . . . . . . . . . . . . . . . . . . . . . . . 40

**Figure 3-3** Plan view of the assembled specimen die . . . . . . . . . . . . . . . . . 41

**Figure 3-4** Three fiber orientations for the tensile specimens . . . . . . . . . . . . 41

**Figure 4-1** The tensile test apparatus . . . . . . . . . . . . . . . . . . . . . . . . . . . . 45

**Figure 4-2** Cantilever style load cell and specimen grips . . . . . . . . . . . . . . 47

**Figure 4-3** Results for the specimen moisture loss test . . . . . . . . . . . . . . . . 49

**Figure 5-1** Schematic of a Hall effect device used to measure specimen elongation . . . . . . . . . . . . . . . . . . . . . . . . . . . . . . . . . . . . 53

**Figure 5-2** Schematic of the Hall effect device used to measure specimen thickness reduction . . . . . . . . . . . . . . . . . . . . . . . . 53

**Figure 5-3** Schematic of an extensometer device used to measure specimen elongation . . . . . . . . . . . . . . . . . . . . . . . . . . . . . 54

**Figure 5-4** The tensile test apparatus with two cameras in place and humidification system . . . . . . . . . . . . . . . . . . . . . . . . . . . 61

**Figure 5-5** Schematic of the test equipment and load-deformation synchronization method . . . . . . . . . . . . . . . . . . . . . . . . . . 63

**Figure 5-6** Photograph of a specimen with markers . . . . . . . . . . . . . . . . . . 65

**Figure 5-7** Distribution of X and Y coordinate values for repeated digitizing a single marker . . . . . . . . . . . . . . . . . . . . . . . . . 66

**Figure 5-8** Linearity of the camera as a measurement device . . . . . . . . . . . . 68

**Figure 5-9** Variation of image magnification with lens extender length . . . . . . 69

## List of Figures

**Figure 6-1** Material line element in undeformed and deformed configurations . . 72

**Figure 6-2** Material line elements used to calculate two dimensional strain . . . 73

**Figure 6-3** Absolute and relative uncertainties in stress for a typical test . . . . . 77

**Figure 6-4** Absolute and relative uncertainties in strain for a typical test . . . . . 80

**Figure 6-5** Strain measurement error due to specimen rotation . . . . . . . . . . . 82

**Figure 7-1** Markers providing four strain measurement regions on the specimen and the corresponding symbols used for each region when plotting results . . . . . . . . . . . . . . . . . . . . . . . . . 85

**Figure 7-2** Surface deformation of the rubber specimen shown by the relative positions of the markers . . . . . . . . . . . . . . . . . . . . . . 86

**Figure 7-3** Stress-strain response for the rubber sample in uniaxial tension showing both longitudinal and lateral strain . . . . . . . . . . . 86

**Figure 7-4** Poisson's ratio characteristics for the rubber sample . . . . . . . . . . 88

**Figure 7-5** Volume change characteristics for the rubber sample in uniaxial tension . . . . . . . . . . . . . . . . . . . . . . . . . . . . . . . 88

**Figure 7-6** Surface deformation on two sides of the parallel fiber specimen shown by relative positions of the markers . . . . . . . . . . 90

**Figure 7-7** Stress-strain response on both sides of the parallel fiber specimen showing both longitudinal and lateral strain . . . . . . . . . 91

List of Figures

**Figure 7-8** Poisson's ratio characteristics on two sides of the parallel fiber specimen . . . . . . . . . . . . . . . . . . . . . . . . . . . . . . 92

**Figure 7-9** Surface deformation on two sides of the perpendicular fiber specimen shown by relative positions of the markers . . . . . . . . . . 94

**Figure 7-10** Stress-strain response on both sides of the perpendicular fiber specimen showing both longitudinal and lateral strain . . . . . . . . . . . . . . . . . . . . . . . . . . . . . . . . . . . . 95

**Figure 7-11** Poisson's ratio characteristics on two sides of the perpendicular fiber specimen . . . . . . . . . . . . . . . . . . . . . . . . 96

**Figure 7-12** Surface deformation of the off-axis fiber specimen shown by the relative positions of the markers. Coordinate system is aligned with the tensile loading axis . . . . . . . . . . . . . . . . . . 98

**Figure 7-13** Surface deformation of the off-axis fiber specimen shown by the relative positions of the markers. Coordinate system is aligned with the fiber direction . . . . . . . . . . . . . . . . . . . . . . 98

**Figure 7-14** Shear strain resulting from a tensile stress. Coordinate system is aligned with the tensile loading axis . . . . . . . . . . . . . . 99

**Figure 7-15** Shear strain and shear stress for the off-axis specimen. Coordinate system is aligned with the fiber direction . . . . . . . . . . 99

**Figure 7-16** Stress-strain response for the off-axis fiber specimen showing both longitudinal and lateral normal strain Coordinate system is aligned with the tensile loading axis . . . . . . 100

**Figure C-1** $\sigma_{22}$ loading . . . . . . . . . . . . . . . . . . . . . . . . . . . . . . . . . 121

**Figure C-2** $\sigma_{11}$ loading . . . . . . . . . . . . . . . . . . . . . . . . . . . . . . . . . 122

**Figure C-3** $\sigma_{33}$ loading . . . . . . . . . . . . . . . . . . . . . . . . . . . . . . . 122

**Figure D-1** Schematic of the load cell . . . . . . . . . . . . . . . . . . . . . . . . . . 124

**Figure D-2** Load cell linearity . . . . . . . . . . . . . . . . . . . . . . . . . . . . . . . 125

**Figure E-1** Schematic of camera lens and lens extender configuration . . . . . . 121

# CHAPTER 1

# INTRODUCTION, ANATOMY AND LITERATURE REVIEW

## 1.1 INTRODUCTION

Biomechanics involves the application of engineering methodologies and techniques to aid in the understanding of medical problems and phenomena. One subgroup of this broad area involves mechanical testing of soft tissues. Ligaments and cartilage are two examples of biological soft tissues. Information regarding their mechanical properties can be used to:

- predict stresses that occur during normal use and stresses that may cause injury,
- evaluate the effects of factors such as aging and exercise,
- provide data needed for numerical modelling,
- compare artificial replacement materials to normal tissue,

as well as many other objectives. Determining mechanical properties of soft tissue is a challenging task and this thesis provides an initial framework in which to address some of the problems.

The objective of this thesis is twofold: (1) develop a test system capable of tensile tests on soft tissue specimens and (2) perform preliminary tests on specimens of knee joint menisci. Due to the nature of soft tissues, many challenging problems are encountered in experimentally determining their mechanical properties. These difficulties include small delicate samples, specimen gripping, strain measurement, nonuniformity of deformation, cross-sectional area measurement and test environment. The majority of this thesis was directed towards the development and application of a testing apparatus to perform tests on samples of meniscal tissue. Emphasis is on the meniscus throughout this thesis but the equipment developed can be readily used for other soft tissues or rubber-like materials where small, delicate specimens are tested. Several tests are presented to provide examples of test results for the meniscus. Before outlining the objectives of this thesis in more detail, background information is presented to help introduce the nature of the problem.

## 1.2 ANATOMY OF THE KNEE JOINT

The knee is the largest articulating joint in the human body. In the simplest of terms the knee could be thought of as a hinge joint, however it is much more complex than a one degree of freedom hinge. The knee joint must satisfy two mutually exclusive requirements (Kapandji 1987). The first is the need for great stability because of the large forces transmitted across the joint resulting from body weight (static and dynamic) and the length of the lever arms (bones). This stability requirement is juxtaposed with the need for great mobility which is essential for optimal orientation of the foot relative to the ground. Mobility is obtained by incongruence of the articular surfaces, however this compromises stability and leaves the joint susceptible to sprains and injuries.

The knee achieves stability by strong ligamentous attachments between the tibia and femur. The main ligaments, shown in Figure 1-1, are the anterior and posterior cruciate ligaments within the joint space and the lateral and medial collateral ligaments

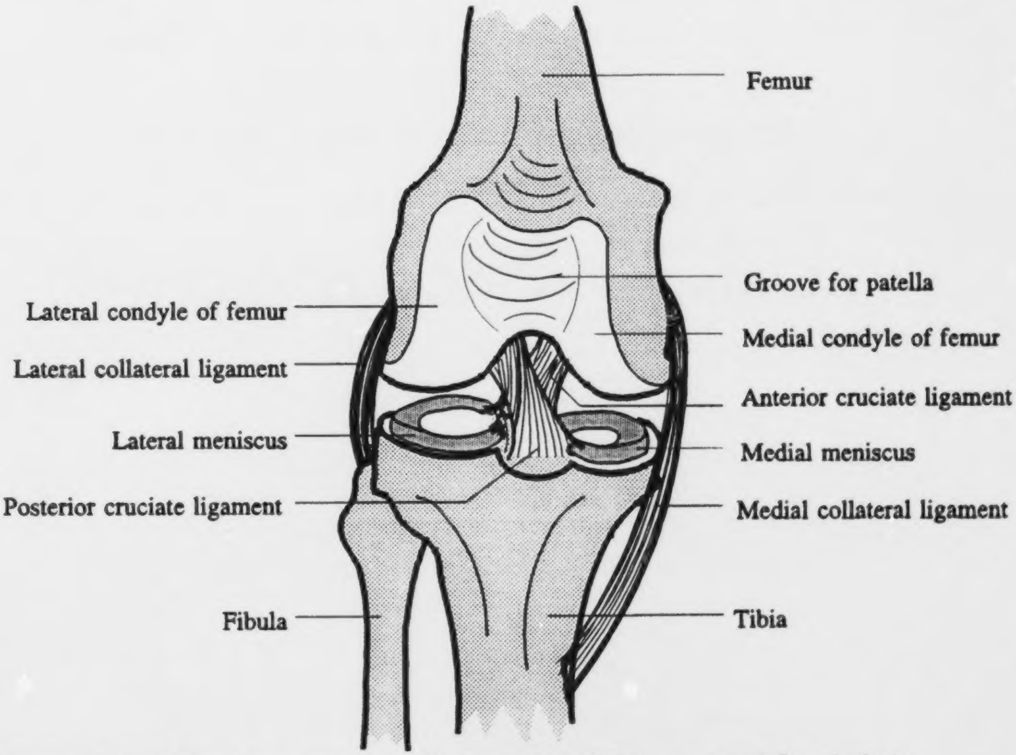
Femur
Groove for patella
Lateral condyle of femur
Medial condyle of femur
Lateral collateral ligament
Anterior cruciate ligament
Lateral meniscus
Medial meniscus
Posterior cruciate ligament
Medial collateral ligament
Fibula
Tibia

**Figure 1-1:** Major components of the knee joint (joint separated for clarity)

on the sides of the joint. The high stiffness of these ligaments and their geometrical arrangement provide limits to the motion of the knee. Active stability and control is also assisted by the musculature crossing the joint.

Weight bearing components of the knee joint consist of the condyles. The long slender bones on each side of the knee become much larger at the knee joint forming the condyles (Figure 1-1). This increases the surface area and improves stability. The intercondylar eminence separates the knee joint into medial and lateral compartments and provides anchor points for the cruciate ligaments and the menisci. The medial and lateral femoral condyles contact the tibial condyle or plateau. These articulating surfaces are covered with a thin (2-4 mm) layer of hyaline cartilage which provide smooth, low friction surfaces where contact takes place. A cross section along a sagittal plane through the lateral compartment, as shown in Figure 1-2, illustrates incongruence of the

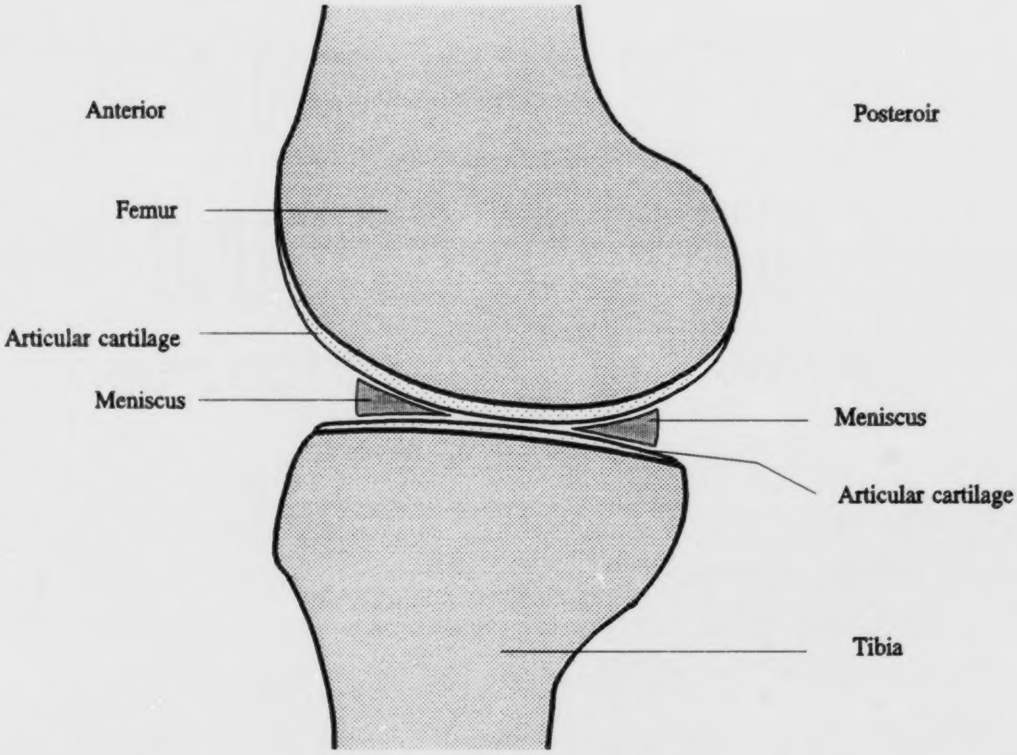

**Figure 1-2:** Section through the lateral compartment of the knee demonstrating incongruence of the articular surfaces and the shape of cross-section of the meniscus

joint. Lack of congruence of the articular surfaces is improved by the interposition of the menisci, which are elements of cartilage-like tissue.

## 1.3 DESCRIPTION OF THE MENISCI

The shape of the menisci can be understood by the following description (Kapandji 1987). If a sphere rests on a plane, contact occurs over a small deformed region. To increase the area of contact a ring is placed between them, bound by the sphere, plane and a cylinder normal to the plane. This ring, equivalent to a meniscus, would be triangular in cross section with the following three surfaces: the concave femoral surface, tibial surface (nearly planar) and the peripheral surface, cylindrical in shape. The intercondylar eminence prohibits the menisci from forming complete rings, hence they are crescent shaped with anterior and posterior horns. The name meniscus originates from the Greek word meniskos, meaning crescent. Menisci are also referred to as semilunar cartilages.

Menisci are firmly fixed to the tibial surface via attachments at their anterior and posterior horns. A view looking down on the tibial plateau is shown in Figure 1-3, illustrating that the knee is not symmetrical with respect to the medial and lateral compartments. The horns of the lateral meniscus are closer together than those of the medial, giving the lateral meniscus a more circular shape covering a larger portion of the articular surface than the medial meniscus. Curvature of the tibial plateau is also different when the medial and lateral sides are compared. The horns are the primary attachments to the meniscus. Secondary attachments have important consequences with respect to the motion of the menisci constraining the medial meniscus, making it less mobile than the lateral. Further details can be found in Kapandji (1987).

The meniscus is forced to undergo significant motion and deformation throughout the range of motion of the knee. The motion of the menisci is governed by passive and active factors. Passive motion is a consequence of the fact that the point of contact between the femoral condyles and tibial plateau moves posteriorly during flexion and anteriorly during extension. The meniscus is trapped between these low friction, cartilaginous surfaces and its wedge shaped cross section is pushed by the femoral

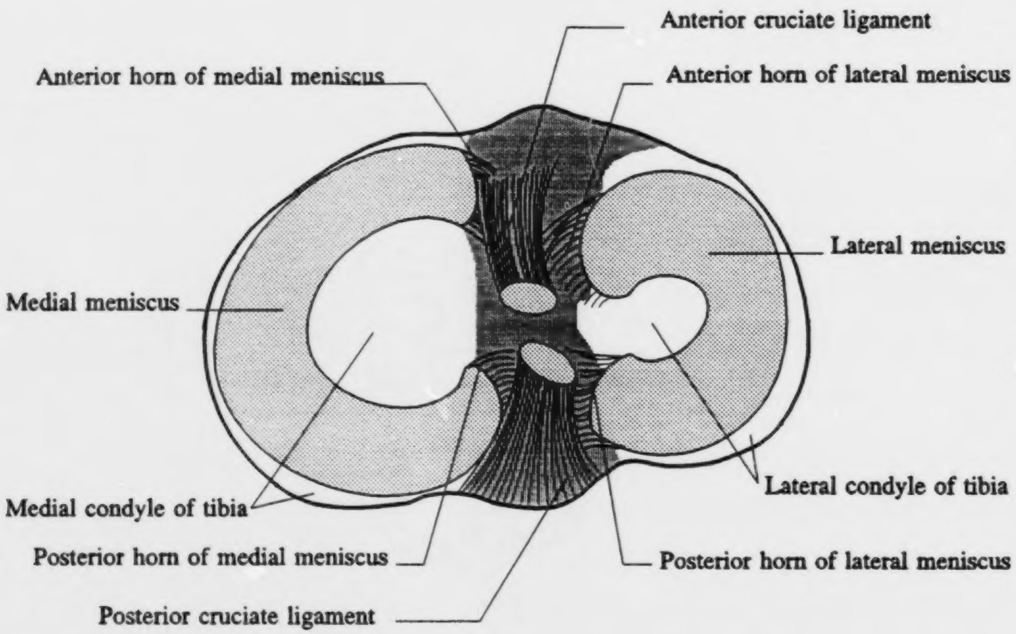
Anterior cruciate ligament
Anterior horn of medial meniscus
Anterior horn of lateral meniscus
Lateral meniscus
Medial meniscus
Medial condyle of tibia
Lateral condyle of tibia
Posterior horn of medial meniscus
Posterior horn of lateral meniscus
Posterior cruciate ligament

**Figure 1-3:** View of the tibial plateau showing the menisci and their attachments to the tibia

condyles. This has been likened to motion when squeezing a cherrystone between two fingers. Active mechanisms contributing to motion include pulling from the fibrous connections between the menisci and various ligaments and tendons. Details are available in Kapandji (1987). A study by Thompson et al (1990) using magnetic resonance imaging (MRI) showed that the lateral meniscus is markedly more mobile than the medial meniscus and the anterior horns are more mobile than the posterior horns, bilaterally. Total excursion of the lateral meniscus near the anterior horn was shown to be as much as 12 mm during flexion. Motion and deformation have important consequences with respect to meniscal injuries. Before discussing the functions of the menisci and injuries to the menisci, the composition and fine structure of the meniscus are presented.

## 1.3 COMPOSITION AND FINE STRUCTURE OF THE MENISCUS

The following description of the meniscus follows from Kelly et al (1990). They describe the meniscus as a soft tissue that consists of two phases; a solid phase (25-30% of wet weight) and a fluid phase (70-75% of wet weight). The solid matrix consists mostly of collagen, 75-80% of the dry weight of the tissue (Mow et al 1990). Collagen forms fibers that are noted for their tensile strength. Fibers are grouped into fiber bundles which are visible to the naked eye. The mechanical response of the meniscus can be thought of as a fiber reinforced material which is also porous and permeable. The fluid phase of the meniscal tissue consists mainly of water, most of which may be forced to flow through the porous permeable matrix. Flow of fluid through this matrix plays an important role in governing the deformational behaviour of the tissue. The viscoelastic response has been modelled as a combination of fluid flow effects coupled with the deformation of the solid matrix. A biphasic theory has been developed and applied to soft hydrated tissues such as cartilage and menisci (Mow et al 1980). This theory models the individual contributions that each phase makes to the overall response. Deformation of the solid matrix is dominated by the presence and orientation of the collagen fiber bundles.

The collagen fiber orientation in the meniscus has an observable pattern. The fine structure of the meniscus has been studied by Bullough et al (1970) and Aspden et al (1985). The outer skin of the meniscus consists of a primarily random orientation of collagen fibers. In the interior of the meniscus, the fibers are grouped together to form large bundles which run predominantly in the circumferential direction. These bundles, approximately 50 to 150 $\mu$m in diameter, appear to be continuous with those of the anterior and posterior ligamentous horns which anchor the menisci to the tibial plateau (Kelly 1990).

## 1.4 FUNCTION OF THE MENISCI

Research was directed towards the function of the meniscus when evidence was presented that removal of the meniscus (meniscectomy) was not a harmless procedure. Complete removal was once a common procedure following injuries to the meniscus. However, clinical studies showed an association between meniscectomy and the development of degenerative changes in the knee joint (Fairbank 1948; Tapper and

Hoover 1969; Johnson et al 1974; Cox et al 1975; Krause et al 1976) A more conservative approach has since been adopted regarding treatment of meniscal tears or lesions.

Biomechanical studies have shown the weight bearing role of the meniscus to be of particular importance. From experimental studies using cadaveric specimens, it has been estimated that the menisci transmit between 50 and 70 per cent of the load applied across the joint (Krause et al 1976; Shrive et al 1978; Seedhom and Hargreaves 1979; Ahmed and Burke 1983). Using pressure sensitive film, Fukubayashi and Kurosawa (1980) and Ahmed and Burke (1983) determined changes in contact area and pressure distribution on the tibial surface resulting from meniscectomy. A 50 to 70 percent reduction in contact area in the medial compartment after removal of the meniscus is reported by Ahmed and Burke. After meniscectomy, the amount of compressive deformation of the articular cartilage and subchondral bone is approximately twice that of the intact joint (Krause et al 1976). Shock absorption in the knee is also attributed to the menisci. Voloshin and Wosk (1983) used accelerometers in vivo to show that normal knees have a greater shock absorbing capacity than knees lacking menisci.

Secondary functions of the meniscus include a role in stabilizing the knee and also lubrication of the articular surfaces. The menisci provide for a more congruous surface and would appear to render the joint more stable. The degree to which this takes place is not precisely known. In the absence of an anterior cruciate ligament, the stabilizing effect is more evident. Levy et al (1982) concluded that in knees that lack an anterior functioning cruciate ligament, the menisci can restrict anterior tibial displacement. Markolf et al (1976) tested cadaveric knees before and after meniscectomy and found measurable changes in stiffness and laxity for certain loading and knee flexion configurations. Menisci are also thought to assist in lubrication and nutrition of the knee joint. The menisci help keep synovial fluid, the lubricating fluid in articulating joints, in contact with the surfaces. In addition, menisci and cartilage depend in part on diffusion through their surfaces for nutrition (Ghosh and Taylor 1987) and contacting surfaces may enhance this effect. The most important function however, is the weight bearing role.

## 1.5 HOW THE MENISCUS TRANSMITS LOAD

Fairbank (1948) described how menisci transmit load. Due to the shape of the menisci and condyles, joint compression causes the meniscus to be forced radially outwards. The horns of the meniscus are firmly anchored to the tibial plateau and therefore tension develops in the circumferential direction, resisting the extruding force. This enables the menisci to share in load bearing. Shrive et al (1978) discuss the mechanism by which the menisci carry load throughout flexion and extension and experimentally confirmed the load carrying capability. Figure 1-4 depicts the radial extruding force on the tibial and femoral surfaces resisted by circumferential tension. This tension is possible because of the tibial attachments at the horns of the menisci (Figure 1-3). The ultrastructure of the meniscus, with a circumferential orientation of

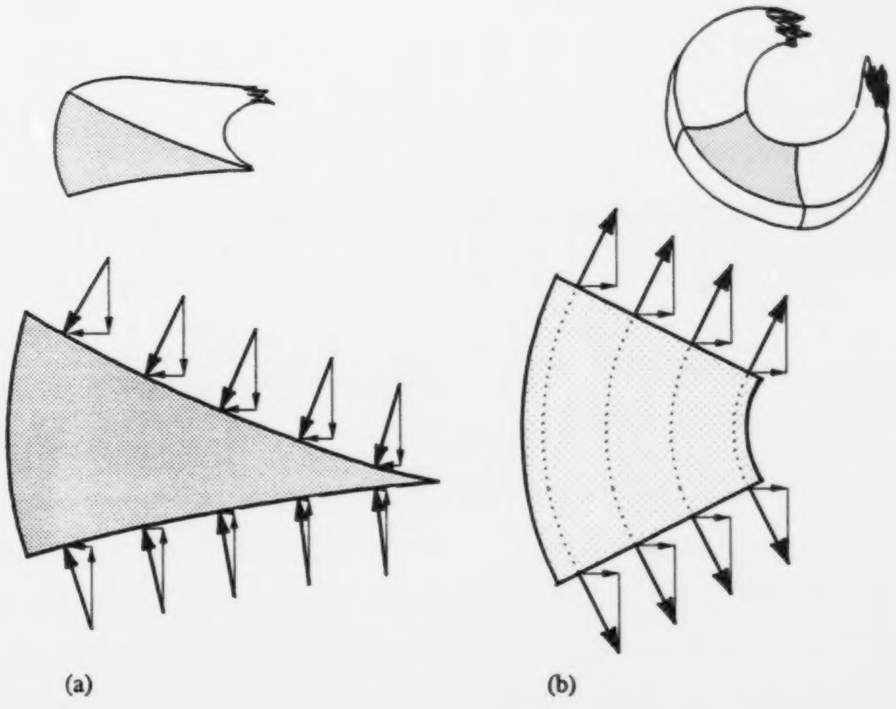

**Figure 1-4:** Forces resisted by the meniscus: (a) radial components due to compression forcing the meniscus out of the joint resisted by (b) radial components of circumferential stress

the collagen fiber bundles, seems well adapted for resisting a hoop stress.

## 1.6 INJURIES TO THE MENISCUS

The majority of injuries to the menisci occur as a split or tear between layers of fibers (Smillie 1970). Two types of these injuries, longitudinal and horizontal tears are shown in Figure 1-5. Less common types are radial and oblique tears which occur across the fibers. Common treatment for a small tear involves trimming and removal of the torn area to prevent further tearing and also prevent lose segments from being trapped between the condyles. Retention of as much of the of the meniscus as possible allows it to maintain a functional role, although reduced. An incomplete meniscus can transmit a portion of the load as long as the circumferential continuity is maintained. Sutured repairs, grafts and the associated healing process associated with these treatments are

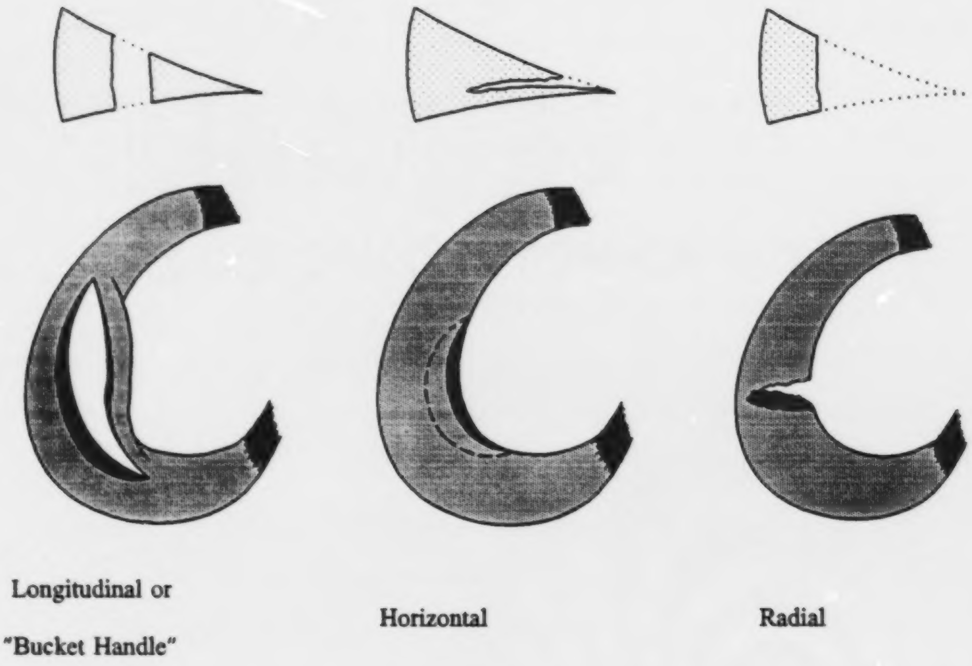

**Figure 1-5:** Types of tears occurring in the meniscus

currently areas of research. Implantable, synthetic meniscal substitutes are also being evaluated (Sommerlath and Gillquist 1992) as another alternative when dealing with a severely damaged meniscus. Information on material properties of meniscal tissue is important for the prediction of the effectiveness of these procedures. Ideal solutions to the treatment of injured menisci would restore material behaviour to that of normal menisci.

## 1.7 TYPICAL STRESS-STRAIN CURVE FOR PARALLEL FIBERED COLLAGENOUS TISSUES

A discussion of general characteristics of soft tissue stress-strain behaviour will help to interpret the meniscal material properties reported in the literature. When a tensile specimen of meniscal tissue is subjected to a low strain rate test, the viscous effects of the interstitial fluid flow are minimized. This "elastic response" is governed

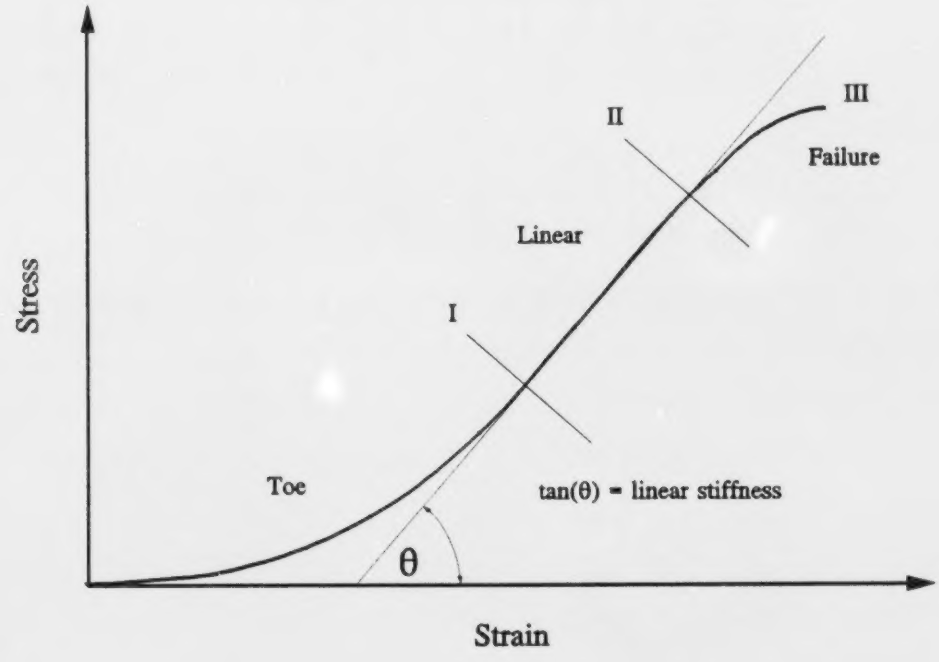

**Figure 1-6:** Typical tensile stress-strain curve for a soft tissue specimen (modified from Viidik, 1990)

by the structure of the solid phase of the tissue. A parallel fibered collagenous tissue subject to uniaxial tension has a characteristic stress-strain curve as shown in Figure 1-6. The stress-strain response consists of several identifiable zones that can be related to structural changes within the tissue as described by Viidik (1990).

The initial part of the stress-strain curve is difficult to define experimentally because of the very low initial stiffness. The definition of zero strain in a soft tissue and how it can be determined is a problem that has not been solved. In a relaxed state, waviness is noted in the collagen fibers of the tissue. As a tensile load is applied, this waviness is gradually straightened out (Viidik 1990). Ghosh and Taylor (1987) have shown this phenomenon for meniscus tissue. This region is referred to as the initial "toe" part of the stress-strain curve and exhibits increasing stiffness with applied load. This region is important because it encompasses most physiological loading. A linear relationship between stress and the corresponding "tangent modulus" or slope of the stress-strain curve was observed by Fung (1967).

The next region of the curve is a linear segment from I to II. The point of inflection that marks the start of this region is the transition from the wavy pattern of the collagen fibers to a straightened configuration of the fibers. In this region, the fibers are elongated at a hierarchial level (Viidik 1990) and the specimen attains its greatest stiffness. A parameter commonly derived from this linear segment is elastic or linear stiffness and is used as a convenient and reproducible way of quantifying tissue response. Material properties for the meniscus are generally reported as a linear stiffness that refers to the slope of this linear zone of the stress-strain curve. Another useful parameter that could be reported in lieu of the complete curve would be the intercept of this line with the strain axis. This would help quantify the toe region of the stress-strain curve.

In the next region, point II to III in Figure 1-6, the slope of the curve begins to decrease until the point of ultimate stress. During this phase, waviness is noted in fiber bundles suggesting rupture and recoil of the fibers (Viidik 1990).

## 1.8 REVIEW OF LITERATURE ON MATERIAL PROPERTIES OF THE MENISCUS

Information on material properties of soft tissues has important applications, some of which were listed in Section 1.1. As discussed in Section 1.6, material properties or stress-strain behaviour is an indicator that is used to experimentally assess the effectiveness of an injury treatment regime. Repaired or synthetic menisci would ideally have the same material properties as normal tissue. In addition, numerical modelling of load-deformation behaviour also requires knowledge of material properties. Numerical modelling can provide a better understanding of the causes of injuries and comparative outcomes of treatments. Accurate knowledge of material properties is therefore a requirement in addition to meniscus shape, loading, nature of constraints and other physiological parameters. Finite element models of varying complexity have been developed to describe the behaviour of the meniscus (Sauren et al 1984; Aspden 1985; Hefzey et al 1987; Spilker et al 1989,1991; Tissahkt and Ahmed 1990; Tissahkt et al 1989,1991). The elastic or low strain rate behaviour of the tissue is required for such models. To account for viscoelastic effects, stress relaxation characteristics are combined with the elastic response in a quasi-linear viscoelastic model (Fung 1981). In the biphasic model (Mow et al 1980) tissue permeability is required along with the elastic response. In the next section, a review of meniscal material properties as reported in the literature is presented.

### 1.8.1 TENSILE PROPERTIES

Mathur et al (1949) studied the tensile strength of human menisci by hanging weights on whole excised menisci until failure occurred. They noted that the average load to failure was less for medial menisci compared to lateral menisci.

Bullough et al (1970) used prepared specimens with a predetermined fiber orientation to perform tensile tests. They recorded tensile strength for each test and showed that the ultimate tensile strength is highly dependent on the orientation of the collagen fibers relative to the tensile loading axis. Ultimate stresses ranged from 3 to 17 MPa for parallel fibered specimens and 0.04 to 3 MPa for perpendicular specimens.

Stiffness and stress-strain curves were not reported.

Uezaki et al (1979) performed tensile tests to study the stress-strain relationship, strain rate dependence and stress relaxation. Linear stiffness varied from 17.2 to 19.4 MPa for strain rates from 0.13 to 16 %/sec, respectively, thus showing minimal strain rate dependence. Stress relaxation data are also given.

Bovine tensile samples with both parallel and perpendicular fiber orientations were tested in tension by Whipple et al (1984, 1985). Figure 1-7a illustrates these fiber orientations. Tensile results indicated that the meniscus exhibits isotropic behaviour in a femoral surface layer that is 200 $\mu$m thick. A mean stiffness of 59.8 MPa was given for this surface layer. Slices 400 $\mu$m thick, parallel to the femoral surface were tested and revealed inhomogeneity and anisotropy. Figure 1-7b shows the orientation of the specimen layers. Statistically significant differences in linear stiffness were noted with respect to depth from the femoral surface. Mean stiffness for parallel fibered specimens from layer 3 and 5 were 194 to 139 MPa, respectively. Specimens with a perpendicular

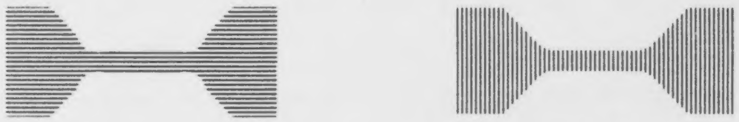

(a) Parallel Perpendicular

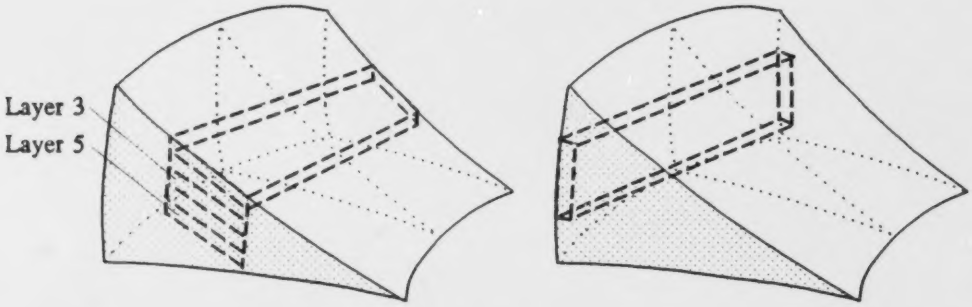

(b) (c)

**Figure 1-7:** (a) Fiber orientations within tensile specimens and orientations of the specimens within the meniscus; parallel to the (b) femoral surface and (c) peripheral surface

fiber orientation had a mean stiffness of 2.8 to 4.6 MPa for layers 3 and 5, respectively, demonstrating material anisotropy.

Proctor et al (1989) reported the same tensile results as Whipple with additional information on inhomogeneity with respect to the anterior and posterior locations. Results from each region are reported as mean stiffness ± standard deviation. Specimens from layers 3 and 5 in the posterior region had a greater stiffness (259 ± 69.2 and 194.9 ± 59.0 MPa, respectively) than layers 3 and 5 from the anterior region (117.8 ± 23.1 and 61.5 ± 25.6 MPa, respectively). These results demonstrate the inhomogeneity of linear stiffness with respect to circumferential location as well as location in the cross section.

The effect of cryopreservation on the tensile properties of canine menisci was studied by Arnoczky et al (1988). Slices parallel to the peripheral surface with a parallel fiber orientation were tested (Figure 1-7c). Linear stiffness and ultimate stress decreased as the specimen location moved inwards from the periphery. The range of tensile moduli and ultimate stresses reported is 99 to 222 MPa and 9 to 31 MPa, respectively. Short term cryopreservation did not appear to affect the tensile properties of the meniscus.

Variation of the tensile moduli of human menisci with respect to location was reported by Fithian et al (1989). Results for parallel fibered specimens for regions of

**Table 1-1:** Tensile results from Fithian et al (1989) expressed as a linear stiffness in MPa (Mean ± SD)

| Region | Medial | Lateral |
|---|---|---|
| Anterior | 159.58 ± 26.2<br>(n=7) | 159.07 ± 47.4<br>(n=10) |
| Central | 93.18 ± 52.4<br>(n=8) | 228.79 ± 51.4<br>(n=11) |
| Posterior | 110.23 ± 40.7<br>(n=12) | 294.14 ± 90.4<br>(n=7) |

both medial and lateral menisci are shown in Table 1-1. Specimens were obtained from slices parallel to the peripheral edge of the meniscus (Figure 1-7c).

Tensile properties of normal canine menisci were studied by Krause et al (1989). Tensile stiffness for parallel fiber specimens from normal menisci ranged from 246 to 362 MPa and ultimate stress ranged from 11 to 16 MPa.

Although the predominate fiber orientation is circumferential, some fibers in the meniscus are oriented in the radial direction. These fibers are termed radial tie fibers since they are oriented radially to the main circumferential orientation. Skaggs and Mow (1990) tested bovine menisci in tension to determine the effect of a single parallel fiber bundle in a predominantly perpendicular fiber specimen (Figure 1-8). They found that the presence of radial tie fibers in a specimen significantly increased its tensile stiffness. Specimens with a radial fiber through the specimen had a mean tensile stiffness of 74 MPa while specimens with no tie fibers had a mean stiffness of 12 MPa. The posterior region of the bovine meniscus contains the greatest number and largest of these fibers (Kelly et al 1990).

Tissakht and Ahmed (1990) presented a finite element model of the meniscus and referred to a recent study of material properties. They used a tensile modulus parallel to the fiber orientation of 127 MPa for the medial meniscus. For the lateral meniscus they used 145 MPa for the central region and 195 MPa for anterior and posterior regions. For perpendicular fiber stiffness they used 14 MPa for lateral and 12 MPa for

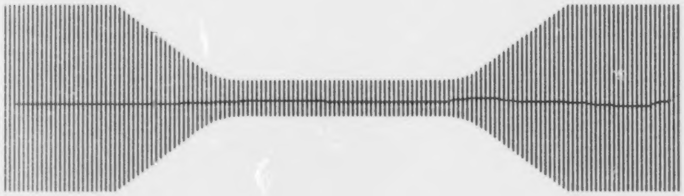

**Figure 1-8:** Radial tie fiber in a perpendicular fiber specimen

medial menisci. Ultimate tensile stresses of 1 to 3 MPa (perpendicular) and 5 to 17 MPa (parallel) were also given.

### 1.8.2 COMPRESSIVE PROPERTIES

Compression studies of bovine menisci are reported by Favenesi et al (1983), Whipple et al (1984) and Proctor et al (1989). Confined compression creep experiments were performed on cylindrical plugs oriented perpendicularly to the tibial surface. An equilibrium elastic modulus of 0.41 Mpa is reported for the compressive creep tests. The equilibrium elastic modulus is the compressive creep stress divided by the strain at equilibrium. It was noted that this is approximately one half the value reported for bovine articular cartilage.

### 1.8.3 SHEAR PROPERTIES

Viscoelastic shear behaviour of the meniscus is reported in two studies. Chern et al (1989,1990) tested disc shaped specimens of bovine meniscus (6.4 mm diameter by 1 mm thick) in torsion at a range of shear strains from 0.5 to 5%. In dynamic shear, the test specimens showed anisotropy and also a dependence on applied axial compressive strain. Increasing axial compressive strain stiffened the specimen in a dynamic shear test. As a measure of the intrinsic shear stiffness of the solid matrix, the equilibrium shear modulus was reported as 0.04 MPa shearing between planes parallel to the fiber direction and 0.03 MPa shearing between planes transverse to the fiber bundle direction.

A dynamic shear testing apparatus was used to measure shear response of equine meniscal tissue by Anderson et al (1990,1991a). A rectangular specimen, 280 $\mu$m thick by 3.4 mm square, was placed between two plates and a sinusoidal shearing motion was generated. Applied shear strains were in the order of 0.01 to 0.001% and frequencies ranged from 100 to 800 Hz. Small shear strains were used to preserve specimen volume and therefore not induce any interstitial fluid flow. Thus they tested the flow independent component of viscoelasticity, the component associated with the solid matrix. They found that shear properties were frequency dependent, anisotropic and nonhomogeneous. They reported values of a complex shear modulus, which is the sum of elastic and viscous shear components in the complex plane. The magnitude of the complex shear modulus at 100 Hz ranged from 0.18 to 0.26 Mpa.

### 1.8.4 DISCUSSION OF LITERATURE REVIEW

The review of literature shows that considerable information exists on the tensile properties of the meniscus, much of it reported in the past two or three years. Evaluation of Poisson's ratio characteristics are not well documented. Due to anisotropy of the meniscal tissue, a single Poisson's ratio is not sufficient to describe the material. A paper by Spilker et al (1991) refers to a study where Poisson's ratios for the meniscus are reported. This is the only information regarding Poisson's ratio characteristics that the author has found. For modelling as a linear elastic solid, Poisson's ratios of the solid phase are required material parameters and further studies are warranted.

Only two papers regarding shear properties are known, both investigating viscoelastic response. Small strains (0.001 to 0.01%) tested by Anderson et al (1991) do not give a complete description of the shear behaviour. A stress-strain curve for shear response has not yet been reported. Both shear testing methods described in Section 1.8.3 do not allow shear failure of the tissue to be observed. Further evaluation of the elastic characteristics of shear moduli would be beneficial. General two dimensional deformation has not been reported for meniscal specimens to assess shear strains as well as normal stains. These areas necessitate further research on the stress-strain behaviour of the meniscus.

## 1.9 OBJECTIVES AND SCOPE OF THESIS

Based on the background information on the meniscus itself and the research into material properties, the objectives of the thesis can now be stated more specifically. The first objective is to ascertain the number and type of tests that would characterize the important aspects of meniscus material properties. A simple linear elastic model based on observed material symmetry provides a starting point. This leads to the second and main objective which is to fabricate and implement a test system capable of obtaining load-deformation data for prepared specimens of meniscal tissue. This presents numerous challenges due to the nature of soft tissues. The third objective is to perform preliminary tests to illustrate the information that can be obtained from the test system.

The scope of this thesis is to model the meniscus as a linear elastic solid. This will allow a finite number of tests to determine parameters and yet provide valuable information on the material properties. Low strain rate tests will be performed to characterize only the elastic response. Viscoelastic models such as the quasi-linear viscoelastic theory (Fung 1981) or the biphasic model (Mow et al 1980) use elastic response as a parameter in the model. Only a limited number of tests will be performed as examples of test results. Extensive testing to obtain a statistical sampling of results will be recommended as a future study.

Before testing equipment can be designed, a theoretical framework is required to determine what types of tests are necessary. This will identify requirements of the load and deformation measurement systems as well as the specimen preparation procedure.

# CHAPTER 2

# THEORETICAL ANALYSIS: CONSTITUTIVE RELATION AND TESTS TO DETERMINE MATERIAL PROPERTIES

## 2.1 INTRODUCTION

A constitutive equation for a specific material relates stress to strain based on specified limitations and assumptions. This chapter outlines a linear constitutive relation to model the solid phase of the meniscus and also describes the tests required to determine a set of material constants. It is desired to determine elastic constants from uniaxial tensile tests to simplify the experimental testing. The objective is to ascertain the number and type of tests required to determine a set of elastic constants that will describe the material over a certain limited range of strain.

## 2.2 CONSTITUTIVE MODELLING

Humphrey et al (1990) describe the formulation of a constitutive relation requiring four basic steps. First, preliminary tests are required to determine the general characteristics of the material, such as elasticity, homogeneity and material symmetry. This first step was accomplished on the basis of a literature review of other researchers' work on the characteristics of the meniscus. Nonlinear response in tension and nonhomogeneous aspects are reported.

The second step, according to Humphrey, requires a theoretical framework necessary to specify the minimum number of possible tests. These restrictions may include material symmetry or internal constraints such as incompressibility. The circumferential orientation of collagen fiber bundles, as discussed in Chapter one, suggests a transversely isotropic model for the solid phase of meniscus tissue. A transversely isotropic material has a preferred direction at every point in the body. For the meniscus, this direction corresponds to the circumferential fiber direction. Distinct material behaviour is noted in this direction. The material exhibits a different response in a plane transverse to the fiber direction and shows no directional preference in this plane, the isotropic plane.

The third step involves developing a specific functional form of the constitutive equation. A linear relationship between stress and strain components is chosen as the form of the constitutive relation. This greatly simplifies the testing required and will provide a starting point for the modelling process. A linear constitutive relationship will provide a starting point that can be further refined.

The fourth step, Humphrey describes as determining the values of the material properties and the evaluation of the validity of the constitutive relation. For a linear elastic solid, a set of elastic constants specified in the constitutive relation, describes the material behaviour.

The rest of this chapter discusses what types of tests are required to determine values for the material properties. Preliminary tests to determine material properties were performed and are discussed in Chapter Seven. Assumptions of linear response, homogeneity and transversely isotropic behaviour are assessed.

Experimental testing required to determine a set of elastic constants for an isotropic medium will be demonstrated as an example of a familiar engineering material. A linear transversely isotropic material will then be presented and the tests required to determine a set of elastic constants will be ascertained.

## 2.3 ANALYSIS OF A LINEARLY ELASTIC ISOTROPIC MATERIAL

The constitutive relation for a linearly elastic solid is

$$\sigma_{ij} = C_{ijkl}e_{kl} \tag{2-1}$$

where $\sigma_{ij}$ are the components of the Cauchy stress tensor, $C_{ijkl}$ are the components of the stiffness tensor and $e_{kl}$ are the components of the infinitesimal strain tensor.
The stiffness tensor for an isotropic material (Spencer 1980) has components

$$C_{ijkl} = \lambda\delta_{ij}\delta_{kl} + \mu(\delta_{ik}\delta_{jl}+\delta_{jk}\delta_{kl}) \tag{2-2}$$

Substituting Equation 2-2 into Equation 2-1 and summing on k and l furnishes the constitutive relation for a linear isotropic material, using the summation convention

$$\sigma_{ij} = \lambda e_{kk} \delta_{ij} + 2\mu e_{ij} \tag{2-3a}$$

or in tensor format

$$\underline{\sigma} = \lambda(tr\underline{e})\underline{I} + 2\mu \underline{e} \tag{2-3b}$$

where $tr\underline{e}$ is the trace operator acting on the tensor $\underline{e}$ and $\underline{I}$ is the unit tensor. Two independent elastic constants, $\lambda$ and $\mu$, describe the material behaviour.

### 2.3.1 DETERMINING CONSTANTS $\lambda$ and $\mu$

In principle, one method to determine the values of these two elastic constants would be to consider a state of uniaxial stress given by $\sigma_{22} \neq 0$ and all other $\sigma_{ij} = 0$. From Equation 2-3, six stress-strain relations are

$$\sigma_{11} = 0 = \lambda(e_{11} + e_{22} + e_{33}) + 2\mu e_{11} \tag{2-4}$$

$$\sigma_{22} = \lambda(e_{11} + e_{22} + e_{33}) + 2\mu e_{22} \tag{2-5}$$

$$\sigma_{33} = 0 = \lambda(e_{11} + e_{22} + e_{33}) + 2\mu e_{33} \tag{2-6}$$

$$\sigma_{12} = 0 = 2\mu e_{12}\ , \quad \sigma_{13} = 0 = 2\mu e_{13}\ , \quad \sigma_{23} = 0 = 2\mu e_{23} \tag{2-7,8,9}$$

Equations 2-7,8,9 demonstrate that $\mu$ is the shear modulus.

Contractile strains $e_{11}$ and $e_{33}$ are equal for this loading case and therefore $e_{11}$ can be substituted for $e_{33}$. Equations 2-4 and 2-5 provide two independent equations from this tensile test.

$$0 = \lambda(2e_{11} + e_{22}) + 2\mu e_{11} \tag{2-10}$$

$$\sigma_{22} = \lambda(2e_{11} + e_{22}) + 2\mu e_{22} \tag{2-11}$$

From experimental measurements $\sigma_{22}$, $e_{11}$ and $e_{22}$ are obtained, allowing $\lambda$ and $\mu$ to be solved for from Equations 2-10 and 2-11 in terms of the known quantities,

$$\mu = \frac{\sigma_{22}}{2(e_{22} - e_{11})} \tag{2-12}$$

$$\lambda = \frac{\sigma_{22} e_{11}}{(e_{22} + 2e_{11})(e_{11} - e_{22})} \tag{2-13}$$

Therefore, for a linear isotropic material, a set of two material constants that describe the behaviour of the material are determined by a single uniaxial tension test.

Relative simplicity of the constitutive equation is obtained by using $\lambda$ and $\mu$ as a set of material constants. However, $\lambda$ does not have a direct physical interpretation and therefore is not readily used in engineering calculations. Another equivalent set of material constants would be a set of engineering parameters. Two common engineering parameters for a linearly elastic isotropic material are Young's modulus or extension modulus E, and Poisson's ratio $\nu$. These moduli can be calculated in terms of $\lambda$ and $\mu$ or determined directly from a tensile test.

### 2.3.2 DETERMINING ENGINEERING PARAMETERS E AND $\nu$

Calculating engineering parameters in terms of $\lambda$ and $\mu$, the extension modulus

$$E = \frac{\sigma_{22}}{e_{22}} \tag{2-14}$$

can be obtained from Equations 2-10 and 2-11.

$$E = \frac{\mu(3\lambda + 2\mu)}{(\lambda + \mu)} \tag{2-15}$$

Poisson's ratio is defined by

$$\nu = \frac{-e_{11}}{e_{22}} \tag{2-16}$$

where $e_{22}$ is the applied extension and $e_{11}$ is the resulting lateral contraction. Poisson's ratio is calculated from Equation 2-10.

$$\nu = \frac{-e_{11}}{e_{22}} = \frac{\lambda}{2(\lambda + \mu)} \tag{2-17}$$

The relation between $\mu$, $\nu$, and E is obtained by substituting Equation 2-14 and 2-16 in Equation 2-12.

$$\mu = \frac{E}{2(1 + \nu)} \tag{2-18}$$

An alternative to determining $\lambda$ and $\mu$ and then using transformation formulas to calculating E and $\nu$ (Equation 2-15 and 2-17) would be to determine the engineering parameters directly from a tensile test. This utilises experimental measurements of $\sigma_{22}$, $e_{11}$ and $e_{22}$ to obtain E, $\nu$ and $\mu$ directly from Equations 2-14, 2-16 and 2-18.

The above discussion has shown that a single tensile test is sufficient to determine two elastic constants to characterize a linear isotropic material. Engineering parameters can be determined directly from experimental measurements or calculated from another set of moduli. A linear transversely isotropic material is now introduced and the tests required to determine a set of material properties are presented.

## 2.4 ANALYSIS OF A LINEARLY ELASTIC TRANSVERSELY ISOTROPIC MATERIAL

### 2.4.1 CONSTITUTIVE RELATION

A transversely isotropic material, as discussed in Section 2-2, is characterized by a single preferred direction at all points in the body. If the fiber direction is given by a unit vector $\underline{a}$, then $\underline{a}$ is normal to the transverse plane which exhibits isotropic behaviour. The stiffness tensor for a linearly elastic material which is transversely isotropic with respect to the $\underline{a}$ direction is (Jaunzemis 1967; Spencer 1984)

$$\begin{aligned} C_{ijkl} &= \lambda\,\delta_{ij}\delta_{kl} + \mu_T(\delta_{ik}\delta_{jl}+\delta_{jk}\delta_{kl}) + \alpha\,(a_k a_l \delta_{ij} + a_i a_j \delta_{kl}) + \\ &\quad (\mu_L - \mu_T)(a_i a_k \delta_{jl} + a_i a_l \delta_{jk} + a_j a_k \delta_{il} + a_j a_l \delta_{ik}) + \beta\, a_i a_j a_k a_l \end{aligned} \tag{2-19}$$

where $\lambda$, $\mu_T$, $\alpha$, $\mu_L$ and $\beta$ is a set of five elastic constants that describe the material behaviour.

Substituting Equation 2-19 into the general constitutive relation for a linearly elastic material, Equation 2-1, yields the constitutive relation for a linearly elastic material, transversely isotropic with respect to a general fiber direction $\underline{a}$ with components $a_i$,

$$\begin{aligned} \sigma_{ij} &= \lambda\, e_{kk}\delta_{ij} + 2\mu_T e_{ij} + \alpha\,(a_k a_l e_{kl}\delta_{ij} + a_i a_j e_{kk}) + \\ &\quad 2(\mu_L - \mu_T)(a_i a_k e_{kj} + a_j a_k e_{ki}) + \beta\, a_i a_j a_k a_l e_{kl} \end{aligned} \tag{2-20a}$$

or in tensor notation

$$\begin{aligned} \underline{\sigma} &= \lambda\,(tr\underline{e})I + 2\mu_T\underline{e} + \alpha\{(a\cdot\underline{ea})I + (tr\underline{e})a\otimes a\} + \\ &\quad 2(\mu_L - \mu_T)\{(\underline{a}\otimes\underline{a})\underline{e} + \underline{e}(\underline{a}\otimes\underline{a})\} + \beta(\underline{a}\cdot\underline{ea})\underline{a}\otimes\underline{a} \end{aligned} \tag{2-20b}$$

A fiber direction is considered where the vector $\underline{a}$ is inclined at an angle $\theta$ to the 2-direction by a rotation about the 3-axis. This configuration is shown in Figure 2-1. The components of $\underline{a}$ are; $a_1 = \sin\theta$, $a_2 = \cos\theta$, $a_3 = 0$.

Using this fiber orientation and displaying the constitutive relation in matrix format results in Equations 2-21. Appendix A shows the matrix representation of the stiffness tensor components. The components of Equations 2-21 are obtained by evaluating Equation 2-20 or by evaluating each of the 21 possible stiffness components in Equation

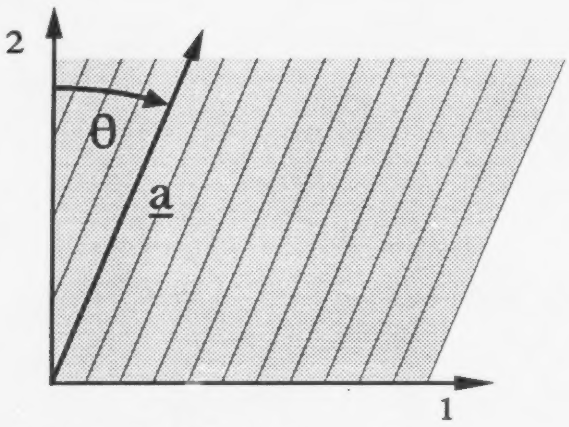

**Figure 2-1:** Fiber orientation defined by vector a

2-19. The stress-strain relationships for a general fiber orientation in the 1-2 plane are

$$\begin{pmatrix} \sigma_{11} \\ \sigma_{22} \\ \sigma_{33} \\ \sigma_{12} \\ \sigma_{13} \\ \sigma_{23} \end{pmatrix} = \begin{pmatrix} C_{1111} & C_{1122} & C_{1133} & C_{1112} & 0 & 0 \\ C_{2211} & C_{2222} & C_{2233} & C_{2212} & 0 & 0 \\ C_{3311} & C_{3322} & C_{3333} & C_{3312} & 0 & 0 \\ C_{1211} & C_{1222} & C_{1233} & C_{1212} & 0 & 0 \\ 0 & 0 & 0 & 0 & C_{1313} & C_{1323} \\ 0 & 0 & 0 & 0 & C_{2313} & C_{2323} \end{pmatrix} \begin{pmatrix} e_{11} \\ e_{22} \\ e_{33} \\ 2e_{12} \\ 2e_{13} \\ 2e_{23} \end{pmatrix} \tag{2-21}$$

where the components of the stiffness tensor are

$$C_{1111} = \lambda + 2\mu_T(1 - 2\sin^2\theta) + 2\alpha\sin^2\theta + 4\mu_L\sin^2\theta + \beta\sin^4\theta \tag{2-22}$$

$$C_{1122} = \lambda + \alpha + \beta\cos^2\theta\sin^2\theta \tag{2-23}$$

$$C_{1133} = \lambda + \alpha\sin^2\theta \tag{2-24}$$

$$C_{1112} = (-2\mu_T + \alpha + 2\mu_L + \beta\sin^2\theta)\cos\theta\sin\theta \tag{2-25}$$

$$C_{2222} = \lambda + 2\mu_T(1 - 2\cos^2\theta) + 2\alpha\cos^2\theta + 4\mu_L\cos^2\theta + \beta\cos^4\theta \tag{2-26}$$

$$C_{2233} = \lambda + \alpha\cos^2\theta \tag{2-27}$$

$$C_{2212} = (-2\mu_T + \alpha + 2\mu_L + \beta\cos^2\theta)\cos\theta\sin\theta \qquad (2\text{-}28)$$

$$C_{3333} = \lambda + 2\mu_T \qquad (2\text{-}29)$$

$$C_{3312} = \alpha\cos\theta\sin\theta \qquad (2\text{-}30)$$

$$C_{1212} = \mu_L + \beta\cos^2\theta\sin^2\theta \qquad (2\text{-}31)$$

$$C_{1313} = \mu_T(1-\sin^2\theta) + \mu_L\sin^2\theta \qquad (2\text{-}32)$$

$$C_{1323} = (\mu_L - \mu_T)\cos\theta\sin\theta \qquad (2\text{-}33)$$

$$C_{2323} = \mu_T(1-\cos^2\theta) + \mu_L\cos^2\theta \qquad (2\text{-}34)$$

Shear coupling is evident for a test specimen with an off-axis fiber orientation. Thus shear strains are associated with normal stresses and vice versa. The component $C_{1112}$ can be interpreted as a coupling of normal stress $\sigma_{11}$ and shear strain $e_{12}$ . Similarly, $C_{1211}$ relates shear stress $\sigma_{12}$ to normal strain $e_{11}$. Symmetry considerations require that these two components be equal. For an angle of $\theta = 0°$ or $\theta = 90°$, which corresponds to a fiber direction parallel to the reference coordinate system, the shear coupling terms drop out.

For an isotropic material, a single tensile test provided two independent equations relating stress and strain and these two equations were solved resulting in values for the material constants. For a transversely isotropic material, tensile tests are preformed to obtain five equations which could be solved for five independent constants. This is procedure is discussed in the next section.

### 2.4.2 DETERMINING CONSTANTS $\lambda$, $\mu_T$, $\alpha$, $\mu_L$ and $\beta$

Since the response of a transversely isotropic material depends on the fiber direction, tensile tests will be conducted with specimens having a specific fiber orientation. Equations 2-22 to 2-34 illustrate the dependence of each of the stiffness components on fiber orientation. A transversely isotropic material, with five elastic constants, would require five independent equations. In principle, five equations could be obtained by testing specimens with different fiber orientations. These stress-strain equations could be solved and the five material constants $\lambda$, $\mu_T$, $\alpha$, $\mu_L$ and $\beta$ would be determined. Engineering parameters are then obtained using transformation formulas which are given in Appendix B.

The determination of $\lambda$, $\mu_T$, $\alpha$, $\mu_L$ and $\beta$ as described above presents several difficulties. More than one fiber orientation is required to solve for the constants and therefore different specimens are required. In Chapter One, the meniscus was shown to be nonhomogeneous. Using specimens with different properties would cause problems when solving the system of equations. The five equations would not be representing the same material and one set of material constants would not satisfy the equations. In addition, the transformation formulas derived in Appendix B are complicated and experimental errors would be compounded. Directly determining engineering parameters from the tests would therefore be an easier method of characterizing the material.

### 2.4.3 ENGINEERING MODULI FOR A TRANSVERSELY ISOTROPIC MATERIAL

In the set of material constants given above, $\mu_T$ and $\mu_L$ represent shear moduli transverse and longitudinal to the fiber direction, respectively. This is concluded by evaluating the shear stress equations in 2-21 when $\theta = 0°$ or $90°$. Additional engineering constants for a transversely isotropic material are also given in terms of the fiber direction. Two extensional moduli are the longitudinal modulus or the modulus in the fiber direction ($E_L$) and the transverse modulus or the extension modulus in an isotropic plane ($E_T$). Three distinct Poisson's ratios are possible. The notation for Poisson's ratio is, $\nu_{ij}$, where the applied strain is in the i direction and the resultant contractile strain is in the j direction. For example, Poisson's ratio $\nu_{LT}$ is the ratio $-e_T/e_L$, where $e_T$ is the contractile strain in a direction transverse to the fiber direction induced by an applied strain in the longitudinal direction, $e_L$. Three Poisson's ratios are $\nu_{LT}$, $\nu_{TL}$ and $\nu_{TT}$. Therefore a set of engineering constants describing a linear transversely isotropic material would be $E_L$, $E_T$, $\nu_{LT}$, $\nu_{TL}$, $\nu_{TT}$, $\mu_T$ and $\mu_L$. Only five of these are independent since two relations exist. The first relation, familiar from an isotropic material, relates properties in the transverse or isotropic plane.

$$\mu_T = \frac{E_T}{2(1 + \nu_{TT})} \tag{2-35}$$

The second relationship, developed in Appendix C, relates extension moduli and Poisson's ratios.

$$\frac{E_L}{E_T} = \frac{\nu_{LT}}{\nu_{TL}} \tag{2-36}$$

This set of engineering parameters can be evaluated directly from uniaxial tensile tests. The tests and experimental measurements that will be performed are now described. Experimental aspects are dealt with in following chapters.

### 2.4.4 TESTS REQUIRED TO DETERMINE ENGINEERING MODULI

The first tensile test has fibers oriented in the direction of the applied loading, as shown in Figure 2-2. Two parameters are determined from this test. Experimental measurements of load and cross-sectional area are used to calculate $\sigma_{22}$ and deformation measurements enable calculation of $e_{11}$, $e_{22}$, and $e_{33}$. A parallel fiber test determines the extension modulus in the fiber direction

$$E_L = \frac{\sigma_{22}}{e_{22}} \tag{2-37}$$

and one Poisson's ratio

$$\nu_{LT} = \frac{-e_{11}}{e_{22}} = \frac{-e_{33}}{e_{22}} \tag{2-38}$$

Using both $e_{11}$ and $e_{33}$ to calculate $\nu_{LT}$ could be used as a check on the validity of a transversely isotropic model.

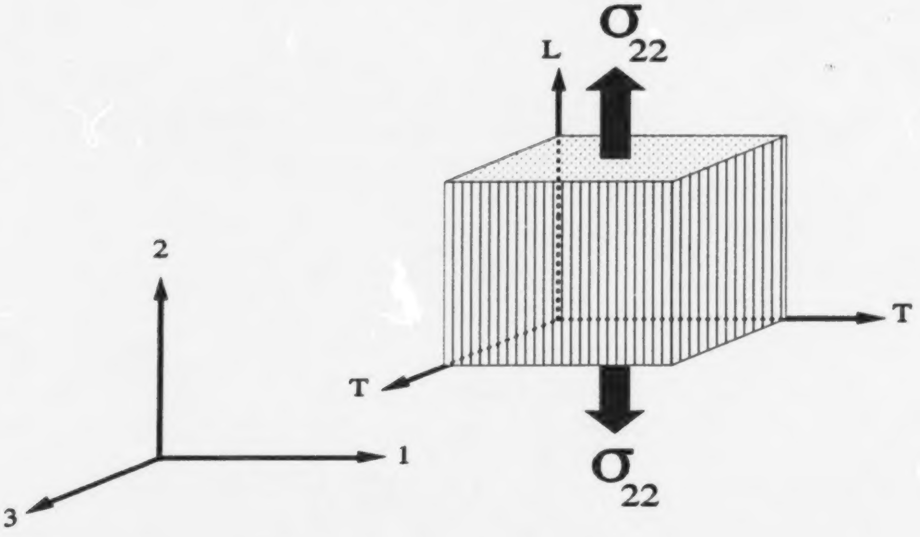

**Figure 2-2:** Parallel fiber test

The second test, shown in Figure 2-3, has a fiber orientation perpendicular to the direction of the applied load. With $\sigma_{22}$, $e_{11}$, $e_{22}$ and $e_{33}$ determined from experimental measurements the following constants can be calculated:

$$E_T = \frac{\sigma_{22}}{e_{22}} \tag{2-39}$$

together with two Poisson's ratios,

$$\nu_{TL} = \frac{-e_{11}}{e_{22}} \tag{2-40}$$

and

$$\nu_{TT} = \frac{-e_{33}}{e_{22}} \tag{2-41}$$

Using the relation given in Equation 2-36, a further check of transversely isotropic

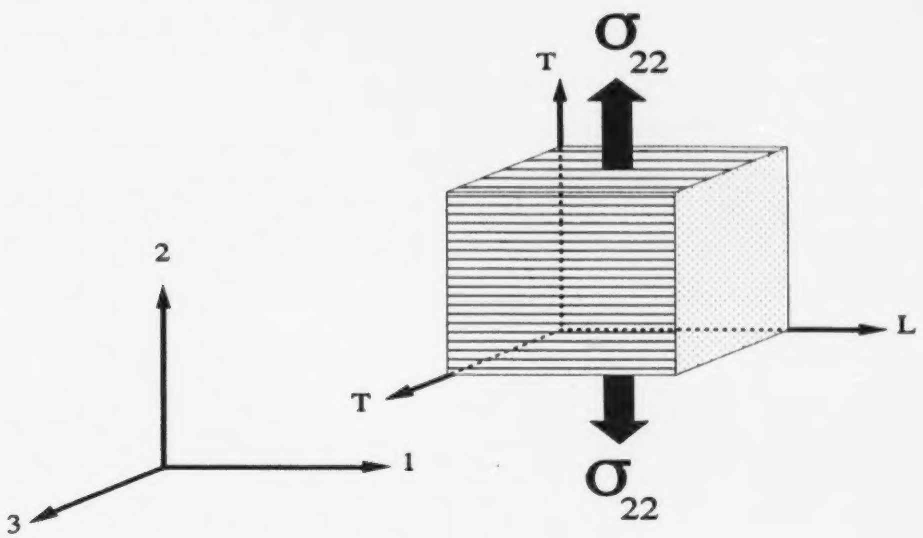

**Figure 2-3:** Perpendicular fiber test

behaviour can be made. The shear modulus in the transverse plane ($\mu_T$) can be calculated using Equation 2-35. After two tensile tests one parameter still remains to be determined, the shear modulus in a longitudinal plane ($\mu_L$).

A third tensile test has fibers oblique to the axis of the tensile load. The fiber direction is inclined at an angle $\theta$ to the 2-direction by a rotation about the 3-axis. This configuration is shown in Figure 2-4. Experimental measurements from this test determine $\sigma_{22}$, $e_{11}$, $e_{22}$ and the induced shear strain $e_{12}$. The longitudinal shear modulus is defined as

$$\mu_L = \frac{\sigma_{LT}}{2e_{LT}} \tag{2-42}$$

Shear stress and shear strain are required in a coordinate system aligned with the material fibers. This requires a transformation of both the stress and strain tensors to determine the components in a new material coordinate system aligned with the fibers. The shear stress along the fibers $\sigma_{LT}$, is given in terms of the applied normal stress $\sigma_{22}$,

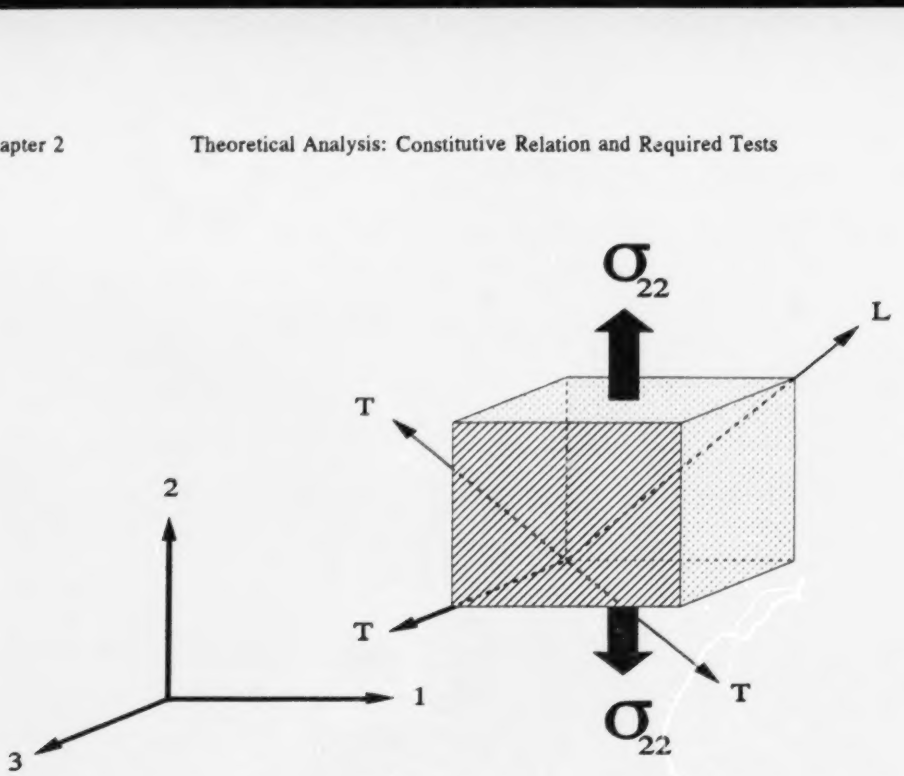

**Figure 2-4:** Off-axis fiber test

$$\sigma_{LT} = -\sigma_{22}\frac{\sin 2\theta}{2} \tag{2-43}$$

Shear strain in a material coordinate system aligned with the fibers is

$$e_{LT} = \frac{1}{2}(e_{11} - e_{22})\sin 2\theta + e_{12}\cos 2\theta \tag{2-44}$$

Therefore the longitudinal shear modulus $\mu_L$, determined from a tensile test is

$$\mu_L = \frac{\sigma_{LT}}{2e_{LT}} = \frac{\sigma_{22}\sin 2\theta}{2(e_{22} - e_{11})\sin 2\theta - 4e_{12}\cos 2\theta} \tag{2-45}$$

which is valid for values of $\theta \neq 0°, 90°, -90°$ etc. The shear modulus determined in this manner is not from a state of pure shear. In addition to the shear stress along the fiber direction, a tensile component normal to the fiber direction exists as well as a tensile component longitudinal to the fibers.

For an isotropic material, the shear strain term is equal to zero in this coordinate system aligned with the tensile direction. Equation 2-45 becomes

$$\mu = \frac{\sigma_{22}}{2(e_{22} - e_{11})} \qquad (2\text{-}46)$$

which is the same as Equation 2-12 from the section on an isotropic material. Dividing the numerator and denominator by $e_{22}$ yields the shear modulus in terms of Young's modulus and Poisson's ratio

$$\mu = \frac{\frac{\sigma_{22}}{e_{22}}}{2(1 - \frac{e_{11}}{e_{22}})} = \frac{E}{2(1 + \nu)} \qquad (2\text{-}47)$$

which illustrates how this technique applies to an isotropic material.

This completes a set of engineering elastic moduli that have been determined directly from three uniaxial tensile tests.

## 2.5 SUMMARY

The constitutive relation for a linearly elastic transversely isotropic material was presented. A set of five material constants is required to characterize this material. Three tensile tests allow calculation of these five moduli. Due to nonlinear response of the tissue, the value of strain at which the moduli were calculated should also be given with the moduli. Each of the three tests will have a specific fiber orientation with respect to the axis of loading; parallel, perpendicular and off-axis. The off-axis configuration will allow measurement of the shear modulus along the fibers, an important but relatively unknown property of the meniscus. The next chapter describes the method used to obtain tensile specimens of meniscus tissue. A summary of considerations pertaining to soft tissue testing is also presented.

# CHAPTER 3

# TENSILE SPECIMEN PREPARATION AND FACTORS AFFECTING SOFT TISSUE PROPERTIES

## 3.1 INTRODUCTION

In Chapter Two, a linear transversely isotropic material was proposed to model the elastic response of the meniscus. The results of Chapter Two showed that three different tensile test specimens are required to experimentally determine a set of five material constants that characterise this model. Each tensile specimen has a specific collagen fiber bundle orientation relative to the axis of the applied load. This chapter describes the procedure used to obtain tensile specimens of precise dimensions from a known location and orientation in the meniscus. In addition, factors that may influence material properties of soft tissues are discussed. These include specimen storage, specimen donor age and test environment variables such as temperature and humidity. Each of these variables has an effect on the value of the material properties and consideration must be given to these variables when assessing results.

## 3.2 FACTORS AFFECTING MATERIAL PROPERTIES

Parameters that may influence the tensile properties of a soft tissue specimen could be separated into two categories: in vivo and in vitro. In vivo factors include donor related variables such as species, age, sex, activity level, nutrition etc. In vitro variables pertain to the soft tissue specimen after it has been excised from the donor and include storage method, moisture content and temperature. Experimental techniques such as measurement of specimen cross-sectional area and deformation significantly affect results and are considered separately in subsequent chapters. The following sections discuss how the material properties of soft tissues may be affected by these variables. The intent is to bring an awareness of the effect these factors may have on test results. Detailed discussions are found in Butler et al (1978), Viidik (1979; 1987) and Woo et al (1990).

## 3.2.1 IN VIVO CONSIDERATIONS

### 3.2.1.1 SPECIES

The relevance of using material properties from animal specimens in studies pertaining to humans was addressed by Athanasiou et al (1991). Differences in biomechanical properties of knee joint cartilage from five species; human, bovine, canine, monkey and rabbit were investigated. In vitro indentation tests were performed and the results showed that significant differences exist in values of stiffness and Poisson's ratio. Noyes and Grood (1976) studied the tensile characteristics of the anterior cruciate using bone-ligament-bone samples from rhesus monkeys and humans. Results showed that elastic stiffness, maximum stress and strain energy to failure from rhesus monkey specimens were 1.7, 1.8 and 1.9 times the respective values for human cadaveric specimens (age group 16 - 26 years).

### 3.2.1.1 DONOR AGE

A relation between donor age and ligament material properties is apparent from several studies. Noyes and Grood (1976) studied the mechanical properties of anterior cruciate ligament bone-ligament-bone complexes obtained from human cadavers. The specimens were divided into two groups: 16 - 26 years and 46 - 86 years. Comparing tensile stiffness, maximum stress at failure and strain energy at failure, the young group had values 1.7, 2.8 and 3.3 times the respective values for the old group. Woo et al (1990) reported tensile tests for anterior cruciate ligament-bone-ligament-bone complexes from two groups of cadaveric knees; a young group (mean age 35) and an old group (mean age 76). The tensile stiffness of the young group was 1.7 times that of the old group. The ultimate load at failure also showed a steady decline with increasing age. It is not known if the meniscus shows a similar decline in material properties with age, however age effects should be considered when comparing results.

### 3.2.1.3 ACTIVITY LEVEL

Ligaments have the ability to adapt to stress levels imposed on them, as do other tissues. Generally, immobilization results in a decreased tensile modulus. After remobilization, the normal state is attained after a period of time. Exercise and increased activity level have a limited ability to increase tensile stiffness. A detailed review is given by Woo et al (1990). A study by Anderson et al (1991b) used sheep with one leg immobilized in a cast for twelve weeks. They concluded that non-weight bearing with early limited motion of the knee does not cause significant deterioration of the mechanical properties of the menisci.

### 3.2.2 IN VITRO CONSIDERATIONS

#### 3.2.2.1 STORAGE

There is no evidence of any significant changes occurring in the mechanical properties of soft connective tissues when the blood circulation in the organism is terminated (Viidik 1986). Short term storage (less than 24 hours) of soft tissue specimens does not require precautions other than the prevention of moisture loss (Viidik 1987). Generally meniscus specimens will not be tested immediately after removal from the donor, thus specimen storage is required. Ghosh and Taylor (1987) showed that exposure to neutral formaldehyde altered the tensile properties of the meniscus, therefore formaldehyde would not be an option for preservation. Experimental studies have shown that careful storage by freezing would not significantly alter the parameters of the stress-strain curve (Galante 1967; Tkaczuk 1968; Noyes and Grood 1976; Butler et al 1978; Woo et al 1986; Arnoczky et al 1988). Prevention of specimen water loss during storage was emphasized in these studies. Arnoczky et al (1988) compared the tensile stiffness of cyropreserved canine menisci (-100°C for one week) to fresh specimens. Their conclusion was that tensile stiffness is not significantly altered by the freezing.

Woo et al (1986) compared properties of fresh rabbit medial collateral ligament specimens to frozen specimens. Their storage protocol involved double wrapping the bone-ligament-bone complex in saline soaked gauze, sealing in an airtight bag and freezing at -20°C. Prior to testing, the bone-ligament-bone complex was allowed to thaw overnight at +4°C and on the day of testing it was allowed to reach 37°C. The bone-ligament bone complex was cycled in tension and then tested to failure. They noted no significant differences in the measured parameters between the fresh and frozen samples.

One exception was the area of hysteresis loops. Frozen samples demonstrated significant decreases in the area of hysteresis during the first few cycles when compared to fresh samples. These differences diminished and became insignificant with further cycling. The storage protocol of Woo et al (1986) is easily duplicated in the lab and will be recommended for the meniscus and should not affect the elastic properties of the meniscus that will be measured in this study.

#### 3.2.2.2 WATER CONTENT

The water content of a soft tissue specimen is important because both overhydration and dehydration will distort the results of a mechanical test. During a single cycle tensile test, overhydration results in a lower elastic stiffness and larger maximum strain values (Viidik 1987).

Exposure to ambient air causes dehydration and a significant stiffening of the soft tissue specimen is noted. Water loss occurs more rapidly in small specimens and an increased stiffness of dehydrated meniscal specimens is noted from our preliminary tests. Specimen preparation should minimize the exposure to ambient air and the specimen should be covered with saline moistened gauze whenever possible. Prevention of moisture loss during testing is addressed in the next chapter.

#### 3.2.2.3 TEMPERATURE

Another important consideration for mechanical testing of soft tissues is specimen temperature during testing. Studies have shown that test specimen temperature will influence the mechanical properties obtained from a tensile test (Hasberry and Pearcy 1986; Woo et al 1987; Lam et al 1990). For cyclic loading between two set extension limits, peak loads decreased with increasing temperature. Woo et al (1987) reported a linear relationship between the decrease in peak load and temperature increase. Also, at higher temperatures an increased extension of the ligament was required before a significant increase in the load was noticed.

Thermal expansion of the soft tissue was discussed by Hasberry et al (1986) and Lam et al (1990). Lam et al (1990) concluded that increased cyclic load relaxation at an elevated temperature was due in part to thermal expansion of the soft tissue. They reported an increased extension in the toe part of the load-deformation curve, however the curves were geometrically similar with an inial offset along the extension axis. Thus the tensile stiffness measured from the linear part of the load-deformation curve was independent of temperature over the range of 25-45°C. They concluded that for a short duration, elastic-dominated test, temperature dependence has a minimal effect on material properties.

Temperature related failure characteristics were not commented on in any of these studies. Testing at room temperature (21°C) would likely result in a contracted toe part of the curve and this could result in a lesser ultimate strain at failure compared to a test at 37°C. This should be considered when interpreting results and warrants further study.

## 3.3. PREPARATION OF TENSILE SPECIMENS

Tensile tests will be performed on prepared specimens with a gauge length of reduced cross section. This reduces the chances of failure occurring at the specimen-grip interface. Specific fiber orientations are required to determine material properties. An outline of the specimen preparation used for preliminary testing is given in the following sections. Based on the preceding sections, specimen storage and exposure to ambient air during specimen preparation are the two most important considerations during the preparation procedure. Proposed preparation techniques are outlined, however methods and specimen dimensions can easily be altered to suit alternative studies.

### 3.3.1 PROCUREMENT OF MENISCI

The majority of specimens used for preliminary testing are from bovine menisci obtained from a local slaughterhouse. Human menisci were also acquired to assess size limitations and carry out preliminary tests. The human samples were obtained under the direction of the HOPE program which enables the use of organs and tissues for transplantation or research purposes. The meniscus is removed from the cadaver donor by trimming the peripheral attachments and cutting the anterior and posterior horns at their tibial attachments. The menisci were then wrapped in saline soaked gauze and placed in air tight containers and frozen at -20°C until the time of testing. Age, sex, and left or right knee location should be recorded for each meniscus.

### 3.3.2 SECTIONING

The sectioning procedure divides the whole meniscus into segments to facilitate further dissection. Sectioning involves cutting the meniscus into three sections; anterior, central and posterior (Figure 3-1a). Four pieces could also be used to obtain more information on nonhomogenous characteristics, however specimen size would then be decreased. Exposure to air is minimized during all procedures by covering the specimens with saline moistened gauze at all possible times. For each section, the inner rim is trimmed away to facilitate flattening out of the specimen on its peripheral edge (Figure 3-1b). This is similar to the technique used by Arnoczky et al (1988). It is assumed that straightening of the initially curved specimen does not induce prestress in the tensile specimen. Flattening the section on its periphery will, to a good approximation, align the collagen fiber bundles parallel to a flat base. This facilitates the next step in the specimen preparation procedure, using a microtome to cut thin slabs of tissue with a parallel fiber orientation.

### 3.3.3 MICROTOME CUTTING

A sliding base microtome is used to cut slabs of tissue of uniform thickness. Components are a sliding base containing the cutting blade, a freezing stage and a vertical adjustment to determine specimen thickness. The freezing stage provides a means of securing the specimen for the microtoming operation. Freezing also prevents specimen deformation during cutting.

An aluminum freezing stage was fabricated and refrigerated glycol is circulated through interior channels. The peripheral edge of a segment is gently pressed down on the -20°C freezing stage and held until it is frozen in place. This results in a tissue sample fixed firmly in place with its collagen fiber bundle orientation in a plane parallel to the cutting plane (Figure 3-1c). The freezing stage is raised or lowered vertically until the desired specimen thickness is obtained.

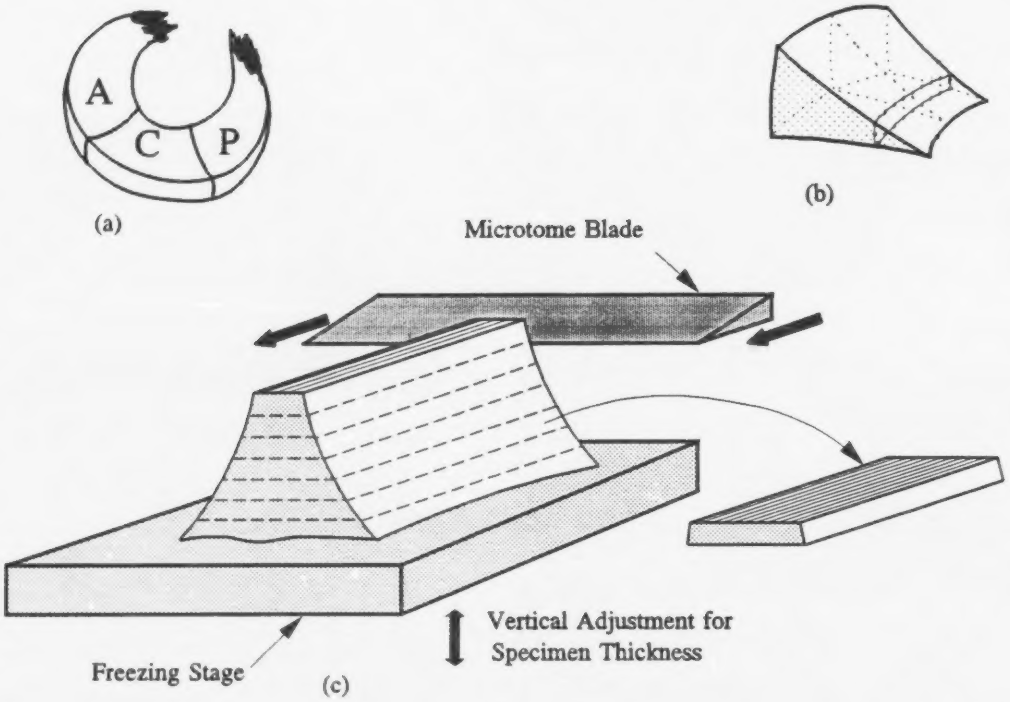

**Figure 3-1:** Steps used to obtain a thin slab of meniscus tissue with a uniform fiber orientation: (a) meniscus is sectioned into three regions, (b) inner rim is trimmed away, (c) thin slabs are sliced with the microtome

### 3.3.4 SPECIMEN DIMENSIONS

Proposed thickness and width for the tensile specimens is approximately 1 to 1.5 mm. Previous studies of meniscus tensile properties have used specimens 0.3 to 0.4 mm thick and 1-1.2 mm wide (Whipple et al 1984; Arnoczky et al 1988; Fithian et al 1989; Proctor et al 1989). Larger cross-sectional dimensions will allow measurement of thickness reduction during testing. Lateral contraction and thickness reduction were not reported in previous studies.

### 3.3.5 CUTTING DIE

The slabs of meniscal tissue obtained from the microtoming operation are not suitable in their present shape for tensile testing. A traditional "dumbbell" shaped tensile specimen with a narrow gauge length is preferred. This ensures that the maximum stress is located in the gauge length and therefore failure is most apt to occur there. Straight sections will usually fail at the grip edge due to distortional effects of the grip.

A die was constructed to furnish tensile specimens from the slab of tissue. The die uses flexible razor blades as the cutting edge. Both the width and length of the gauge section are adjustable and the cutting edges are easily replaced. The components of one side of the die are shown in Figure 3-2. Two razor blades are separated by a central piece which determines the width of the gauge section. Two outside blocks press the razor blades against the central section forcing the blades to conform to shapes of the end blocks. Several sets of blocks allow flexibility in determining both the gauge length and width of the specimen. A plan view of the die is shown in Figure 3-3.

Tensile specimens are pressed out of the slabs of tissue yielding test samples of tissue with a known collagen fiber bundle orientation. Frozen slabs minimize tissue deformation and provide more uniform dimensions. The three types of samples required

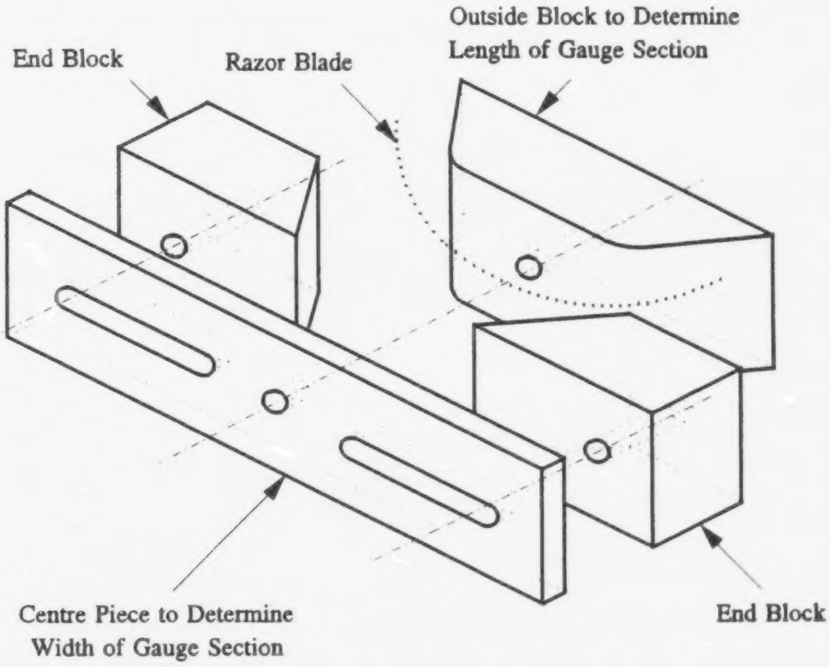
End Block
Razor Blade
Outside Block to Determine Length of Gauge Section
Centre Piece to Determine Width of Gauge Section
End Block

**Figure 3-2:** Components of the adjustable die used to obtain tensile specimens (only one side shown)

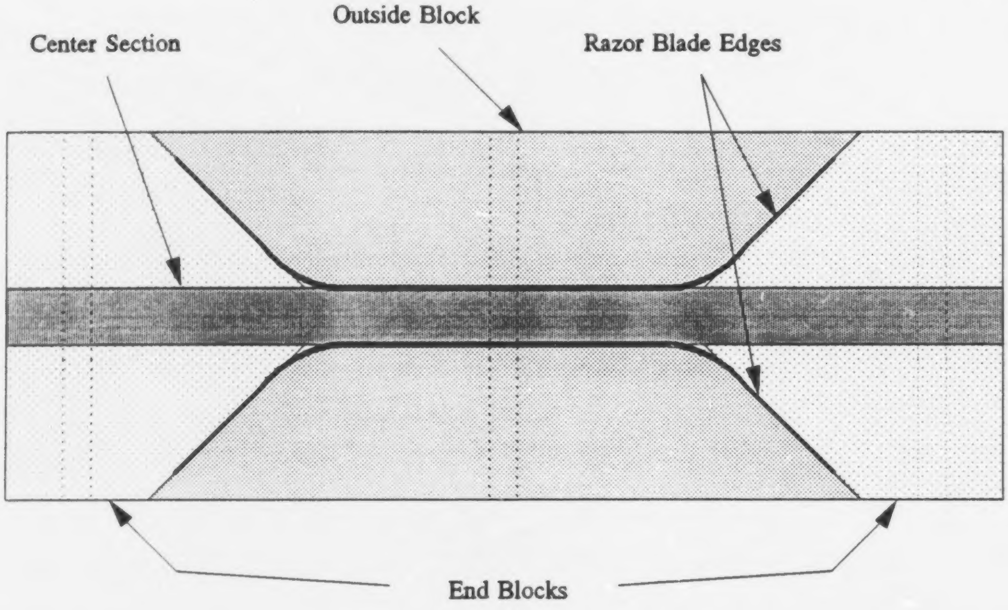
Outside Block
Center Section
Razor Blade Edges
End Blocks

**Figure 3-3:** Plan view of the assembled specimen die showing the components

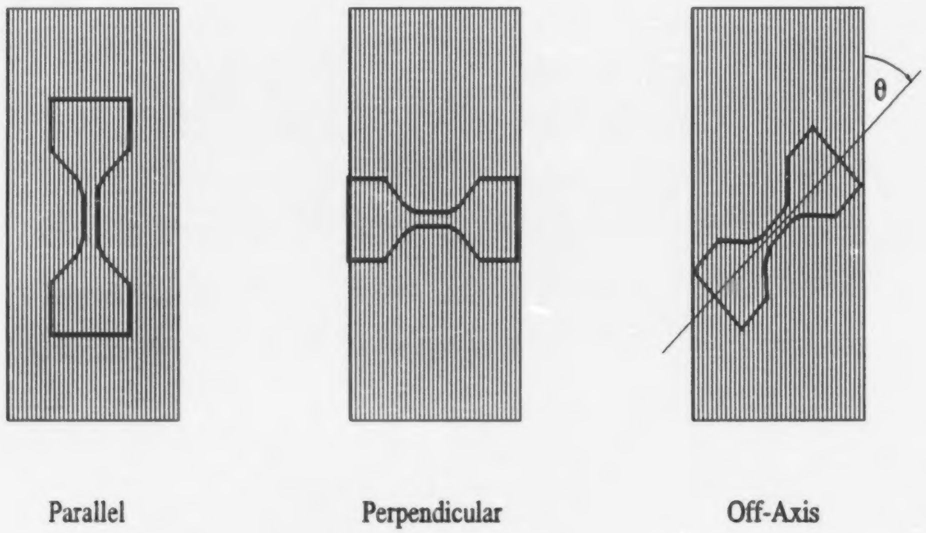
θ
Parallel
Perpendicular
Off-Axis

**Figure 3-4:** Tensile specimens with three fiber orientations obtained from the microtomed slices of tissue

for testing are shown in Figure 3-4.

## 3.4 SUMMARY

This chapter has outlined the procedure for obtaining tensile test specimens. Dimensions of the tensile test specimens can be easily altered to accommodate different studies. Variables that may affect the properties of soft tissue specimens were also presented and the effects of these must be considered when analyzing test results. With the knowledge of meniscal material properties from a literature review and proposed dimensions for the test specimens, anticipated loads can be calculated. This allows the design and fabrication of the testing apparatus.

# CHAPTER 4

# TENSILE TEST APPARATUS

## 4.1 INTRODUCTION

The previous chapters included details that specify the main features of a test apparatus for soft tissue samples. The literature review of material properties in Chapter One provided values of ultimate stress that will be expected. Chapter Two confirmed that uniaxial tension tests are sufficient to characterize the elastic moduli. Specimen size was proposed in Chapter Three and therefore calculation of anticipated forces is possible. Specimen moisture loss during testing was also shown to be an important consideration that must be dealt with during testing. This chapter describes a tensile test apparatus that was fabricated to test small, soft tissue specimens in uniaxial tension.

## 4.2 SPECIAL CONSIDERATIONS FOR SOFT TISSUE TENSILE TESTING

In Section 1-7, a typical tensile stress-strain curve for soft tissues illustrated an initial loading region of very low stiffness. This characteristic puts stringent requirements on load cell resolution. This requires measurement of initial forces that are a small percentage of the anticipated full scale load. Small specimen size also necessitates precautions regarding handling and alignment to avoid tissue damage.

Testing of isolated specimens of tissue requires grips that will resist slippage of the specimen in the grips during the tensile test. Gripping must not be so severe as to cause premature failure at the specimen-grip boundary. Numerous types of gripping methods have been implemented to overcome this problem.

Small soft tissue specimens exposed to ambient air rapidly dehydrate. The effects of moisture loss on soft tissue were discussed in Section 3.2. During the tensile test, steps must be taken to preserve moisture content. This has been accomplished previously by immersion in a solution, humidified environment, wrapping in moist gauze, brushing or spraying saline or coating with oil.

## 4.3 REVIEW OF LITERATURE

Commercial tensile testing machines have been used for soft tissue testing by many researchers. The development of a small scale test apparatus was motivated by concerns about the ability of commercial machines to handle small delicate specimens and measure small forces during initial loading.

Many innovative test machines have been developed for soft tissue testing. Machines have been developed for specific tests: tissue bending (Vesely and Boughner 1985), creep testing (Vogel and Pananicolaou 1983), high strain rate tensile testing (Mabuchi et al 1991), biaxial testing (Lanir and Fung 1974; Vito 1980), shear testing (Chern et al 1989; Anderson et al 1991a; Talman et al 1991). Specially constructed apparatuses for uniaxial tensile testing have also been developed (Uezaki et al 1979; Woo et al 1979; Kerr 1980; Schwerdt et al 1980; Vossonghi and Vaishnav 1980; Sikoryn et al 1988; Aspden et al 1991). The tensile test apparatus designed for this study is described in the next section.

## 4.4 TENSILE TEST MACHINE DESIGN AND CONSTRUCTION

The test machine fabricated to perform tensile testing is shown in Figure 4-1 (Goertzen et al 1991). A variable speed electric motor is linked to a threaded shaft through a reduction gearbox. The upper specimen grip is attached to the load cell which is mounted on a threaded block. This forms the crosshead which translates up or down by rotation of the threaded shaft. The lower grip is fixed to the frame of the test machine. The requirements of the components are discussed.

### 4.4.1 STRAIN RATES AND ELECTRIC MOTOR

A variable speed DC electric motor was selected based on low cost and availability. The electric motor has a speed range from 0.25 to 3.5 revolutions per second. Based on strain rates reported in the literature review, a minimum elongation rate of approximately 0.001 mm/s was selected. This will provide a strain rate of 0.01 percent per second for a grip to grip distance of 10 mm. The actual strain rate in the gauge length of the specimen will depend on the specimen dimensions and shape. Low

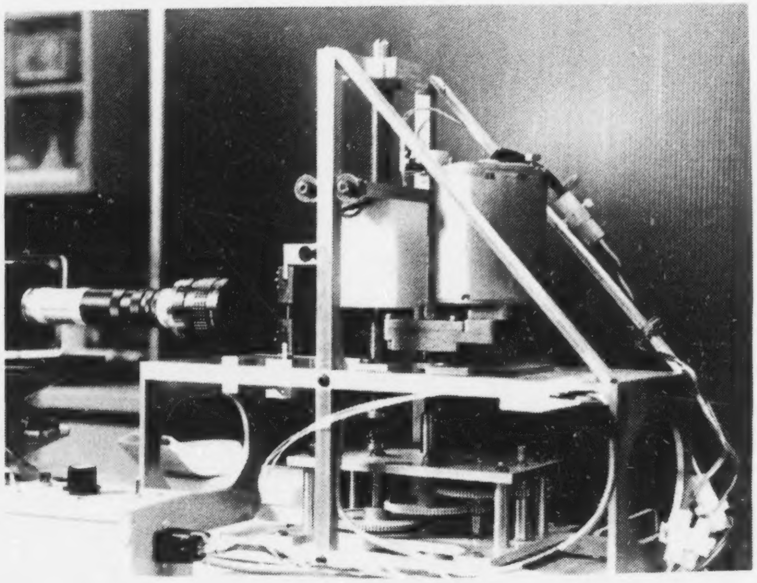

**Figure 4-1:** The tensile test apparatus

strain rates are important to minimize viscous effects.

Translation of the upper specimen grip is obtained by rotation of a threaded shaft acting on a threaded Delrin block. The combination of steel and Delrin was selected for its low coefficient of friction and good wear characteristics and ease of machining. A fine thread was selected for the shaft and block to minimize the reduction necessary to achieve the low strain rate. A gearbox reduction ratio of approximately 350 to 1 is required to give the minimum elongation rate based on the minimum speed of the electric motor and the thread pitch.

A suitable reduction gearbox could not be obtained from a commercial source. Available models where capable of transmitting relatively large torques at high speeds and were too robust for this application. A gearbox was fabricated using Delrin spur gears. The maximum reduction that could be attained in three steps is 8:1, 6.66:1 and 6:1 for an overall reduction of 320:1. The electric motor can be removed and fixed on a new input shaft to attain a different reduction ratio. Connections to the gearbox input and output shafts are made with flexible couplings. Speed control of the electric motor and three input shafts provides a continuous range of crosshead speeds from 0.001 to 0.6 mm/s.

A crosshead assembly stabilizes the upper grip and resists torque from the rotating shaft. Limit switches stop the electric motor at selected upper and lower limits. The load cell is attached to the crosshead assembly.

### 4.4.2 LOAD CELL

The load cell fabricated is a cantilever style fitted with four strain gauges (Measurements Group Inc.) forming a full bridge circuit. Circular cutouts at the strain gauge locations improve sensitivity and retain stiffness. This style has been used previously in this department by Fuchshuber (1987). The maximum load was calculated from values of the ultimate tensile strength reported for menisci. Appendix D provides further details about the load cell design.

The load cell is attached to a strain gauge conditioner (Vishay 2120). Output voltage is sent to a X-Y plotter or to a microcomputer with a 12 bit analog to digital converter (Dash-16, Metrabyte Corporation). The microcomputer samples the strain conditioner output voltage at a user specified time interval and stores the data for further manipulation.

### 4.4.3 SPECIMEN GRIPS

Grips or clamps designed for soft tissue tensile specimens have featured many ideas. Important grip requirements are to hold the tissue with minimal slippage during loading and also avoid specimen failure at the specimen-grip interface. A wide range of gripping techniques have been reported: hooks for biaxial testing of rabbit mesentery (Fung 1967), a standard drill chuck (Schwerdt et al 1980), specimens glued to disposable plastic grips (Wu et al 1976), freezing (Riemersa and Schamhardt 1982), self tightening (Woo et al 1981), spring-loaded for constant clamping force (Roth and Mow 1980) and various configurations of serrated type grips (Butler et al 1984, Galante 1967, Tkaczuk 1968).

After evaluation of these possibilities and considering the complexity of some of the devices, a simple serrated type grip was fabricated. An alignment jig is used to ensure that the grips are properly positioned when the specimen is being loaded. Each grip is attached to the test machine by means of a pin connection. The lower grip attachment point is capable of positional adjustment in order to ensure precise alignment of the upper and lower grips. The specimen grips and their attachments to the test machine are shown Figure 4-2.

### 4.4.4 MEASUREMENT OF GRIP TO GRIP DISPLACEMENT

An attachment for mounting a linear variable displacement transducer (LVDT) was also incorporated. The LVDT measures the displacement of the moving grip relative

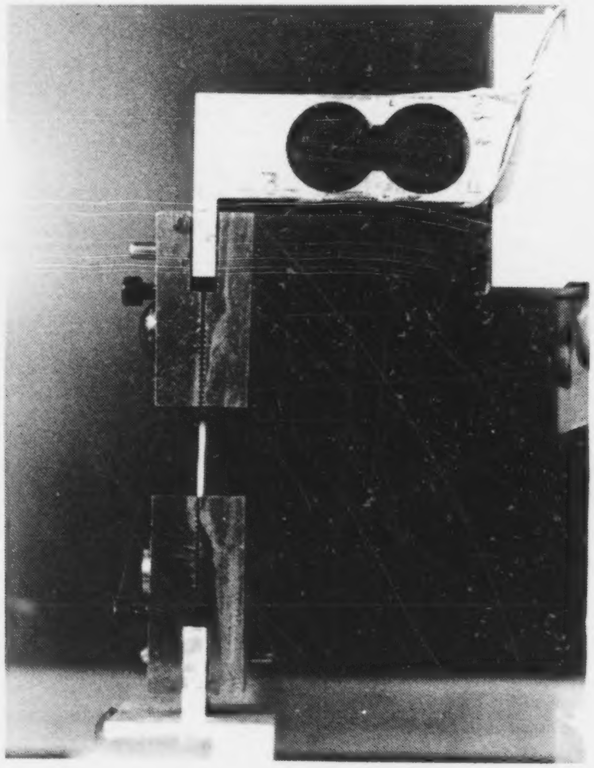

**Figure 4-2:** Cantilever style load cell and attachment of specimen grips

to the fixed grip. This enables analog output of both load and grip to grip displacement to be represented on a X-Y plotter. The LVDT core rests on the grip attachment end of the cantilever load cell and therefore load cell deflection will not affect the recorded specimen deformation.

The next chapter discusses deformation measurement applied to soft tissue samples and will show that a grip to grip measure is not suitable for this study. However, LVDT displacement measurement improves the versatility of the test apparatus and has applications to soft tissue testing.

### 4.4.5 TEST SPECIMEN ENVIRONMENT

The influence of test environment on material properties was discussed in Section 3.2. Dehydration of soft tissue results in increased stiffness. The test apparatus incorporates a high humidity environment to maintain specimen moisture content. An ultrasonic humidifier supplies a stream of high humidity air which encompasses the specimen. A shroud around the specimen contains the humid environment.

The effectiveness of the humidified chamber was tested by comparing the weight loss of a specimen in ambient air (22°C and 25% RH) to that of a specimen immersed in the high humidity air stream. Two sections of bovine meniscus approximately 15 mm wide, 25 mm long and 1 mm thick were used. Each specimen was placed on a small wire holder and initial weights of the tissue samples were determined using a digital scale (Sartorius 1207 MP2) with a resolution of 0.001 gmf. The specimens were placed in their respective test environments and specimen weight was measured over time. Results are presented in Figure 4-3. The humidified air stream was effective at preventing moisture loss. Water drops condensing on the specimen in the humidified stream resulted in a slight increase in specimen weight. The dehydrated specimen approached 30% of its original weight which agrees with the solid content composition of menisci given in the literature (Section 1.3).

Temperature regulation of the air stream has not been incorporated, thus the specimen was tested at room temperature (22° C). Temperature control of the humidifier water tank could be implemented to provide temperature versatility.

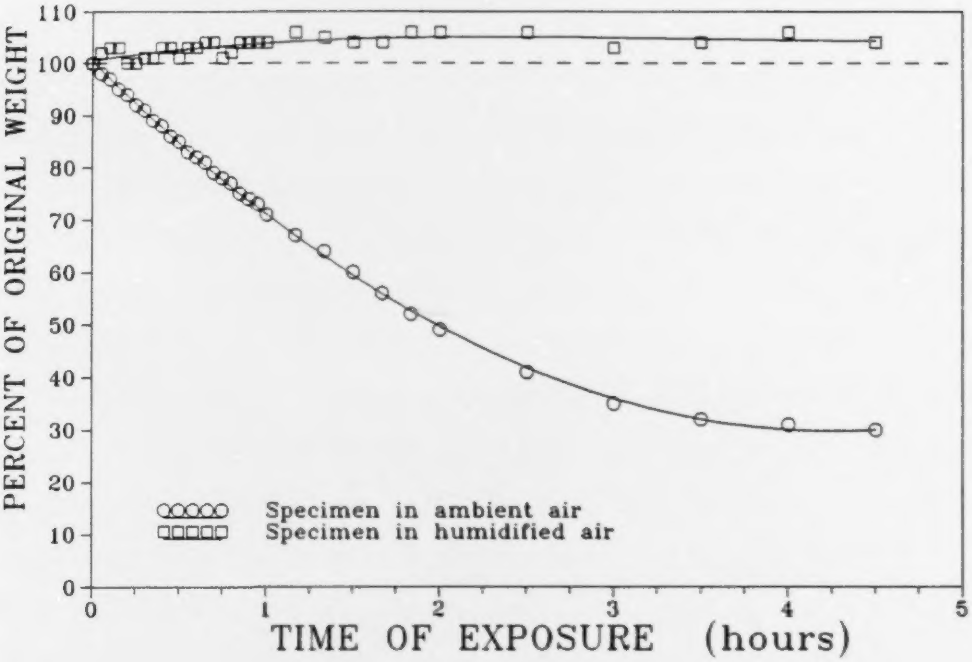

**Figure 4-3:** Results for the specimen moisture loss test showing the effectiveness of the humidified air stream

## 4.5 SUMMARY

This chapter has described a tensile test apparatus developed for soft tissue testing. It is equally applicable to any small tensile specimen where small loads are expected. Application of the equipment to test specimens of meniscus tissue is given in Chapter Seven. Stress-strain calculation requires measurement of force applied to the specimen and the corresponding deformation of the specimen. Measurement techniques such as extensometers and strain gauges have limitations for soft tissue applications. The next chapter discusses these concerns and presents the deformation measurement method.

# CHAPTER 5

# SOFT TISSUE DEFORMATION MEASUREMENT SYSTEM

## 5.1 INTRODUCTION

The purpose of this chapter is to present the system that will be used to measure the surface deformation of soft tissue specimens. The measurement system described in this chapter monitors the relative coordinates of a number of markers on the surface of the specimen throughout the deformation. Two dimensional strain is then calculated based on this information. Special considerations for soft tissue measurements and a review of other strain /deformation measurement techniques are also given.

## 5.2 CONSIDERATIONS FOR SOFT TISSUE DEFORMATION MEASUREMENT

Determining strain in soft tissue specimens provides many challenging problems. The small soft tissue specimens are anisotropic, nonhomogenous, very compliant and undergo large strains. Large strains are experienced by the specimen at failure, however low strains ($<5\%$) correspond to the normal physiological range and are also of interest. Typical methods used to determine strain in engineering materials include strain gauges, extensometers and measuring grip to grip displacement. These methods present problems when applied to soft tissue specimens, especially the small samples used in this study.

### 5.2.1 GRIP SLIPPAGE

A common method to determine strain is to record the crosshead or grip displacement and, based on an initial distance, provide an average strain along the specimen. This method has its limitations when utilized for soft tissue specimens. Chapter four discussed problems associated with specimen gripping. Slippage at the grips will show up as an apparent tissue strain when using a grip to grip measurement technique. In addition, gripping may alter the strain at the specimen-grip interface and this may distort the average grip to grip strain recorded.

### 5.2.2 SPECIMEN REINFORCEMENT AND DAMAGE

Strain gauges and extensometers have been proven as reliable and accurate strain measurement devices for many engineering materials. They may not be suitable for compliant specimens. A strain gauge or extensometer could be thought of as a spring connected in parallel with the specimen. Specimen deformation can be significantly altered by the added stiffness of the measurement system. Attaching a transducer to a hydrated and compliant specimen also presents problems. Standard extensometers will cut through most samples and will interfere with the deformation by constraining the tissue at the region of contact. Bonding a strain gauge type transducer on to a specimen will also interfere with the specimen deformation.

Ideally for fragile, compliant and small specimens, the measurement technique will be noncontacting. This will overcome the aforementioned problems of reinforcement, damage and constraint of the specimen. However, the ability to measure small strains ($<5\%$) is a concern with a noncontact method. This limitation is assessed in Chapter Six.

## 5.3 SOFT TISSUE STRAIN/DEFORMATION MEASUREMENT METHODS

The above considerations have resulted in the development of many devices for strain/deformation measurement for soft tissue testing. A brief review of techniques that have been used for small specimens will be presented. Each method was developed for a specific measurement and has relative advantages and disadvantages depending on the tissue samples and the purpose of the specific study. The deformation measurement system required for this study is to be applied to tensile specimens with a cross sectional area of approximately 2 mm$^2$ and a gauge length of $\approx 5$ mm. This puts severe restrictions on the method of measuring deformation.

### 5.3.1 GRIP TO GRIP STRAIN MEASURE

Soft tissue tests measuring a grip to grip displacement provide a relatively simple method for determining an average strain in the tissue. A displacement transducer such as a linear variable differential transformer (LVDT) provides an output from which strains are calculated. This method has been used on tensile tests of isolated specimens by Galante 1967; Tkaczuk 1968; Uezaki et al 1979 and Haut 1983. Haut (1983) used grip to grip measurements for rat tail tendon tests. Photographs of the specimen-grip interface ensured that slippage did not occur. Uezaki et al (1979) tested samples of menisci using crosshead displacement to calculate strain. This method gives an average strain along the length of the specimen and includes the possible disruption and/or slippage at the grip.

### 5.3.2 MERCURY TUBE STRAIN GAUGE

Edwards et al (1970) constructed a strain gauge using 0.25 mm internal diameter latex rubber tube filled with mercury. Similar in principle to a wire strain gauge, a change in an electrical resistance results from a change in the tube length. The strain gauge was used to measure in vitro strain in the collateral and cruciate ligaments of the human knee. The gauge, approximately 20 mm long, was slightly prestressed and sutured to the ligament. This provided a strain gauge with low stiffness compared to that of the ligament. Meglan et al (1988) constructed a mercury strain gauge using a rubber tube (0.3175 mm ID and 0.625 mm OD). A 20 mm length of tube had a stiffness of 0.0024 N/mm.

### 5.3.3 HALL EFFECT STRAIN MEASUREMENT

A Hall effect device was implemented by Arms et al (1983) as a soft tissue strain transducer. The device, shown in Figure 5-1, consists of wire magnet sliding inside a Teflon tube. A Hall effect generator was bonded to the outer surface of the teflon tube. Fixation pins at each end are pressed into the tissue. A voltage change is proportional to the relative displacement of the pin attached to the wire core and the pin on the teflon tube. This transducer is light weight and offers minimal tissue reinforcement. In vivo strain measurement of the human anterior cruciate ligament (ACL) was reported by Beynnon et al (1989) where a Hall effect device was implanted and retrieved arthroscopicly. This allowed an evaluation of strain in the ACL during selected motions of the knee.

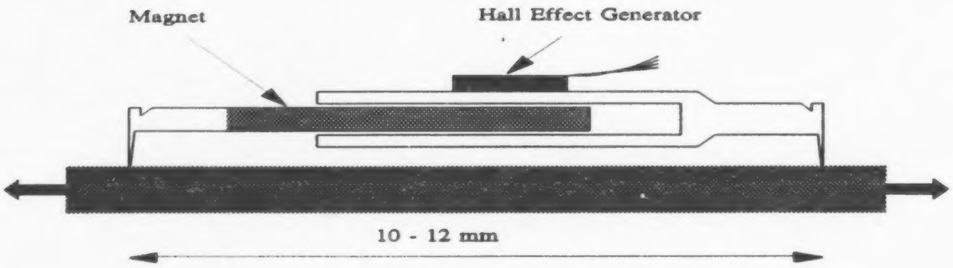
Magnet
Hall Effect Generator
10 - 12 mm

**Figure 5-1:** Schematic of a Hall effect device used to measure specimen elongation (modified from Arms et al 1983)

### 5.3.4 HALL EFFECT THICKNESS REDUCTION MEASUREMENT

A system for measuring the thickness reduction of a tensile test specimen was developed by Woo et al (1979). The system employed a tensile test machine that incorporated a variable impedance transducer to monitor thickness reduction. A simplified illustration is shown in Figure 5-2. The specimen was tested in a horizontal

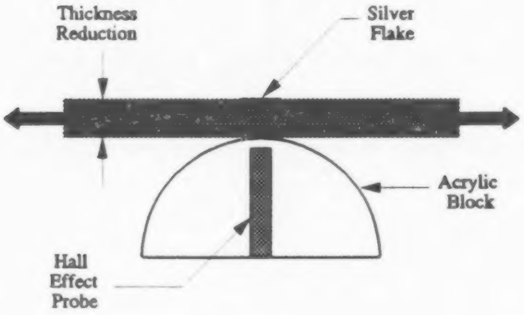
Thickness Reduction
Silver Flake
Acrylic Block
Hall Effect Probe

**Figure 5-2:** Schematic of the Hall effect device used to measure thickness reduction (modified from Woo et al 1979)

orientation with the transducer probe mounted in an acrylic block contacting the bottom surface of the specimen. A small silver flake was placed on the top surface of the specimen directly over the probe tip. The original specimen thickness was ≈0.25 mm. The thickness reduction of the specimen during uniaxial tensile testing results in a decrease in the distance between the transducer tip and the silver flake. This results in a change in transducer voltage corresponding to the change in thickness.

### 5.3.5 EXTENSOMETER TECHNIQUES

Various types of extensometers have been developed for soft tissue applications. Manak (1980) used a device shown in Figure 5-3 to measure strain in aorta tissue. Sutures were used to fasten the device to the tissue. Krause et al (1976) used an extensometer type "hump-backed displacement transducer" to measure circumferential strain in menisci when the knee joint was subjected to compressive loading in vitro.

An extensometer under development has been reported by Shrive (1991). The extensometer incorporates cantilever extensometer arms that employ strain gauges as sensing elements. The cantilever arms are supported by flexible proving rings which maintain contact between the specimen and transducer. Sensitivity of at least 0.02%

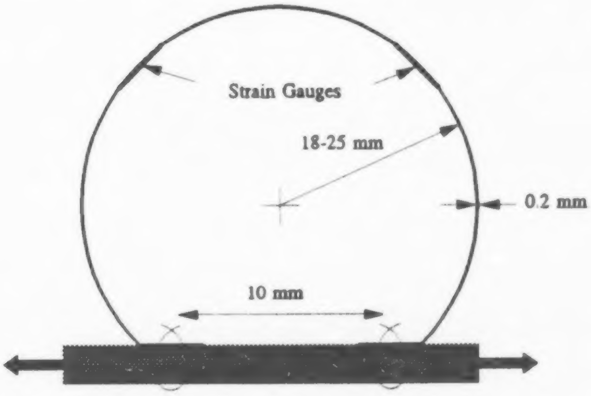

**Figure 5-3:** Schematic of an extensometer device used to measure specimen elongation (modified from Manak et al 1980)

strain is achieved with this device (Shrive 1991).

### 5.3.6 LASER METHOD TO MEASURE LATERAL CONTRACTION

A noncontacting method of measuring the lateral contraction during tensile testing was developed by Knauss and Kenner (1981). Their system employed a laser with a 50 mm circular beam. A soft tissue specimen is placed between the laser and a photo detector. The photo detector senses the width of the shadow cast by the specimen and provides an output proportional to the specimen width.

### 5.3.7 NONCONTACTING OPTICAL DEFORMATION MEASUREMENT

A noncontacting optical method for measuring specimen deformation generally uses two or more markers placed on the surface of the specimen to define a length or relative positions. An initial length or marker position is measured from discrete photographs or digitized video camera images. Deformed length or position are measured and strain is calculated based on the initial and deformed configurations. This method has the advantages of no physical contact therefore no reinforcement or tissue disruption from the measurement system and therefore is often the method of choice for small soft tissue specimens. However, tissue damage may result from the type of marker used and the relative uncertainty in strain for small deformations may be large.

#### 5.3.7.1 ONE DIMENSIONAL DEFORMATION MEASUREMENT FROM DISCRETE PHOTOGRAPHS

A photographic method for measuring dimensional changes in specimens of articular cartilage is outlined by Roth and Mow (1980). This measurement technique was duplicated in studies on the tensile properties of the meniscus (Whipple et al 1985; Arnoczky et al 1988; Proctor et al 1989). The method reported by Roth and Mow used tensile specimens 1.5 mm wide with a 2 mm gauge length identified by two lines stained on the specimen. Discrete photographs of the specimen were taken during the test. The film negatives were then analyzed using a stereomicroscope to measure the change in length between the stained lines. Accuracy of the measurement system was assessed by taking eighteen photographs of a gauge wire of known diameter (0.12475 +0.0000/-0.0001 inches). Four individuals analyzed each of the film negatives. Standard deviations from each of the four sets of measurements ranged from 0.00043 to 0.00095 inches (0.011 - 0.024 mm). Repeatability of measurements made between stained lines was not given.

### 5.3.7.2 VIDEO DIMENSION ANALYZER

A video dimension analyzer (VDA) is a device utilized by many researchers for determining strain in soft tissues (Woo et al 1979; Fithian et al 1989; Sabiston et al 1990). The VDA was developed by Yin et al (1972) and is commercially available (Instrumentation for Physiology and Medicine Inc., San Diego, California). The VDA is a self contained video processor that provides an analog output proportional to the distance between two edges contained in a viewing window. For soft tissue applications, an edge is the contrast between a black dye line on a white specimen. Two black lines form the gauge length on the test specimen. The video camera scans horizontally and senses the black to white contrast. This triggers a timer to turn on and the scan sensing the second edge triggers the timer to turn off. The scan time between the two edges corresponds to the length between the edges and is represented by a voltage. Comparison to the original voltage (length) provides a strain output. Thus a continuous measurement of strain is achieved during a test.

A modification of the VDA technique was developed by To et al (1988) to assess the uniformity of strain through the specimen. They used an optical rear projection device to simultaneously measure tensile strains on opposite sides of soft tissue specimens.

Biaxial measurement of normal strains is possible with the VDA device. Woo et al (1979) measured extensional and lateral strains in articular cartilage tensile specimens using a VDA system. A tensile test was performed with the VDA recording extensional strain. A recording of the test was then replayed on a television monitor with the viewing window of the VDA device oriented to measure lateral contraction as seen on the television monitor. Lanir and Fung (1974) performed biaxial stress tests on sheets of rabbit skin. Using two VDA's and a beam splitter, they were able to simultaneously record strain in both directions of applied stress.

### 5.3.7.3 TWO DIMENSIONAL DEFORMATION MEASUREMENT

The performance of an optical measurement system relies in part on its ability to identify surface markers accurately and repeatably. Discrete particles generally provide better edge detection than ink or stain lines thus improving the repeatability of measurements. In addition, coordinates of a specific point on the surface can be obtained in order to calculate two dimensional strain.

To measure a general two dimensional deformation during uniaxial tensile tests, Hoffman et al (1981) used markers that consisted of 0.1 mm platinum wire sharpened at one end and the other end melted to 0.3 mm ball. Coordinates of the ball ends were determined from photographic enlargements using an X-Y digitizer. They reported a strain values within ±1% for strains of 20%.

Hoffman and Grigg (1984) used 0.6 mm discs affixed to the specimen surface with grease or mineral oil. Marker centroids were calculated utilizing a computer program. A location error associated with centroid values was determined from 100 measurements of a single marker. They reported that 95% of the centroid values lie within a 0.0144 mm radius of the mean value.

Humphrey et al (1987) used dried vanilla bean specks ($\approx 250\ \mu m$) as markers. They used super glue to fix the markers on sheets of tissue and performed bi-axial stress tests. Automatic tracking of the marker position accurate to within one pixel was reported.

A method for making dimensional measurements using a video camera is given by Aspden et al (1988). Dimensional measurements were made on the computer screen and a precision of 0.4% was given based on one pixel resolution out of 256 pixels vertically on the computer screen. Repeatability or marker selection was not discussed.

Butler et al (1990) reported that the ability to provide better edge detection prompted the use of suture as markers. Previous studies by their group used ink or stain as identifying marks. They calculated regional one dimensional strains by projecting a slide on a 1000 x 360 mm board with 1 mm grid lines providing 100x magnification. A strain accuracy of 0.4% is reported.

Omens and Fung (1990) used stainless steel balls (60-100 $\mu$m) sprinkled on the surface of sections of heart muscle to investigate zero stress conditions. Measurements of marker centroid values were made from digitized images. Each location was measured five times and averaged. Distances measured from enlarged photographs were 10 mm and a digitizing error for this length was ± 0.2 mm. They report a 2.85% uncertainty in the value of the stretch ratio.

Neumann et al (1991) calculated regional one dimensional strain along lumbar anterior longitudinal ligaments in vitro using an array of 1.5 mm plastic beads sewn onto the tissue surface with suture. Digitized images were analyzed to calculate strain.

#### 5.3.7.4 THREE DIMENSIONAL DEFORMATION MEASUREMENT

Several studies of general three dimensional deformations of soft tissues have been made using biplanar stereophotogrammetry. Stokes and Greenapple (1985) used 0.8 mm circular paper targets as markers on the surface of intervertebral discs during compression testing. Three dimensional coordinates of the markers were determined using photographs from the two cameras. An expected positional error of less than 0.15 mm for 95% of the measurements was reported.

Brown et al (1991) performed tests on cadaver knees by implanting five, 1 mm steel ball markers into the periphery of each meniscus and subjected the knee to axial compression. They used biplanar X-ray stereophotogrammetry techniques to determine displacements of steel balls during compression tests. A resolution of 0.1mm was reported.

### 5.3.8 DISCUSSION OF MEASUREMENT TECHNIQUES

The previous sections have shown that many methods have been employed to determine strain in soft tissues. Each method has relative advantages and limitations and these must be assessed for each particular study. For the proposed study, specimen size presents the greatest restriction. All contacting techniques for determining strain could not be used because of the reinforcement concerns and tissue damage at the transducer-tissue interface. The Hall effect displacement transducer in Section 5.3.3 would probably offer the least resistance or reinforcement of the contacting type transducers, however fixation pins would cause tissue disruption in such small samples. Therefore a noncontacting method is required.

A grip to grip measurement technique is noncontacting and even with the assumption that grip slippage does not take place, the grip-specimen interface produces abnormal strain conditions that are also included in the measurement. Grip to grip strain measure has been compared to local strain measurement techniques by Zernicke et al (1984) and Woo et el (1981). Both studies reported a significant variation in strain along the length of the tissue sample. Zernicke et al (1984) used ink lines to mark five regions along a 70 mm long rectangular section tendon. Tissue strain was measured on a regional basis using an optical technique and compared to a grip to grip strain measure. They showed that grip to grip consistently results in larger calculated strain values than those measured locally. Grip to grip strains were 2 - 3 times average local strains. They also noted smaller measured strains at the tissue mid length and increasing in the zones closer to the grips. In the proposed meniscus study, a localized strain measure would provide a more representative value of the material properties. In addition, lateral and shear strains must also be determined and this requires another technique.

A video dimensional analyzer (VDA) discussed in Section 5.3.7.2, provides a noncontact method to determine the normal strains. The system provides an immediate analog output of the test and therefore does not require any manual data reduction. Concerns with this system are cost, uncertainty in results and measurement of only normal strains. The video processor alone costs approximately $8000. Relative uncertainties reported ≈80% at 1% strain and ≈10% at 10% strain (Shrive 1991).

Noncontacting optical methods using discrete photographs or video cameras have the advantage of no physical contact, ability to measure deformation at multiple regions to assess nonhomogeneous characteristics and also determine general two dimensional strains. In addition, a visual account of the test is recorded on video tape for analysis. Disadvantages of such systems are relative uncertainties in results at low strain levels, misinterpretation of rigid body rotation as strain, obtaining suitable markers to define points from which repeatable measurements can be made, marker interference with the deformation and time consuming data reduction. A description of the system follows and an uncertainty analysis of strain values is given in Chapter Six.

## 5.4 DESCRIPTION OF THE DEFORMATION MEASUREMENT SYSTEM

A noncontact optical method was chosen as the deformation measurement system based on the discussions in the previous sections. The basic configuration used two charge coupled device (CCD) video cameras. Two cameras provided views on two perpendicular sides of the test specimen. Markers were placed on the specimen and a magnified image of the specimen was recorded on video tape during the test. The test was then replayed into a computer with an image capture board and selected images were digitized. Using the accompanying software, the coordinates of markers were determined and the two-dimensional strains were calculated from the relative deformations in the marker region. Details of each component are discussed next.

### 5.4.1 CAMERA, LENS AND MAGNIFICATION

Two charge coupled device (CCD) cameras (JVC Model TK S210U) were used. The image was focused on an image sensor containing 694 horizontal and 491 vertical image sensing elements in a 8.8 mm by 6.6 mm area. Each camera was fitted with a standard 50 mm lens and magnification was achieved using a lens extender. The lens extender is an extension tube fitted between the camera and the lens. This provides a simple way of obtaining the required magnification without expensive lenses or microscopic equipment. Magnification is important because the uncertainty in the dimensional measurement is minimized if the test specimen image is magnified to occupy the full field of view. This is discussed further in Chapter Six.

A standard 50 mm lens with a 170 mm extension tube provides a resolution of 250 pixels/mm allowing 1.75 mm to fill the vertical distance of the screen. This lens combination also provides sufficient distance from the lens to the specimen for specimen lighting. Details of the lens and lens extender selection are given in Appendix E. The

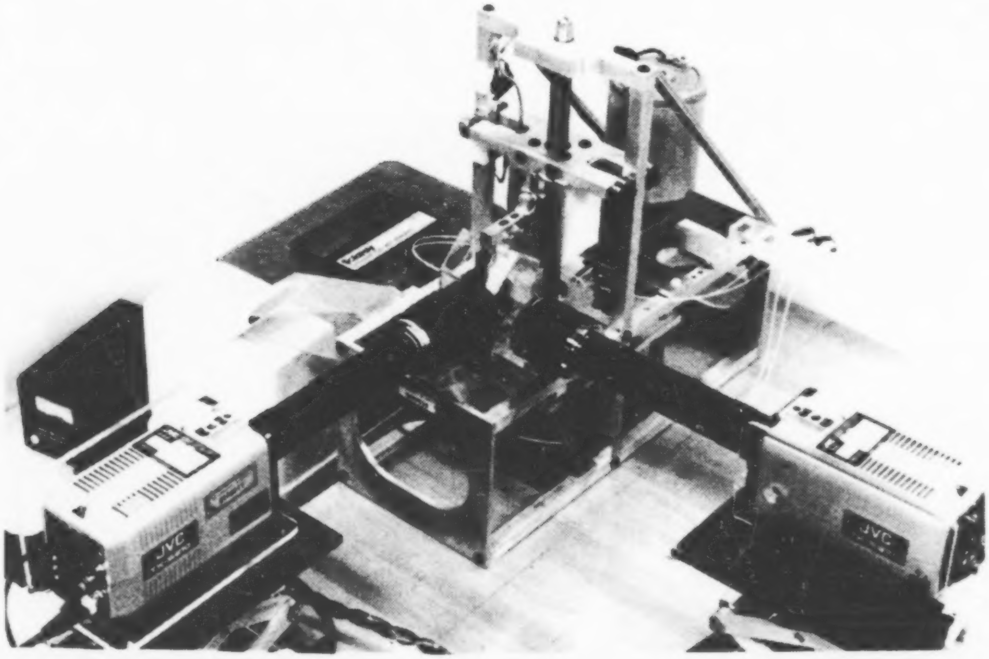

**Figure 5-4:** The tensile test apparatus with two cameras in place and the humidification system

light source is a 20 W quartz halogen lamp positioned $\approx 0.5$ m from the specimen. The increase in specimen temperature due to the light source is not significant. Both cameras were mounted on stands that allow three dimensional translations required for positioning as well as focusing. The complete test system is shown in Figure 5-4.

### 5.4.2 VIDEO IMAGE CAPTURE AND SYNCHRONIZATION WITH LOAD DATA

Each test was filmed with a video camera, viewed on a television monitor and recorded on video tape. In order to analyze specimen deformation, the tape of the test was replayed into a computer with an image capture board (Scion Corp., 152 West Patrick St, Frederick, MD. 21701). With a user command, a single frame was captured from the running video tape and shown on the computer screen. The captured image was represented as a 640 x 480 array of pixels with 256 levels of grey. The window on the computer screen provides a region of 555 x 435 pixels where the image can be analyzed. Software supplied with the image capture board features image enhancement, zoom and thresholding. A capture rate up to 30 frames a second is possible. The intermediate step of the video tape as a transfer medium between the camera and the image capture board may result in a loss of image quality but this was necessary because the image capture board was not available in the test laboratory.

The image captured for deformation measurement must correspond to the same time at which the load was sampled. This provides the load and deformation measure for one data point during the test. The load cell output was sampled at a specified time interval during the test. Ideally, the image capture would be triggered at the same time that the A-D converter samples the load and this would ensure that the image saved corresponds to the load reading recorded. However, the computer with the image capture was not available in the lab, so the test was recorded on video tape for analysis at another location. This required an alternative method of synchronizing the load-deformation data.

The computer in the lab (IBM-PC) that contains the A-D converter also accomplishes the synchronization task. Figure 5-5 shows a schematic of the system. A program was written (Microsoft QuickBASIC 4.5) to control the A-D board. At the time that the load is sampled by the A-D board in the computer, the A-D board also sends a voltage to illuminate a LED light source. This light source is flashed next to the test specimen in the field of view of the camera by means of a 0.6 mm diameter fiber optic cable. Therefore, the frames on the video tape that show the light source correspond to the time that the load is sampled. This allows synchronization of the load and deformation data.

To help match each of the images during a test with its corresponding load reading, multiple LED's and fiber optic cables are used. For one camera, two fiber optic cables are visible. With two lights, three combinations are possible with at least one light on. The fourth combination, both lights off, corresponds to the time between data points. The first data point is denoted by both lights on, the second with the top light

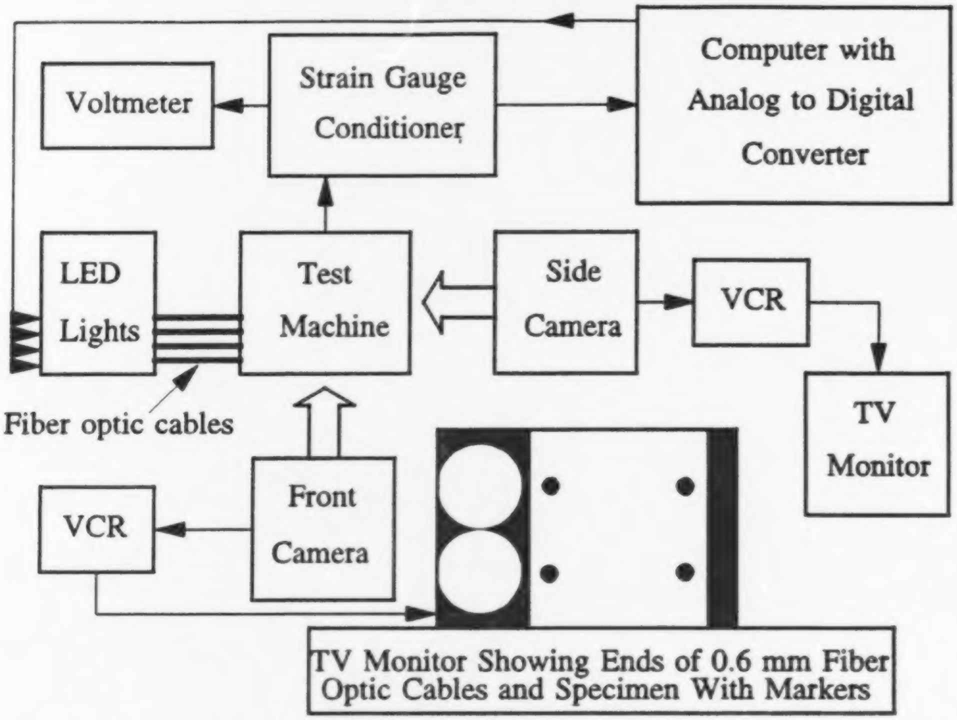
Computer with Analog to Digital Converter
Voltmeter
Strain Gauge Conditioner
LED Lights
Test Machine
Side Camera
VCR
TV Monitor
Fiber optic cables
Front Camera
VCR
TV Monitor Showing Ends of 0.6 mm Fiber Optic Cables and Specimen With Markers

**Figure 5-5:** Schematic of the test equipment and load-deformation synchronization method

on and bottom off and the third data point is top off and bottom on. This helps differentiate each of the data points during digitization.

The digitization procedure is as follows. The video tape is replayed at normal speed into the computer with the image capture board. When the flash of light appears ($\approx 0.1$ sec), a click of the mouse captures a single frame on the computer screen. The time between the data points (sampling interval) for a typical low strain rate test is about 20-30 seconds and any time lag between the flash of light and clicking the mouse is considered negligible. The perimeter of each specimen marker is traced manually using the mouse. Software supplied with the image capture board calculates the X and Y coordinates of the centroid of each marker area. The coordinates are stored and later used to calculate two dimensional strain in the region of the markers. The selection and placement of markers on the specimen is described in the next section.

## 5.5 SPECIMEN MARKERS

An important aspect of optical deformation measurement is the selection of markers to define points on the surface of the tissue. The relative motion of these markers determines the deformation of the surface of the specimen. Before the calibration and repeatability of the measurement system can be evaluated, a suitable marker must be selected.

For a noncontacting optical system, the ideal surface marker would provide a small distinct point, adhere to the surface when fluid is exuding from the specimen and not restrict the natural deformation. From the review of optical methods presented in Section 5.3, many different types and methods of marker placement have been used. Variations of these methods were tried in order to find a suitable technique for the small meniscus samples. An ink band on the specimen did not provide a sharp edge at high magnification and at large values of strain, fluid exuding from the specimen distorted the edge even more. Histological stains were also tried. Verhoffs elastin stain is a histological stain that reacts with collagen to turn the collagen substance black. This overcomes the problem of the stain flowing with the fluid but under high magnification the edge of the stained line was not detectable with sufficient repeatability. As another possibility, small sutures were sewn through the specimen and this provided a distinct point. Although the suture itself was probably small enough to minimize damage, the needle used to sew the suture in place damaged the tissue. Another method used fine needles obtained from entomology. The needle end was pierced into the specimen and trimmed off to provide a distinct circular point. However several pins through the thickness of the specimen may interfere with the deformation and this method was not used.

Small particles on the specimen surface proved to be the best solution. A black marker provided the best edge contrast on the white tissue. Coal granules were obtained in several different size groups. Particles from the group with an average size ranging from 0.075 - 0.1 mm were found to be the most suitable. The small size made them distinct points, yet they were large enough to be placed individually on the specimen with the use of a microscope (Figure 5-6). The particles would be washed away by the

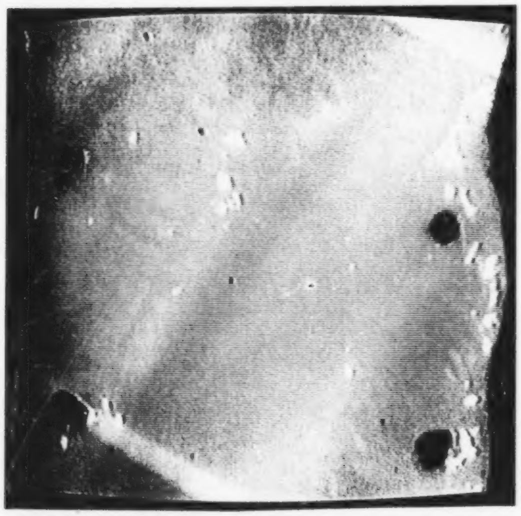

**Figure 5-6:** Photograph of a specimen with markers (specimen width $\approx 1.2$ mm)

exuding fluid during the test and this necessitated the use of a cyanoacrylate adhesive to fix the particles on the surface. The adhesive must be used carefully to avoid disturbing the surface of the specimen. Excess adhesive would impair the natural deformation of the tissue.

The tensile specimen was prepared as described in Chapter Three and placed in the grips using the mounting jig. A drop of cyanoacrylate glue was placed on the surface of a small plastic plate. A small number of coal particles were placed in the adhesive. Using a binocular microscope and a fine needle, individual coal particles were mixed with the adhesive and placed on the specimen at the desired position. Any number of markers can be placed on the surface to form a grid. The adhesive only coats the surface of the marker and therefore the amount of the tissue being fixed by the specimen placement is less than a 0.075 mm diameter area. This corresponds to approximately 5% of the width of the gauge section on the specimen and it was assumed that this does not significantly affect the surface deformation. This marker placement technique resulted in a distinct point that adhered to the surface and did not significantly interfere with the deformation.

## 5.6 VERIFICATION OF MEASUREMENT SYSTEM PERFORMANCE

### 5.6.1 REPEATABILITY OF SUCCESSIVE MEASUREMENTS

A repeatability test was performed to assess the ability in determining the centroid location of typical marker. The lens configuration used was a 50 mm lens with a 170 mm lens extender providing a resolution of 250 pixels/mm. A marker on a test specimen was measured 40 times to determine the centroid location. The results are shown in Figure 5-7 as a frequency distribution of pixel values for both the X and Y coordinate location. For both cases the range of values is three showing minimal scatter in the measurements. The standard deviation of centroid coordinates provides the variability between individual measurements in the sample. Based on this test, a standard deviation ($\sigma$) of 0.5 pixel is used for a given marker location. Therefore 95% of the X and Y coordinate measurements are expected to be within ∓ 1 pixel of the mean values. The standard error of the mean (SEM) involves repeated measurements of the same value and provides a measure of the precision of an estimate of the population. The standard error of the mean is defined by

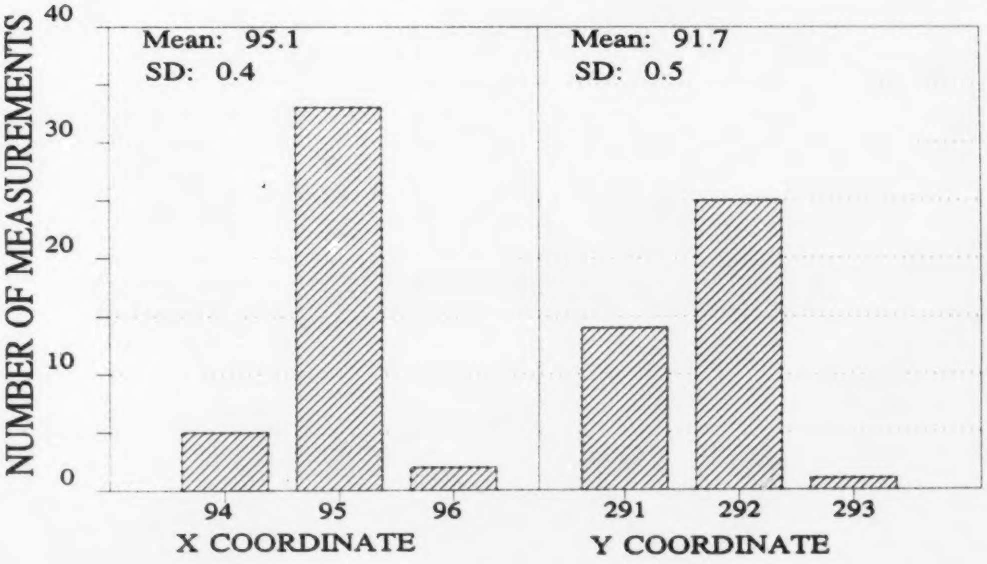

**Figure 5-7:** Distribution of X and Y coordinates (pixels) for repeated digitizing a single marker.

$$SEM = \frac{\sigma}{\sqrt{n}} \tag{5-1}$$

where n is the number of measurements used to calculate the mean and $\sigma$ is the standard deviation of the population. An improved estimate of the location can be obtained with repeated measurements. A single measurement has an uncertainty of ±1 pixel and for a measurement repeated five times an uncertainty of ±0.5 pixel is assumed, both values with 95% confidence. In Chapter Six these results will be used in an uncertainty analysis of the strain values.

### 5.6.2 LENS ABERRATION

A test was performed to evaluate possible distortion of the image due to the lens configuration. Two markers were bonded to a piece of white plastic to represent a line of fixed length. The distance between the two markers was 1.25 mm (312 pixels) which corresponds to 75% of the full height of the field of view with a 50 mm lens and 170 mm lens extender. The markers were oriented to form a vertical line. The distance between the centroid locations was measured at five locations across the field of view. Differences in the five line lengths were less than one pixel (0.3%). The markers were then oriented horizontally and length measurements were taken at five locations from the top to the bottom of the screen. No significant differences in length were noted for this orientation and it was concluded that the lens configuration was free of any spherical aberration.

However this test revealed that the horizontal measurements differed from the vertical measurements by 2.7%. Line lengths in the vertical direction averaged 312 pixels while the same distance in the horizontal direction measured 321 pixels. The aspect ratio of the pixel elements was not 1:1. A correction of 2.7% was used to correct the X values of subsequent measurements. The horizontal or X direction was deemed "incorrect" because calibration was carried out in the Y direction.

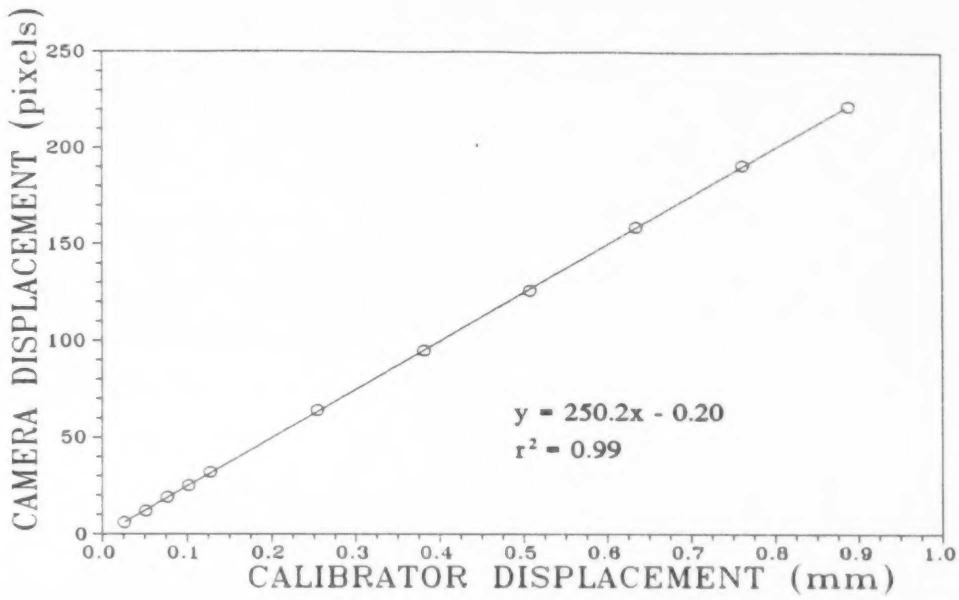

**Figure 5-8:** Linearity of the camera as a measurement device

### 5.6.3 LINEARITY AND CALIBRATION

Linearity and calibration of the camera as a distance measuring device was determined using a micrometer calibrator (MTS Calibrator, Model 650.03). The test was performed with a 50 mm lens focused to infinity and a 170 mm lens extender. One marker was bonded to the fixed edge of the calibrator and another marker was bonded to the moving edge. Displacement increments were made with the calibrator and the relative locations of the two centroids were determined. Test results, shown in Figure 5-8, show linear response and also provide a calibration factor to relate pixel measurements to physical distances. A conversion of 250.2 pixels per millimeter was determined from Figure 5-8. It should be noted that strain calculations are based on pixel measurements and the conversion is only necessary for calculation of the cross-sectional area.

Calibration tests for other lens extender lengths were completed and the results are shown in Figure 5-9. This provides calibration data for other lens extender lengths using the 50 mm lens. A lens extender length of 200 mm provides a sensitivity of 295 pixels/mm and is a feasible upper limit for this test apparatus. For lens extender lengths

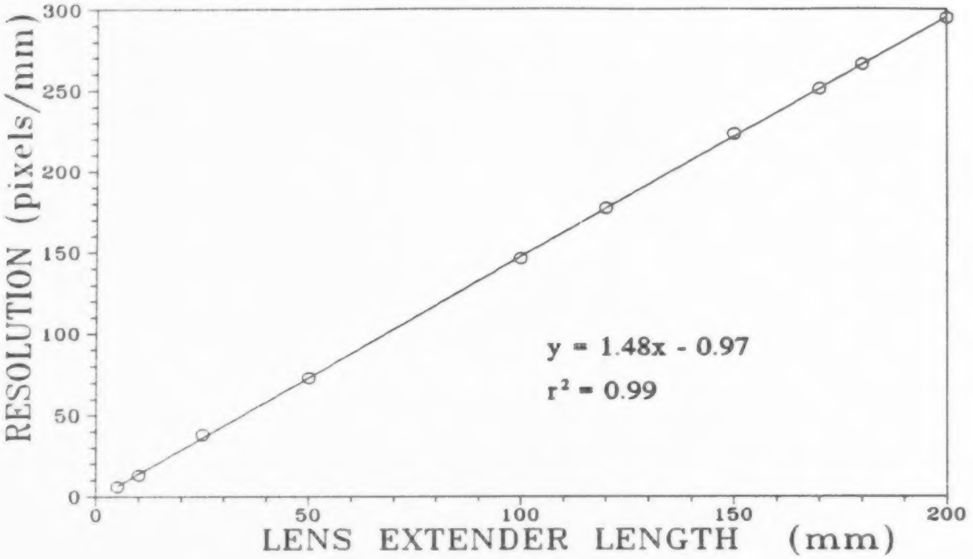

**Figure 5-9:** Variation of image magnification with lens extender length

over 200 mm, illumination and focusing become increasingly difficult. One or two quartz halogen lights were used for specimen illumination, depending on the application. Also, with increasing lens extender lengths, the distance between the lens and specimen decreases (Appendix E) and the lens interferes with the incoming light. The lens to specimen distance for a 200 mm lens extender and 50 mm lens is approximately 20 mm.

## 5.7 SUMMARY

The deformation system described provides the information required to calculate two dimensional strain on the surface of the specimen during testing. The main features are that the method is noncontacting which avoids any specimen reinforcement or disruption and the capability to measure a general two dimensional deformation. The load - deformation data must now be converted into stress - strain data. Chapter Six describes the calculation of stress and strain from the load - deformation data. In addition, an uncertainty analysis of the computed results is given.

# CHAPTER 6

# CALCULATION OF STRESS AND STRAIN AND UNCERTAINTY ANALYSIS

## 6.1 INTRODUCTION

For a typical laboratory test, tensile load was recorded by the computer and the corresponding locations of specimen surface markers were determined by analyzing the video tape of the test. From this data, stress and strain which were the quantities of interest, were then calculated from the experimental load and deformation data. This chapter outlines the calculation of stress and strain values and provides an uncertainty analysis of the results. The assessment of uncertainties associated with calculated results can help evaluate the reliability of the method and attention can be given to variables that have the greatest effect on the calculated results.

## 6.2 STRESS CALCULATION

The stress measure used was based on the initial cross-sectional area of the soft tissue specimen. Measurement of load (force) values was described in Chapter Four. The load cell reading was recorded at a specified time interval and the data were stored for subsequent stress calculation.

### 6.2.1 CROSS-SECTIONAL AREA MEASUREMENT

The measurement of cross-sectional area of soft tissue specimens introduces difficulties due to the compliance and irregular shape of many specimens. Numerous techniques have been implemented. Non-destructive methods have incorporated a laser beam (Lee and Woo 1988), optical beam (Iaconis et al 1987), area micrometers (Walker et al 1964), micrometers sensing contact (Woo et al 1979) and an instrumented calliper (Shrive et al 1988). Questions have also been raised regarding the definition of cross-sectional area (Butler 1978). Should the fluid component of the soft tissue be included as part of the load carrying area?

The method of specimen cross sectional area measurement used in this study is based on the assumption that the test specimen has a rectangular cross-section. This assumption follows from the test specimen preparation procedure described in Chapter Three. A noncontacting method for measuring surface deformation was described in Chapter Five and this is also used for specimen dimension measurements. The cross-sectional area measurement uses two cameras that are positioned perpendicular to two adjacent surfaces of the specimen. One camera measures the width and the second camera measures thickness. Measurements are made at the time defined to be the start of the test. This initial point of the test is also where the undeformed configuration of the deformation measurement markers is recorded. Width and thickness are calculated from an average of each set of measurements made along the gauge length of the specimen. Stress is calculated at each data point based on this original cross-sectional area which includes both the solid and fluid components.

## 6.3 STRAIN CALCULATION

For an arbitrary two dimensional finite deformation, a systematic method of calculating strains is required. Kinematics of finite deformation is covered in Spencer (1980) or Fung (1990) as well as many other references. A deformation gradient is formulated to describe the deformation of the material. If the deformation gradient is known for a region then strains can be calculated for that region.

As shown in Figure 6-1, a material line element has endpoints $\underline{x}$ and $\underline{x} + \underline{dx}$ in the undeformed or reference configuration. In the deformed configuration the line element has endpoints $\underline{\chi}$ and $\underline{\chi} + \underline{d\chi}$. Greek letters will refer to the deformed configuration. The deformation gradient tensor for a body maps a material line element from the undeformed to the deformed configuration or vice versa. Referring to Figure 6-1, the deformation gradient tensor is given by

$$F_{ij} = \frac{\partial \chi_i}{\partial x_j}$$

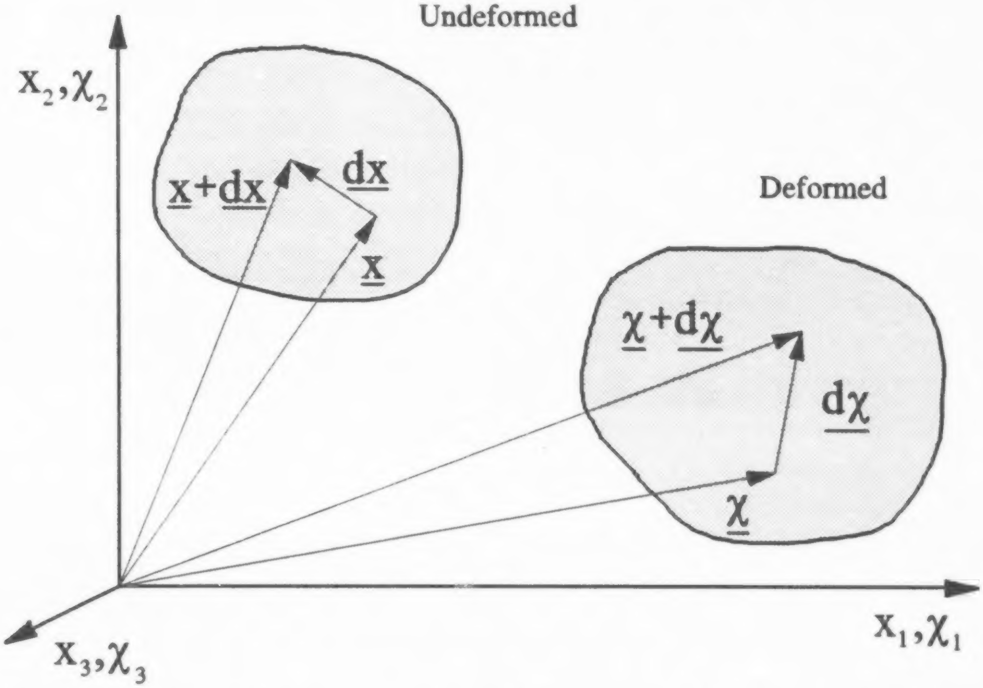
Undeformed
$x_2, \chi_2$
$\underline{x}+\underline{dx}$
$\underline{dx}$
$\underline{x}$
Deformed
$\underline{\chi}+\underline{d\chi}$
$\underline{d\chi}$
$\underline{\chi}$
$x_1, \chi_1$
$x_3, \chi_3$

**Figure 6-1:** Material line element in undeformed and deformed configurations

of two markers, forming a line element, are known in the undeformed and deformed configurations at specified times during the test. Knowing the relative motion of three noncollinear points (markers), a two dimensional deformation gradient can be calculated based on a finite version of Equation 6-1. This is written as

$$F_{ij} = \frac{\Delta \chi_i}{\Delta x_j} \quad or \quad \Delta \chi_i = F_{ij}\, \Delta x_j \qquad i,j = 1,2 \tag{6-2}$$

When Equation 6-1 is written as Equation 6-2, the deformation is assumed to be homogeneous in the region enclosed by the markers. The method of determining the deformation gradient tensor is outlined below and is similar to that given by Waldman (1986). This method provides a systematic way of reducing the X and Y coordinate data of the markers into two dimensional strains.

As shown in Figure 6-2, a triangular region in the undeformed configuration is

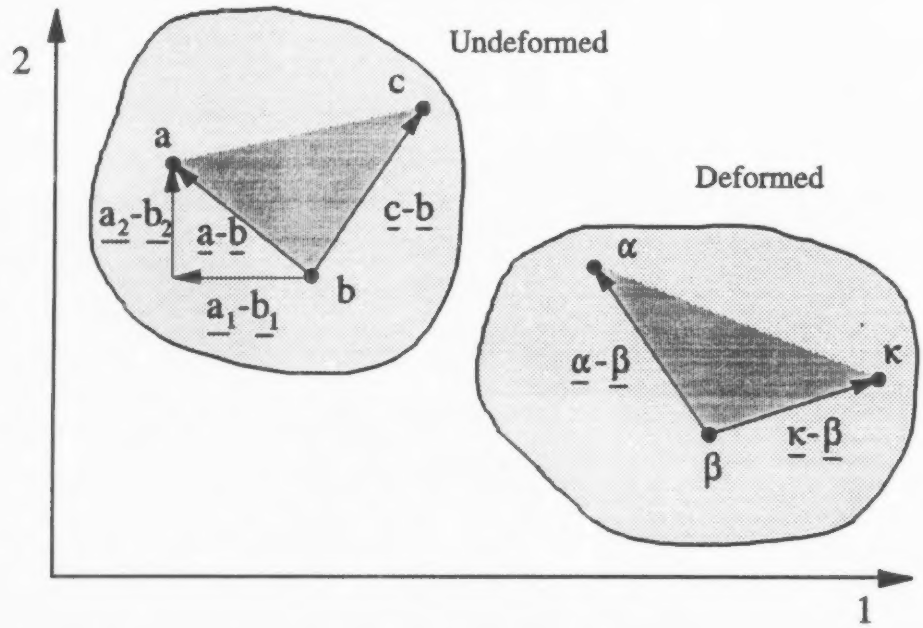
2
Undeformed
c
a
Deformed
$\underline{a}_2$-$\underline{b}_2$
$\underline{a}$-$\underline{b}$
$\underline{c}$-$\underline{b}$
α
b
$\underline{a}_1$-$\underline{b}_1$
$\underline{\alpha}$-$\underline{\beta}$
κ
$\underline{\kappa}$-$\underline{\beta}$
β
1

**Figure 6-2:** Material line elements used to calculate two dimensional strain

enclosed by three points; $\underline{a}$, $\underline{b}$ and $\underline{c}$. After the material has deformed, the locations of the three points are given by $\underline{\alpha}$, $\underline{\beta}$ and $\underline{\kappa}$. Two line elements are formed from the three points; $\underline{a}$ - $\underline{b}$ and $\underline{c}$ - $\underline{b}$ in the reference configuration and $\underline{\alpha}$ - $\underline{\beta}$ and $\underline{\kappa}$ - $\underline{\beta}$ in the deformed configuration. From Equation 6-2, each line element provides two equations relating components of the undeformed and deformed line elements by means of the deformation gradient components. For the line element from $\underline{b}$ to $\underline{a}$,

$$(\alpha_1 - \beta_1) = F_{11}(a_1 - b_1) + F_{12}(a_2 - b_2) \tag{6-3}$$

$$(\alpha_2 - \beta_2) = F_{21}(a_1 - b_1) + F_{22}(a_2 - b_2) \tag{6-4}$$

Similarly for a line element from point $\underline{b}$ to $\underline{c}$,

$$(\kappa_1 - \beta_1) = F_{11}(c_1 - b_1) + F_{12}(c_2 - b_2) \tag{6-5}$$

$$(\kappa_2 - \beta_2) = F_{21}(c_1 - b_1) + F_{22}(c_2 - b_2) \tag{6-6}$$

The four components of the deformation gradient describing the surface deformation of the test specimen are solved for from Equations 6-3 to 6-6. In terms of the coordinates of the three markers, the components of the deformation gradient are

$$F_{11} = \frac{(\alpha_1 - \beta_1)(c_2 - b_2) - (a_2 - b_2)(\kappa_1 - \beta_1)}{(a_1 - b_1)(c_2 - b_2) - (a_2 - b_2)(c_1 - b_1)} \tag{6-7}$$

$$F_{22} = \frac{(a_1 - b_1)(\kappa_2 - \beta_2) - (\alpha_2 - \beta_2)(c_1 - b_1)}{(a_1 - b_1)(c_2 - b_2) - (a_2 - b_2)(c_1 - b_1)} \tag{6-8}$$

$$F_{12} = \frac{(a_1 - b_1)(\kappa_1 - \beta_1) - (\alpha_1 - \beta_1)(c_1 - b_1)}{(a_1 - b_1)(c_2 - b_2) - (a_2 - b_2)(c_1 - b_1)} \tag{6-9}$$

$$F_{21} = \frac{(\alpha_2 - \beta_2)(c_2 - b_2) - (a_2 - b_2)(\kappa_2 - \beta_2)}{(a_1 - b_1)(c_2 - b_2) - (a_2 - b_2)(c_1 - b_1)} \tag{6-10}$$

where Greek letters refer to marker coordinates after deformation. With these four components, two dimensional deformation is defined in the region of the points and strains can be calculated in this region.

Cauchy's infinitesimal strain tensor is given by

$$e_{ij} = \frac{1}{2}(F_{ij} + F_{ji}) - \delta_{ij} \quad or \quad \underline{\varepsilon} = \frac{1}{2}(\underline{F} + \underline{F}^T) - \underline{I} \tag{6-11}$$

with components

$$e_{11} = F_{11} - 1 \tag{6-12}$$

$$e_{22} = F_{22} - 1 \tag{6-13}$$

$$e_{12} = \frac{1}{2}(F_{12} + F_{21}) \tag{6-14}$$

and the Lagrangian or Green finite strain tensor is

$$E_{ij} = \frac{1}{2}(F_{ki}F_{kj} - \delta_{ij}) \quad or \quad \underset{\sim}{E} = \frac{1}{2}(\underset{\sim}{F}^T\underset{\sim}{F} - \underset{\sim}{I}) \tag{6-15}$$

with components

$$E_{11} = \frac{1}{2}(F_{11}^2 + F_{21}^2 - 1) \tag{6-16}$$

$$E_{22} = \frac{1}{2}(F_{22}^2 + F_{12}^2 - 1) \tag{6-17}$$

$$E_{12} = \frac{1}{2}(F_{11}F_{12} + F_{22}F_{21}) \tag{6-18}$$

Equations 6-16 to 6-18 show that for finite strains, shearing components of the deformation gradient are related to normal strains and vice versa.

## 6.4 UNCERTAINTY ANALYSIS OF CALCULATED STRESS AND STRAIN VALUES

Error is the difference between the "true" value and the measured value while uncertainty is the probable range of values that is thought to encompass the error (Taylor 1982). Uncertainties and errors can be classified into two groups: random and systematic (Taylor 1982). Random errors or uncertainties can be revealed by repeated measurements and are treated statistically. There is an equal chance of overestimation as there is of underestimation. Systematic errors or uncertainties relate to calibration and initializing (zeroing) equipment and will not be detected by repeated measurements. It was assumed that calibration and initialization of equipment have reduced systematic errors or uncertainties and they will be neglected.

For a function of several variables,

$$f = f(x_1, x_2, \dots, x_n) \tag{6-19}$$

where the variables $x_1$ to $x_n$ are measured with random uncertainties of $\epsilon_{x_1}$ to $\epsilon_{x_n}$, respectively, the absolute uncertainty in the value of the function f is expressed as a summation of partial derivatives

$$\epsilon_f = \sqrt{\sum_{i=1}^{n} \left( \frac{\delta f}{\delta x_i} \epsilon_{x_i} \right)^2} \tag{6-20}$$

Relative uncertainty is obtained by dividing the absolute uncertainty by the value of the function to obtain uncertainty as a percentage of the value of the function at that point. An uncertainty analysis based on Equation 6-20 was applied to the stress and strain calculations.

### 6.4.1 UNCERTAINTY IN STRESS VALUES

Stress as defined in Section 6.2 is a function of three variables,

$$\sigma = \sigma(P,w,t) = \frac{P}{wt} \tag{6-21}$$

The same technique was used to measure the width and the thickness, therefore the uncertainty in measuring the width was the same as the thickness ($\epsilon_w = \epsilon_t$). From Equation 6-20 and 6-21, the absolute uncertainty in stress is

$$\epsilon_\sigma = \sqrt{\left( \frac{1}{wt} \epsilon_P \right)^2 + \left( \frac{1}{w^2} + \frac{1}{t^2} \right) (\sigma \epsilon_w)^2} \tag{6-22}$$

The relative uncertainty in the stress calculation is

$$\frac{\epsilon_\sigma}{\sigma} = \sqrt{\left(\frac{\epsilon_P}{\sigma w t}\right)^2 \epsilon_P^2 + \left(\frac{1}{w^2} + \frac{1}{t^2}\right)\epsilon_w^2} \qquad \textbf{(6-23)}$$

Both uncertainties depend on the value of stress and the initial (fixed) dimensions. Both relative and absolute uncertainties were evaluated for a typical test. A width and thickness of 300 pixels (1.2 mm) was used for the initial dimensions. Uncertainty in the load value ($\epsilon_P$) was assumed to be ∓1 bit of the analog to digital converter (0.02 N) for loads up to 4 N. For loads greater than 4 N, the uncertainty was 0.5% of the load value. Uncertainty in the width and thickness measurements ($\epsilon_w$) was ∓5 pixels on the digitized image or 0.020 mm at the magnification used (250 pixels/mm). Uncertainty estimates for the stress calculation are shown in Figure 6-3. For stresses greater than

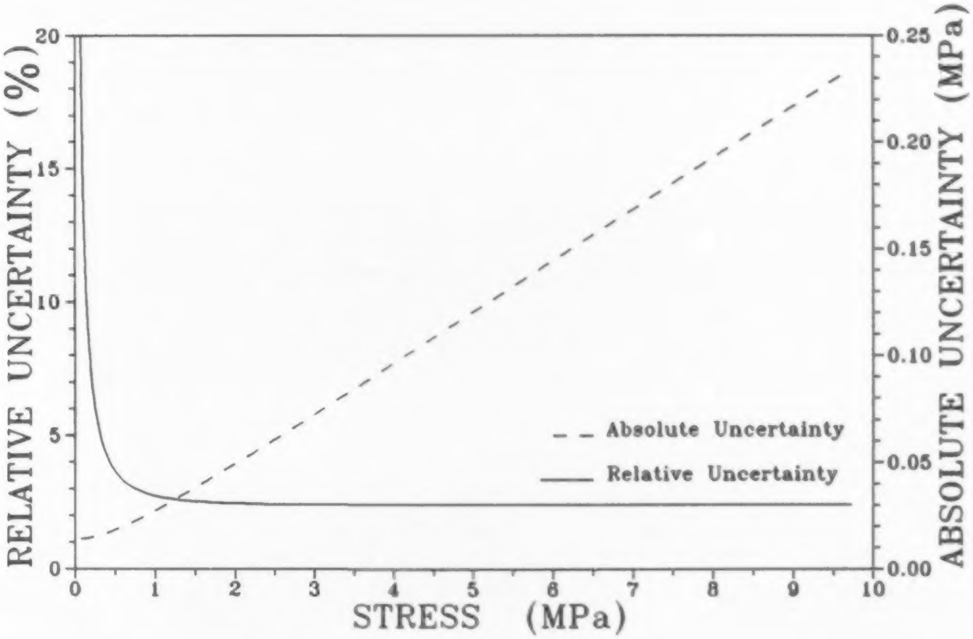

**Figure 6-3:** Absolute and relative uncertainties in stress for a typical test

1 MPa, the relative uncertainty approaches 2.5%. Uncertainty in the stress value plays a lesser role in the reliability of the calculated results than strain uncertainties, therefore attention to uncertainties in strain values is of greater importance.

### 6.4.2 UNCERTAINTY IN STRAIN CALCULATION

Two dimensional strain was calculated in Section 6.3 by calculating deformation gradients based on the centroid coordinates of the three markers. The most complete method to assess the uncertainty in strain would be to calculate the uncertainty in each deformation gradient component from Equations 6-8 to 6-10 with an uncertainty associated with each coordinate value. These uncertainties would be combined in Equations 6-11 or 6-15 to give the uncertainty in strain. However, a simple one dimensional case is easier to interpret and will indicate the important factors regarding the reliability of strain values.

For one dimensional strain given by

$$e = \frac{L - L_o}{L_o} \tag{6-24}$$

the absolute uncertainty is

$$\begin{aligned} \epsilon_e &= \sqrt{\left(\frac{1}{L_o}\right)^2 \epsilon_L^2 + \left(\frac{L}{L_o^2}\right)^2 \epsilon_{L_o}^2} \\ &= \frac{1}{L_o}\sqrt{\epsilon_L^2 + (e+1)^2\,\epsilon_{L_o}^2} \end{aligned} \tag{6-25}$$

and the relative uncertainty is

$$\frac{\epsilon_e}{e} = \frac{1}{e L_o}\sqrt{\epsilon_L^2 + (e+1)^2\,\epsilon_{L_o}^2} \tag{6-26}$$

As seen from Equations 6-25 and 6-26, the initial length ($L_o$) is an important parameter in the strain uncertainty as well as the uncertainties associated with the measurement of the two lengths, $\epsilon_L$ and $\epsilon_{L_o}$.

Ideal magnification would have the initial length occupy as much of the viewing screen as possible. This requires an estimate of the maximum strain that will be reached during the test. If specimen failure is of interest, the markers must remain in the field of view during failure and this requires an initial estimate of the strain at failure.

When calculating strain, all measurements are referred to the original measurement. Therefore, the uncertainty in the coordinates of the initial marker configuration is of particular importance. Repeating the initial measurement to reduce $\epsilon_{L_o}$ would be recommended. The time requirement to repeat all measurements and reduce $\epsilon_L$ would have to be evaluated for each test.

Uncertainty in a finite strain measure is determined similarly. In uniaxial tension, a finite strain measure is given by

$$E = \frac{1}{2}\frac{L^2 - L_o^2}{L_o^2} \tag{6-27}$$

The absolute uncertainty is

$$\begin{aligned} \epsilon_E &= \sqrt{\left(\frac{L}{L_o^2}\epsilon_L\right)^2 + \left(\frac{L^2}{L_o^3}\epsilon_{L_o}\right)^2} \\ &= \frac{1}{L_o}\sqrt{(2E+1)\left[\epsilon_L^2 + (2E+1)\,\epsilon_{L_o}^2\right]} \end{aligned} \tag{6-28}$$

The same parameters are of importance in the uncertainty in the finite strain measure.

To assess the uncertainty in strain, values for $\epsilon_L$ and $\epsilon_{L_o}$ must be determined. Calculation of tensile strain using a noncontacting optical method requires the calculation of an initial length $L_o$ and a deformed length L. Each length is calculated by subtracting the centroid coordinates of two markers. Therefore, the uncertainty in the length measurement ($\epsilon_L$) in terms of the uncertainties in the centroid coordinates ($\epsilon_x$) is

$$\epsilon_L = \sqrt{2}\,\epsilon_x \tag{6-29}$$

Uncertainty in a centroid coordinate measurement was determined in Section 5.6.1. For a single measurement an uncertainty of ±1 pixel was determined and for a measurement repeated five times an uncertainty of ±0.5 pixel is given, both values with 95% confidence. The initial measurement is repeated five times and the remaining measurements are made once. Therefore from Equation 6-29, $\epsilon_{L_o}$ and $\epsilon_L$ would have uncertainties of ±0.7 and ±1.4 pixels respectively. Realistic values for testing are ±1 and ±1.5 for $\epsilon_{L_o}$ and $\epsilon_L$, respectively. A plot of strain uncertainty and strain is given in Figure 6-4 for these uncertainties and an initial length ($L_o$) of 300 pixels. This represents a typical test situation. Relative uncertainty falls below 10% after a strain of 6% has been attained.

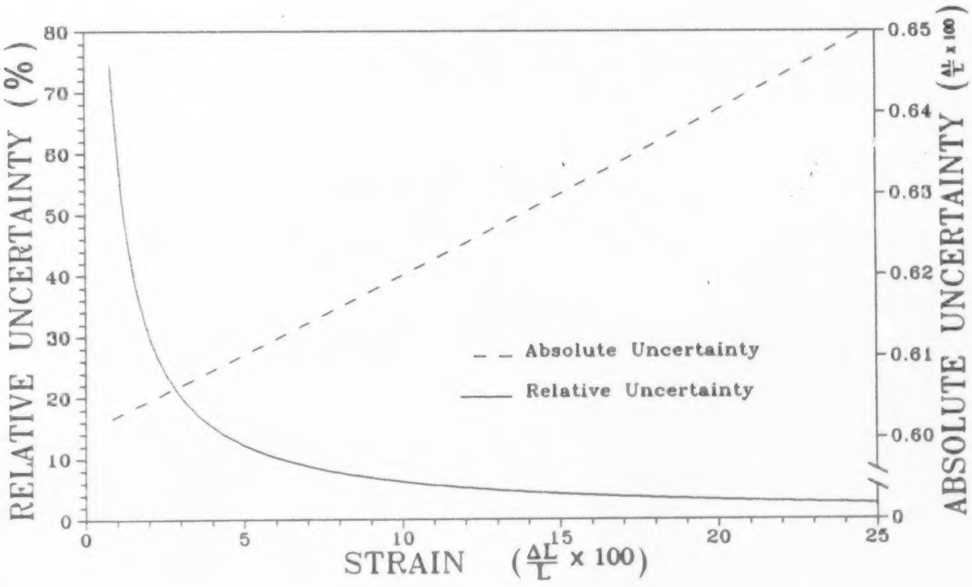

**Figure 6-4:** Absolute and relative uncertainties in strain for a typical test

**Table 6-1:** Sensitivity of relative uncertainty in strain measurement

| PARAMETER | | | STRAIN VALUE | | |
|---|---|---|---|---|---|
| $L_o$ | $\epsilon_{L_o}$ | $\epsilon_L$ | 1% | 5% | 10% |
| 300 | 1 | 1.0 | 47 | 10 | 5 |
| | 1 | 1.5 | 60 | 12 | 6 |
| | 1 | 2.0 | 75 | 15 | 8 |
| 400 | 1 | 1.0 | 36 | 7 | 4 |
| | 1 | 1.5 | 45 | 9 | 5 |
| | 1 | 2.0 | 56 | 11 | 6 |
| 500 | 1 | 1.0 | 28 | 6 | 3 |
| | 1 | 1.5 | 36 | 7 | 4 |
| | 1 | 2.0 | 45 | 9 | 5 |

The sensitivity of relative uncertainty in strain for possible combinations of experimental variables is given in Table 6-1. Length values are given in pixels because the digitized image is represented by a grid of 555 horizontal by 435 vertical pixels. Magnification was adjusted for different sized specimens so that the maximum number of pixels are used. An initial length of 500 pixels could be used for tests up to 10% strain. The benefit of maximizing the initial length is evident from the values in Table 6-1. The uncertainty for the finite strain measure given in Equation 6-27 does not differ significantly compared to the strain defined in Equation 6-24 for a given value of strain.

An additional error could be introduced if the specimen undergoes an angle change as shown in Figure 6-5. An apparent strain given by

$$e = \cos\theta - 1 \tag{6-30}$$

would be indicated for an angle change of $\Theta$. An inclination of 5° would result in an error in strain of 0.4%. The specimen grips and test machine mounts maintain a vertical specimen orientation. The second camera will also detect any change in angle of the specimen. The cross-sectional area measurement is also susceptible to an angle

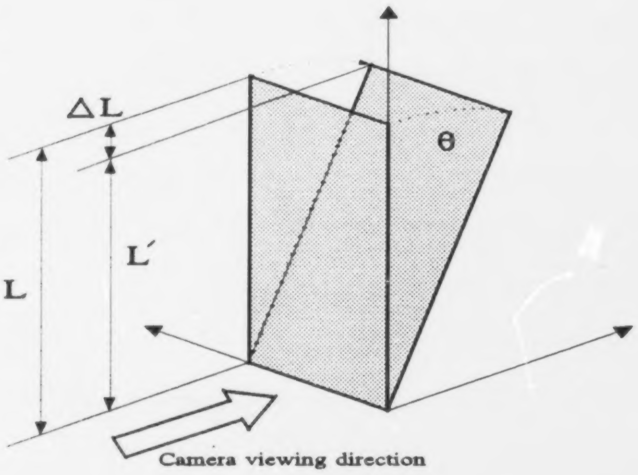

**Figure 6-5:** Strain measurement error due to specimen rotation

alignment error.

### 6.4.3 DISCUSSION OF UNCERTAINTY ANALYSIS

The optical technique used by Roth and Mow (1980) to determine strain in cartilage specimens is of interest because this technique was also used in tests on the menisci (Whipple et al 1985; Arnoczky et al 1988; Proctor et al 1989). Roth and Mow tested articular cartilage in tension using an optical strain measurement technique described in Section 5.3.7.1. Based on an uncertainty analysis it was determined that the relative uncertainty in strain measurement was less than 4%. The value of strain for this uncertainty was not given. Their calculations in the appendix show that this relative uncertainty was evaluated at 33.7% strain. If the uncertainty is evaluated at 1% and 10% strain, the relative uncertainty in strain is 68% and 7%, respectively. Uncertainties for each of the measurements were given as the accuracy given by the manufacturer's instrument specifications. For length measurements, the uncertainty was given as 0.0127 mm for an initial length of approximately 2.5 mm. The repeatability of measuring the length between the two stained lines used as markers was not discussed.

A video dimensional analyzer (VDA) was described in section 5.2.7.2. Papers employing this method state errors in linearity and accuracy are less than 0.5%. Shrive

(1991) refers to values of relative error in strain measurement as 80% at 1% strain and 10% at 10% strain. Properties of the meniscus reported by Fithian et al (1989) were determined using a VDA.

## 6.5 SUMMARY

Two dimensional strains are calculated from the relative motion of markers on the specimen surface. An uncertainty analysis has shown which parameters are most important when assessing uncertainty in both stress and strain. Maximizing the initial length between markers will reduce uncertainties associated with strain. Measurement of the initial configuration also is of particular importance in the uncertainty of the strain results. Analysis shows the system to be capable of measurements with uncertainties comparable to other published optical systems. The complete test apparatus will now be applied to meniscus specimens to show an example of test results.

# CHAPTER 7

# APPLICATION OF THE TEST SYSTEM TO MENISCUS SPECIMENS

## 7.1 INTRODUCTION

Previous chapters have described the components of the test system and assessed their performance. This chapter presents some applications of the test system. First, a specimen of vulcanized rubber was tested as an example of a "well behaved" material. Examples of tests on bovine meniscus tissue are then presented. Chapter two described three tensile tests that are proposed to determine material constants for a linear transversely isotropic material. An example of each of the three tests is presented as an application of the system. The results presented are intended to show the information that can be obtained from a test. A larger number of samples must be tested before any material properties can be inferred.

## 7.2 GENERAL TEST PROCEDURES

The starting point for a meniscus tissue tensile test is difficult to define due to the low initial stiffness of the specimen. The most common method is to prescribe a given preload as the starting point of the test. A preload of 0.01 N ($\approx$0.025 MPa prestress) has been used previously (Woo et al 1979; Arnoczky et al 1988; Fithian et al 1989; Proctor et al 1989). An initial prestress of $\approx$0.01 MPa was used in the tests presented here.

Tests on meniscal tissue were carried out in a humidified air stream to prevent moisture loss. An elongation rate of 0.01 mm/s was used for the example tests. For a 5 mm gauge length this would correspond to a strain rate of 0.2%/sec. The actual strain rate of the specimen gauge length was determined after the test from the strain axis of the stress-strain curve, knowing the time interval between data points.

Four surface markers were used to measure the specimen deformation. Three markers would be sufficient to characterize two-dimensional deformation in a triangular region enclosed by the points. The addition of a fourth marker allows deformation in four regions to be analyzed. This allows an evaluation of the homogeneity of

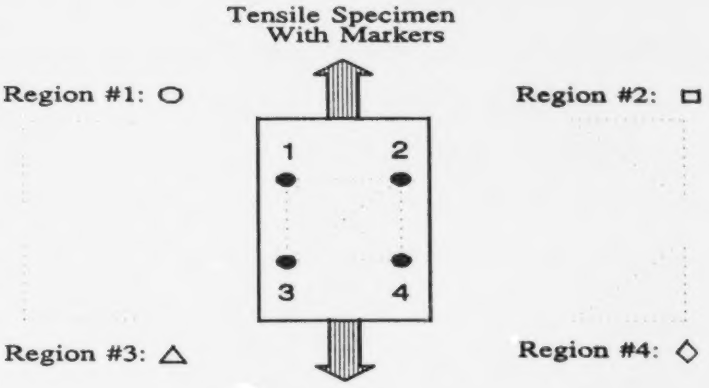

**Figure 7-1:** Markers providing four strain measurement regions on the specimen and the corresponding symbols used for each region when plotting results

deformation of the material in the region of the markers. The four regions are shown in Figure 7-1 along with the symbol that is used when plotting stress-strain results for each region. For a uniform material like rubber, the four stress strain curves should be the same. Results also include a marker position history. This illustrates the movement of three markers relative to a fourth marker and enables a visualization of the deformation during the test.

## 7.3 EXAMPLE OF A TENSILE TEST FOR A RUBBER SPECIMEN

A strip of vulcanized rubber was tested in tension to provide an example of test results for a uniform material. Specimen dimensions are similar to those used by Rivlin (1951); 7.85 mm wide, 0.81 mm thick, 10 mm gauge length and 50 mm between grips. The deformation at each data point is shown in Figure 7-2 as the relative positions of three of the markers relative to marker #4. The initial and a deformed configuration are noted by dashed lines. The direction of the applied tensile stress is also shown in the figure. Relative movement of the markers reveal a uniform deformation on the material surface.

Both longitudinal and lateral strains are plotted against the applied tensile stress in Figure 7-3. The strain measure used is that given by Equation 6-11. A finite strain

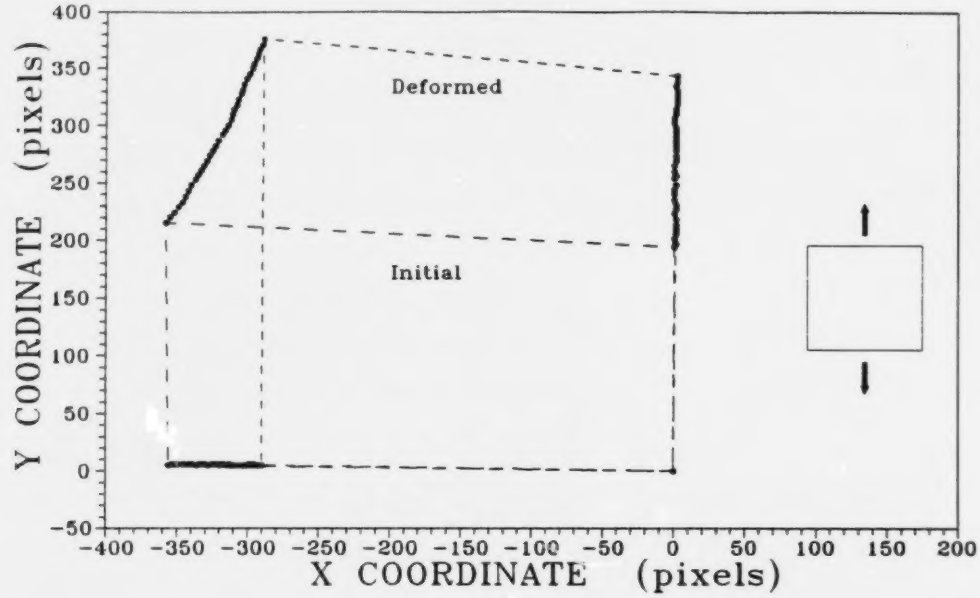

**Figure 7-2:** Surface deformation of the rubber specimen shown by the relative positions of the markers

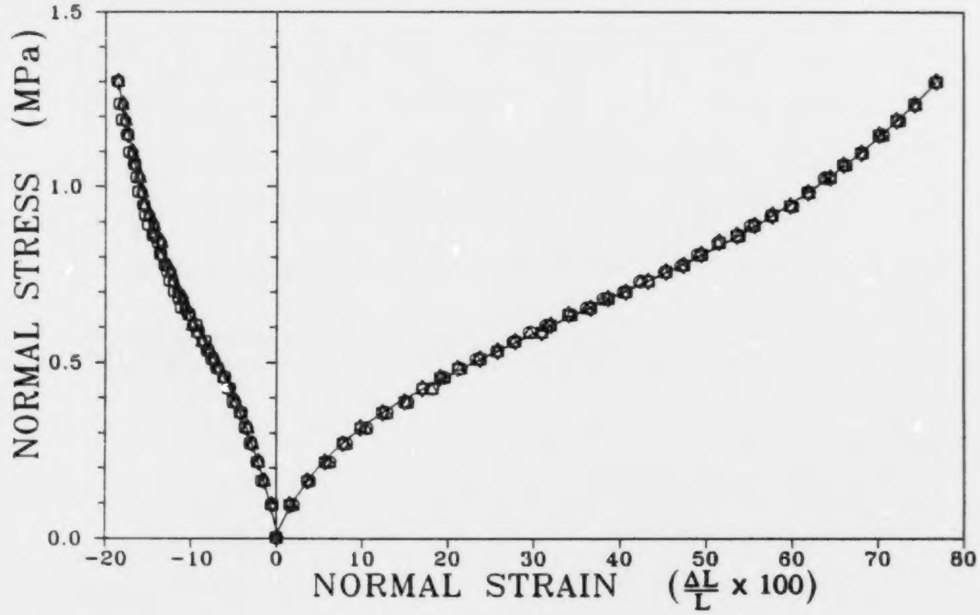

**Figure 7-3:** Stress-strain response for the rubber sample in uniaxial tension showing both longitudinal and lateral strain

measure given by Equation 6-15 could be calculated but these results are not presented. Stress-strain curves for the four regions overlap to form one curve showing that each of the four regions experience the same strain. The shape of the stress-longitudinal strain curves are characteristic of those shown in literature (Rivlin 1951). Experimental results for stress-lateral strain were not found in literature. Lateral strains for rubber testing are normally calculated using the incompressibility condition.

Rubber is normally assumed to be incompressible and for small strains, a Poisson's ratio of 0.5 satisfies this constraint. Poisson's ratio $\nu$, is defined by

$$\nu = \frac{-e_{11}}{e_{22}} \quad or \quad -e_{11} = \nu e_{22} \tag{7-1}$$

where $e_{11}$ and $e_{22}$ are lateral and longitudinal strains given in Equations 6-12 and 6-13, respectively. Poisson's ratio characteristics for the rubber sample are shown in Figure 7-4 where the slope of the curve represents $\nu$ defined in Equation 7-1. The ratio of strains does not remain constant over the duration of the test. With increasing strain, the value of Poisson's ratio decreases. Initially the slope is approximately 0.5 but a more detailed test at low strains would be necessary to determine the value with greater certainty.

Incompressibility or change in volume can be evaluated by examining the condition

$$\lambda_1 \lambda_2 \lambda_3 = 1 \tag{7-2}$$

where $\lambda_i$ are principal stretches. For uniaxial tension in the 2-direction lateral stretches $\lambda_1$ and $\lambda_3$ are assumed to be equal, therefore Equation 7-2 can be written

$$\frac{1}{\lambda_1^2} = \lambda_2 \tag{7-3}$$

Plotting Equation 7-3 shows the incompressibility characteristics of the vulcanized rubber sample during tensile testing (Figure 7-5). The sample does not satisfy the condition of

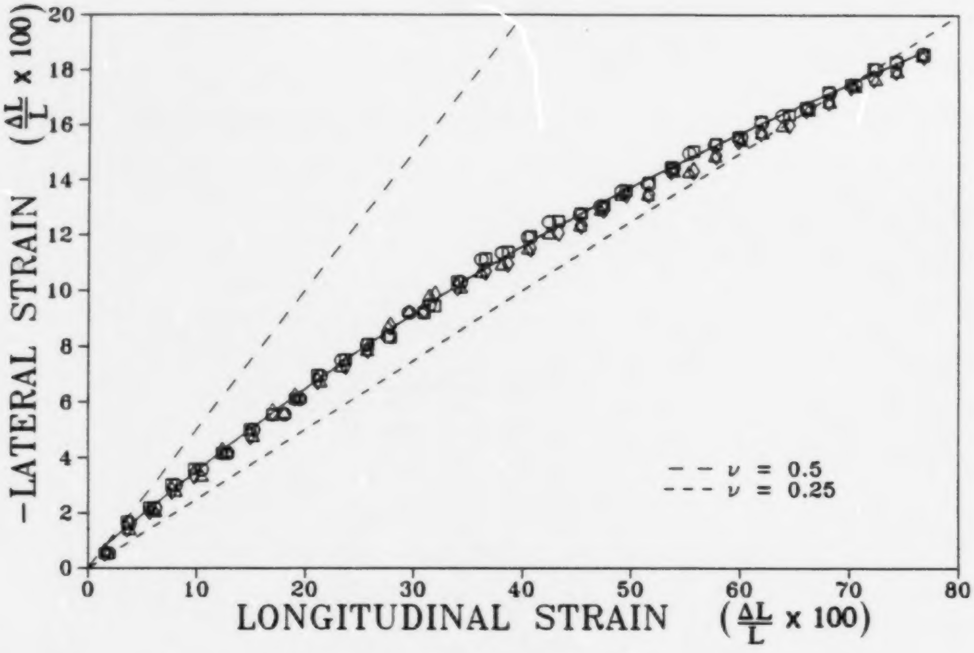

**Figure 7-4:** Poisson's ratio characteristics for the rubber sample

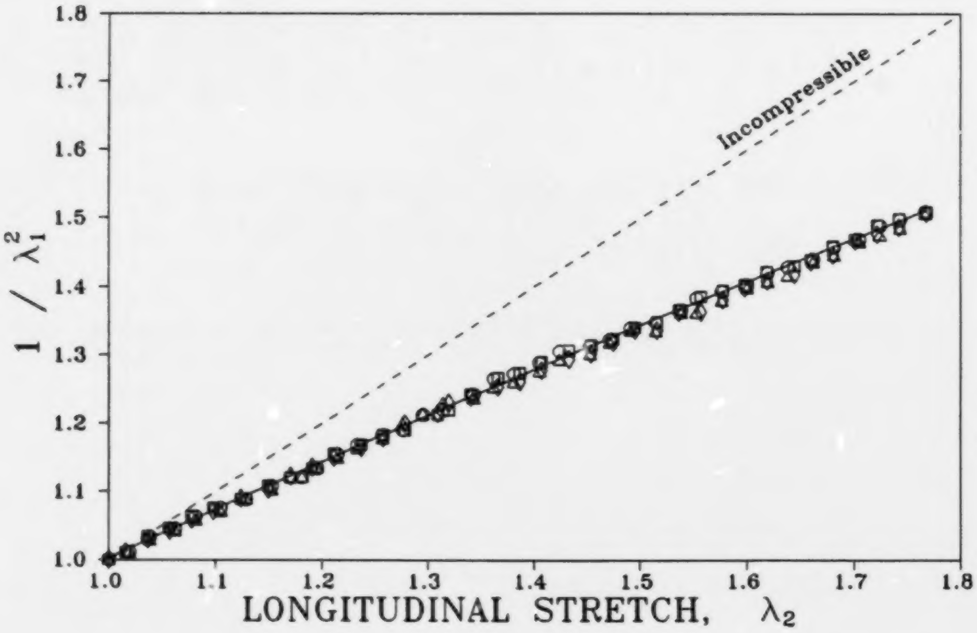

**Figure 7-5:** Volume change characteristics for the rubber sample in uniaxial tension

Equation 7-3 and this may be due to the assumption that $\lambda_1$ and $\lambda_3$ are equal. The two stretches may not be equal due to type of rubber or manufacturing processes such as rolling of the rubber sheet.

## 7.4 EXAMPLE OF A PARALLEL FIBER TEST FOR MENISCUS TISSUE

A sample of bovine meniscus was prepared with a collagen fiber orientation parallel to the axis of the tensile load. From the results of Chapter two, this test characterizes two elastic moduli; $E_L$, the longitudinal elastic modulus and $\nu_{TL}$, Poisson's ratio for tension applied in the longitudinal direction. Verification of the assumption of transverse isotropy can be made by comparing deformations of two sides of the specimen. The two cameras recording specimen deformation are designated the front view and side view.

The test specimen dimensions for the parallel fiber test are a front width of 1.65 mm and a side thickness of 1.45 mm. Relative deformation of the markers is shown in Figure 7-6 with the initial configuration and a deformed configuration noted by dashed lines. The applied stress relative to the fiber orientation is also shown in the figure. The material deformation shows uneven straining on each surface. For a transversely isotropic material, deformations of these surfaces should be the same. From Figure 7-6 it is evident that these surfaces did not deform similarly.

Lateral and longitudinal strains were plotted with the applied tensile stress in Figure 7-7. At a stress of 15 Mpa, the regions on each side of the common edge show longitudinal strains of $\approx 25\%$ while the outside edges of both surfaces experience only $\approx 10\%$ strain. Substantial shearing occurs along the fibers on the side view surface, as seen from the relative deformation of this side shown in Figure 7-6b. Calculations of a tensile modulus are normally based on a tangent to the linear section of the longitudinal strain curve. For this case where uneven strains occur in the different regions, estimates of material stiffness may not be valid. The different regions may not be carrying the same load due to different fiber arrangements and this would make the estimation of tensile stiffness difficult. From Figure 7-7, the tensile modulus $E_L$ based on the regions adjacent to the common edge (regions #2 and #4 on the front surface and #1 and #3 on

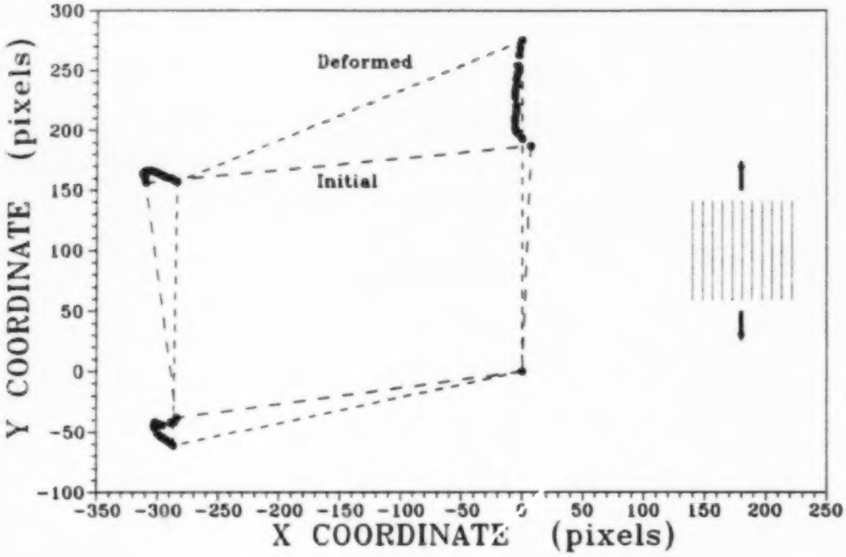

**7-6a:** Front surface

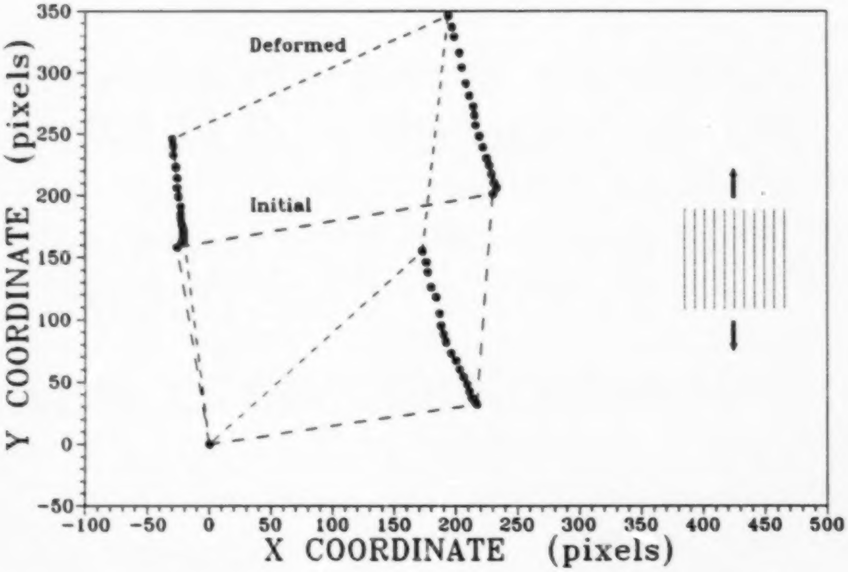

**7-6b:** Side surface

**Figure 7-6:** Surface deformation on two sides of the parallel fiber specimen shown by relative positions of the markers

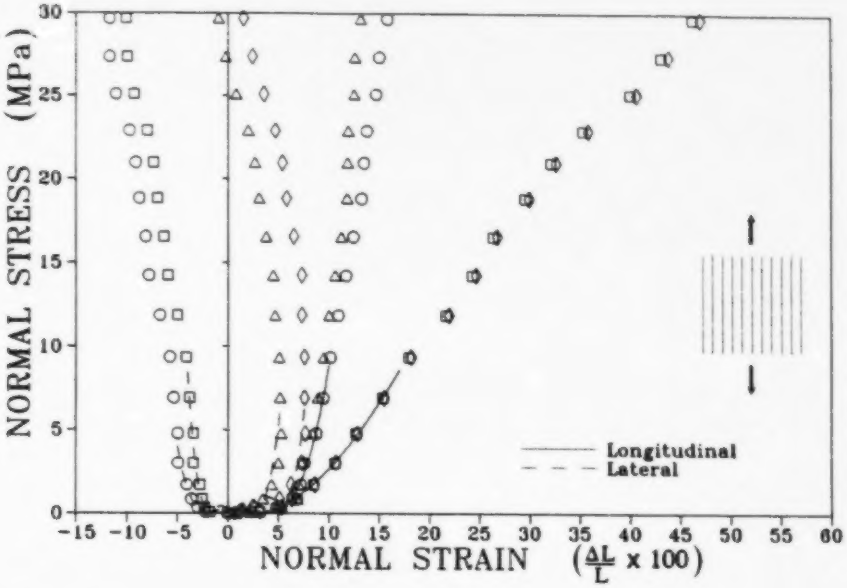

**7-7a:** Front surface

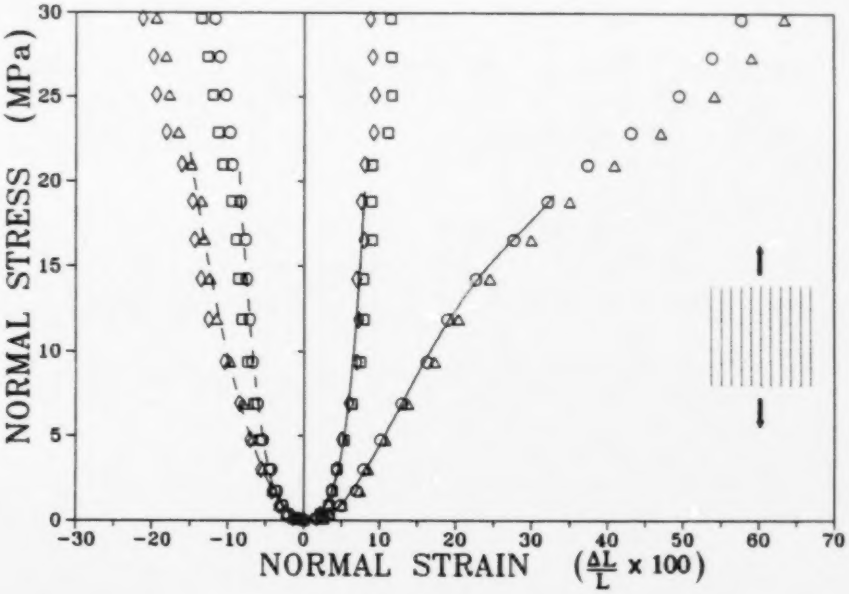

**7-7b:** Side surface

**Figure 7-7:** Stress-strain response on both sides of the parallel fiber specimen showing both longitudinal and lateral strain (symbols defined in Figure 7-1)

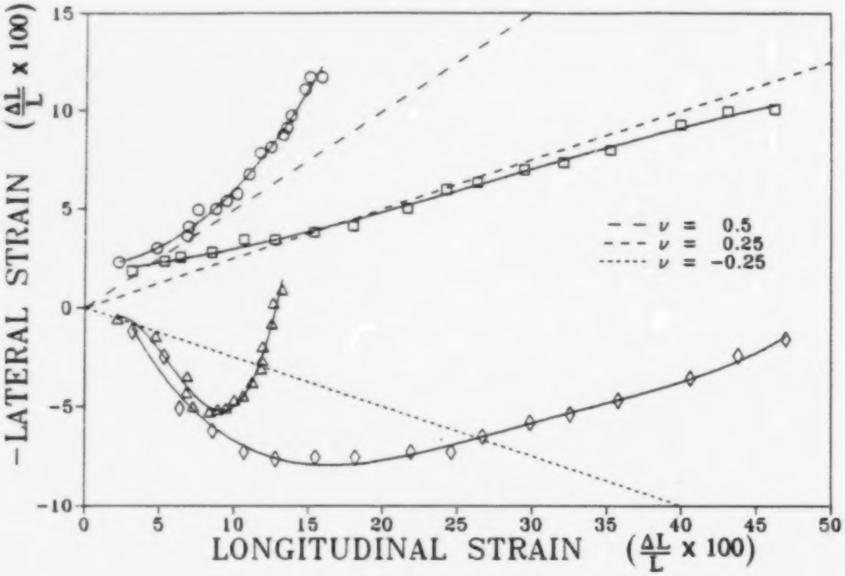

**7-8a:** Front surface

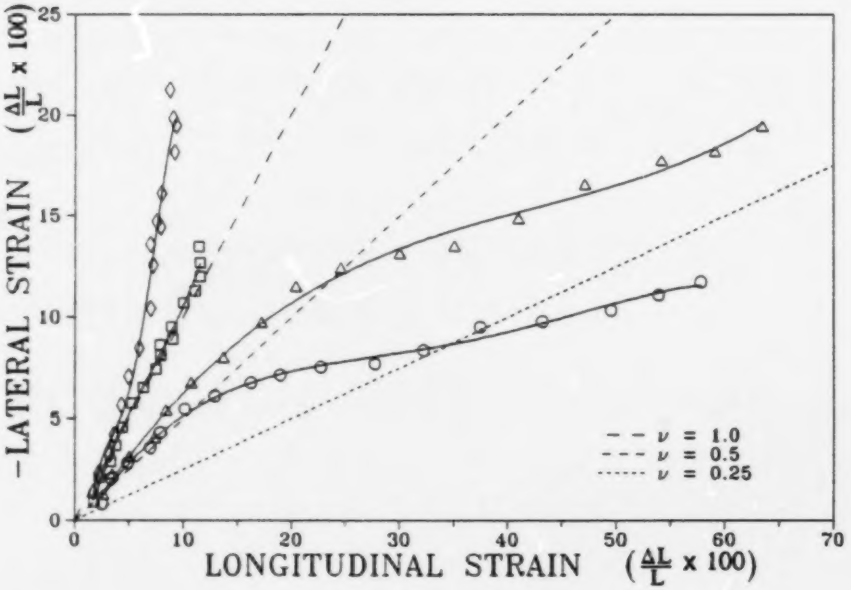

**7-8b:** Side surface

**Figure 7-8:** Poisson's ratio characteristics on two sides of the parallel fiber specimen (symbols defined in Figure 7-1)

the side surface) would be in the range of 80 MPa while the modulus calculated for the low strain regions would be approximately 400 MPa.

Lateral strains on the front surface (Figure 7-7a) show an interesting response that also occurred with other parallel fiber tests. A positive lateral strain occurred during the tensile test. The exact reason for this is not known but the following discussion offers some possibilities.

A demonstration of Poisson's ratio characteristics is shown in Figure 7-8 by plotting Equation 7-1. The slope of the curves indicate Poisson's ratio and this value changes with increasing strain. The positive lateral strain mentioned above results in a negative values for Poisson's ratio in two of the regions on the front surface. This result along with uneven strain on the surfaces would make evaluation of Poisson's ratio characteristics unreliable for this test. For the 5-10% strain range on the side surface, $\nu_{LT}$ is between 0.5 and 1.0.

Specimen volume change could be assessed for Equation 7-2. A three dimensional plot with each stretch represented on an axis would depict the volume change. The uneven strain condition should be investigated further before Poisson's ratio and volume change can be evaluated properly.

## 7.5 EXAMPLE OF A PERPENDICULAR FIBER TEST FOR MENISCUS TISSUE

The perpendicular fiber test was used to evaluate the tensile modulus transverse to the fiber direction, $E_T$, as well as two Poisson's ratios $\nu_{LT}$ and $\nu_{TT}$. A further check on a transversely isotropic model can be made using Equation 2-36. The shear modulus in the isotropic plane, $\mu_T$, can also be evaluated with these test results using Equation 2-35.

Dimensions of the meniscus test specimen for the perpendicular fiber test were a front width of 1.43 mm and a side thickness of 1.63 mm. These two sides have different fiber orientations relative to the applied stress. The fiber orientation and the relative marker positions for the two surfaces are shown in Figure 7-9. Lateral and longitudinal strains for each surface are shown in Figure 7-10. Tensile stiffness $E_T$ was

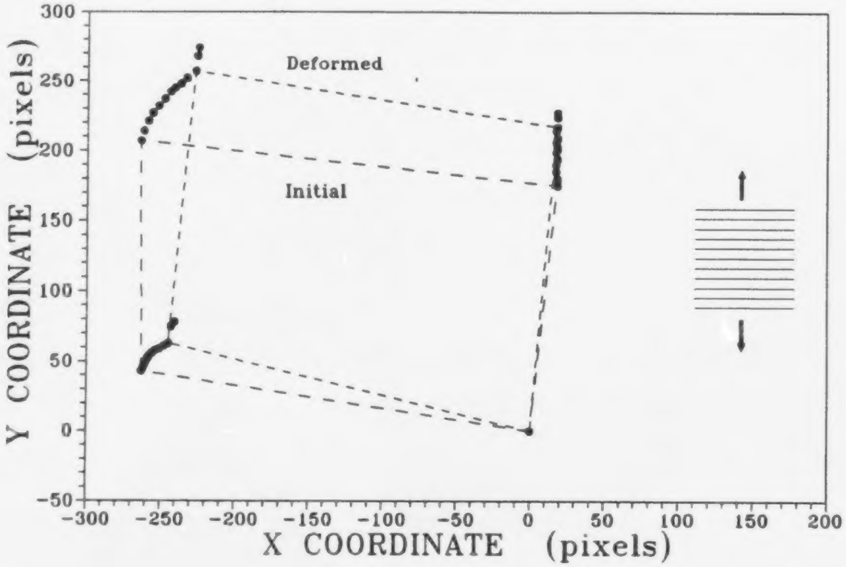

**7-9a:** Front surface

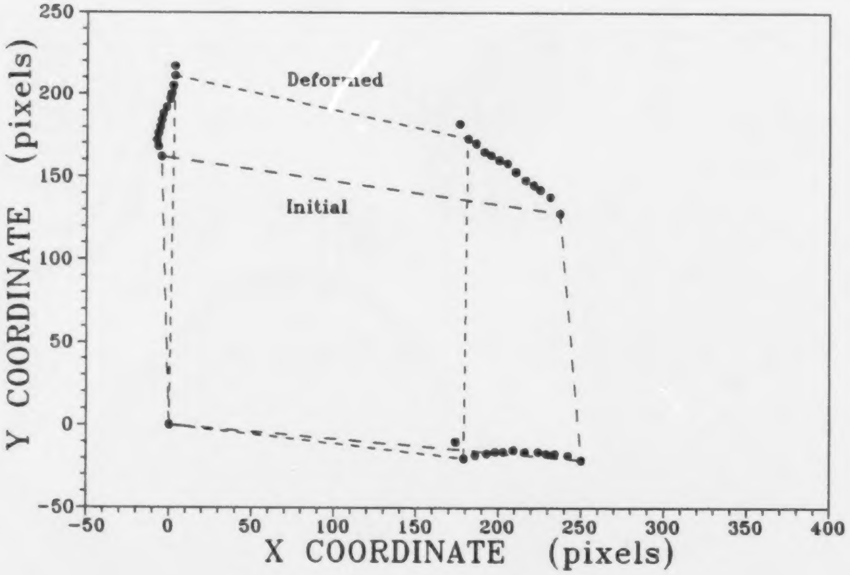

**7-9b:** Side surface

**Figure 7-9:** Surface deformation on two sides of the perpendicular fiber specimen shown by relative positions of the markers

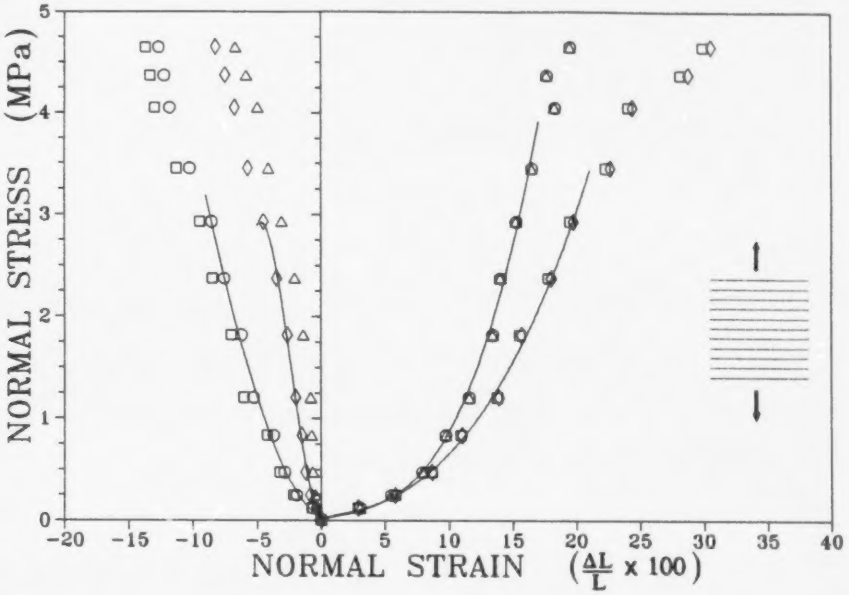

**7-10a:** Front surface

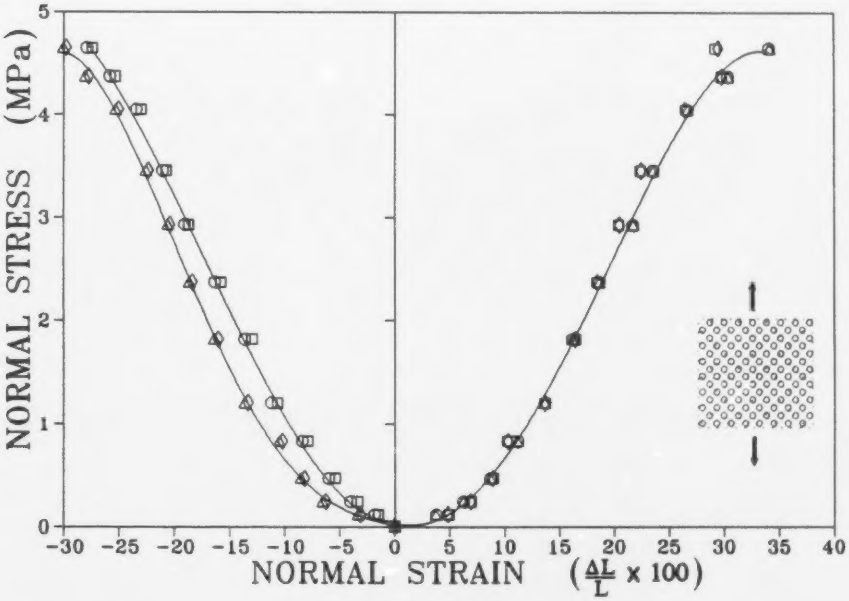

**7-10b:** Side surface

**Figure 7-10:** Stress-strain response on both sides of the perpendicular fiber specimen showing both longitudinal and lateral strain

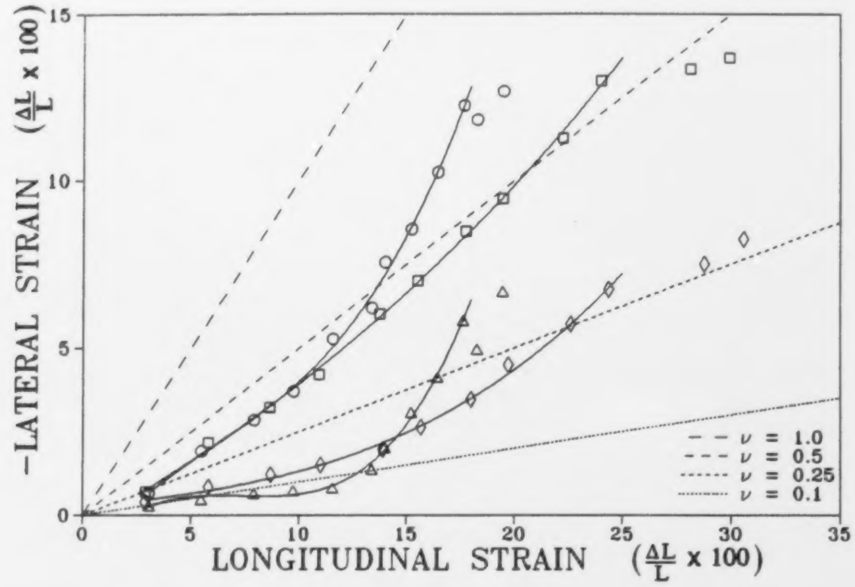

**7-11a:** Front surface

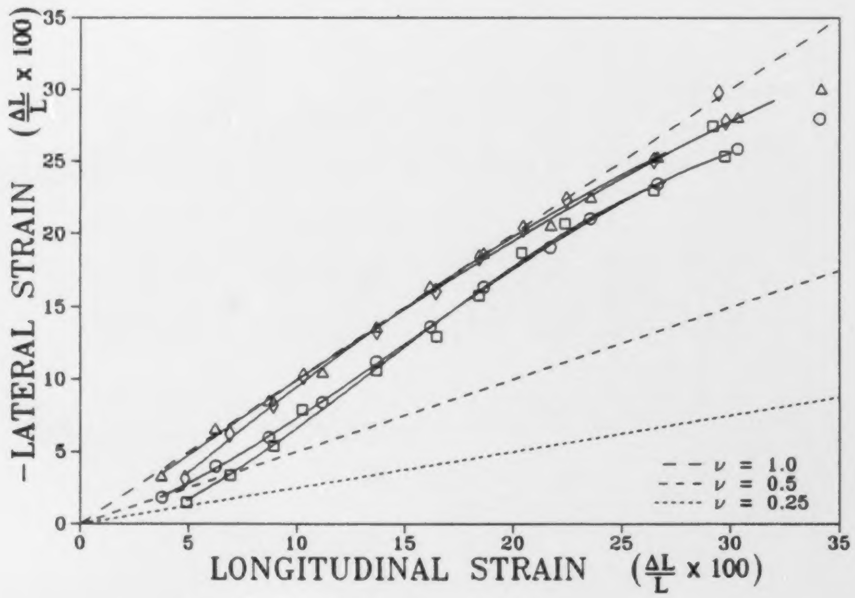

**7-11b:** Side surface

**Figure 7-11:** Poisson's ratio characteristics on two sides of the perpendicular fiber specimen

approximately 20 MPa for this specimen and both surfaces showed comparable longitudinal strains. The side surface showed similar strains in each of the four regions. Poisson's ratio characteristics for the two fiber orientations are shown in Figure 7-11. On the side surface, Poisson's ratio $\nu_{TT}$ had a value of $\approx 1.0$ in the 5-10% strain range. On the front surface for the strain range of 5-10%, Poisson's ratio $\nu_{TL}$ was $\approx 0.1$ for regions #3 and #4 while #1 and #2 showed $\nu_{TL}$ to have a value of $\approx 0.5$. The shear modulus $\mu_T$ was calculated using Equation 2-35 and based on this test $\mu_T \approx 5$ MPa.

## 7.6 EXAMPLE OF AN OFF-AXIS FIBER TEST FOR MENISCUS TISSUE

The off-axis tensile test provides a method for investigating shear behaviour along the collagen fiber bundles. Only the front camera was used to measure the surface deformation. Specimen dimensions were 1.23 mm front width and 0.82 mm side thickness. The specimen was prepared with the fiber orientation inclined at an angle of 30° to the axis of the tensile load. This fiber orientation and the relative marker deformation in a coordinate system aligned with the tensile load axis are shown in Figure 7-12. Figure 7-13 shows the state of stress and relative deformation in a coordinate system aligned with the fiber direction. The shear deformation along the fibers is seen in these figures. A normal stress resulted in a shear strain in a coordinate system aligned with the loading axis as shown in Figure 7-14. In a coordinate system aligned with the fibers, the shear stress acting along the fibers and resulting shear strain are shown in Figure 7-15. "Engineering" shear strain was used as the strain measure so the tangent to the curve corresponds to the value of the shear modulus ($\mu_L$) at that point. Engineering shear strain is two times the value of the tensorial shear strain which is given by Equation 6-14. A third order polynomial was used to fit the curves in Figure 7-15, the shear modulus $\nu_L$ had a value of 0.001 MPa at 20% shear strain. The state of stress is not pure shear and the normal stresses present may have an effect on the shear modulus.

The tensile stiffness of the off-axis fiber specimen was evaluated from Figure 7-15. The tensile modulus for this off-axis orientation was $\approx 25$ MPa.

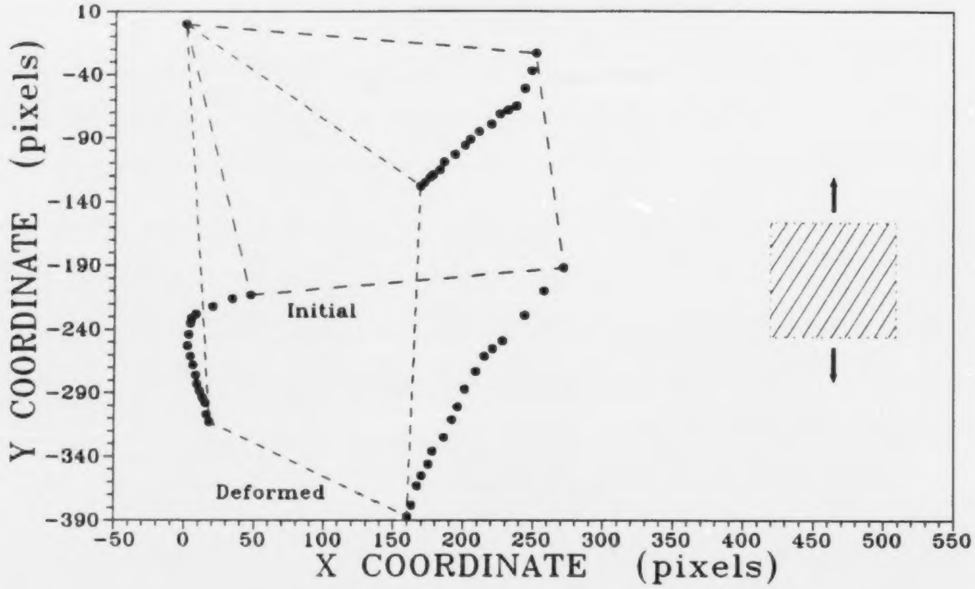

**Figure 7-12:** Surface deformation of the off-axis fiber specimen shown by the relative positions of the markers. Coordinate system is aligned with the tensile loading axis.

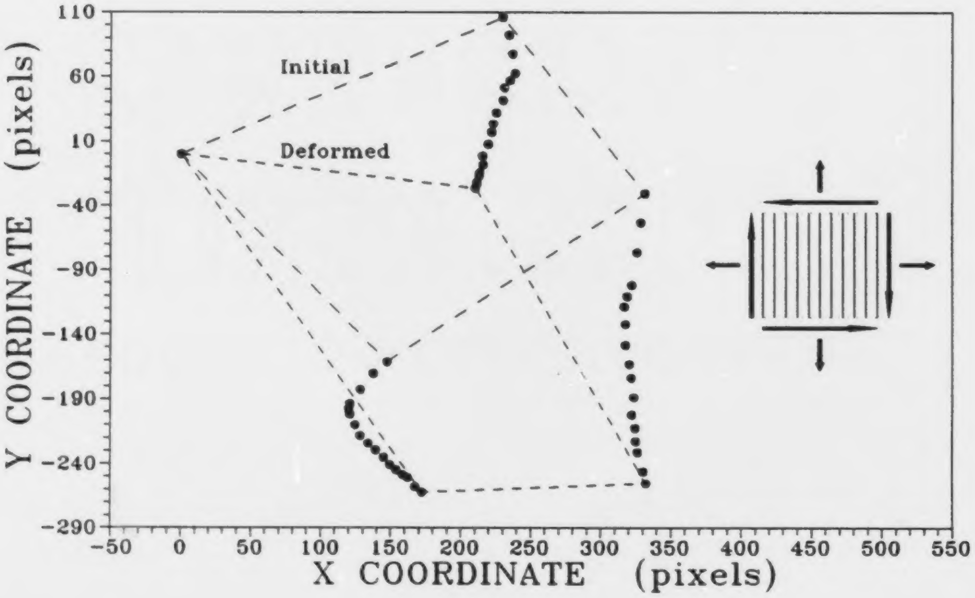

**Figure 7-13:** Surface deformation of the off-axis fiber specimen shown by the relative positions of the markers. Coordinate system is aligned with the fiber direction.

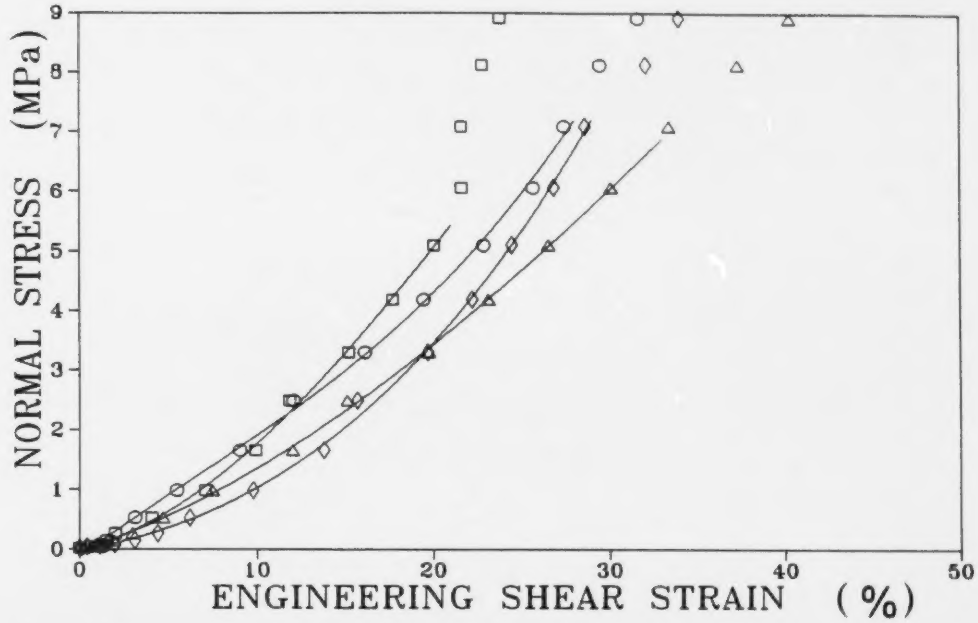

**Figure 7-14:** Shear strain resulting from a tensile stress. Coordinate system is aligned with the tensile loading axis.

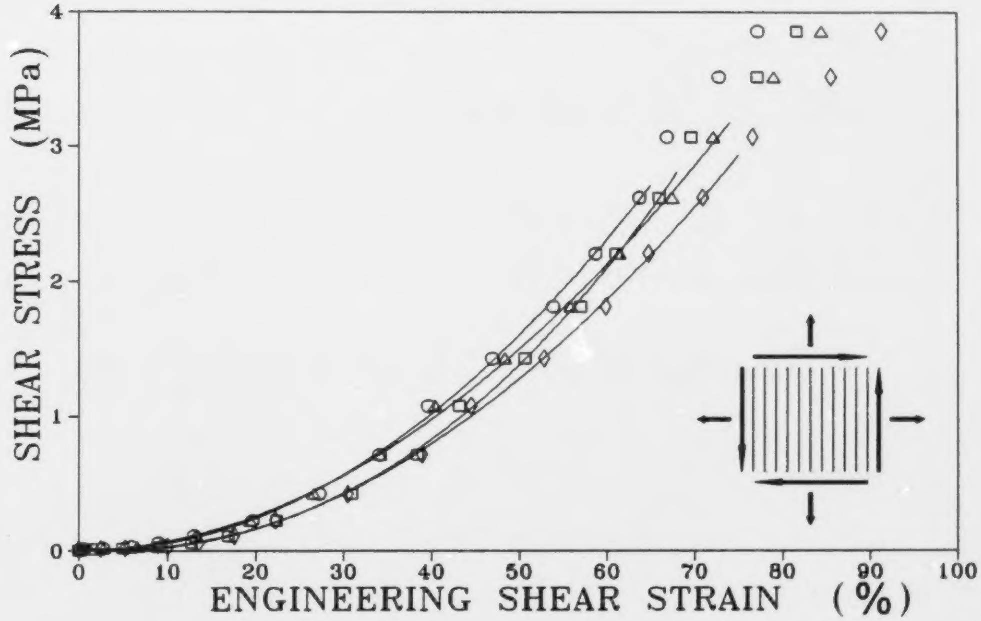

**Figure 7-15:** Shear strain and shear stress for the off-axis specimen. Coordinate system is aligned with the fiber direction.

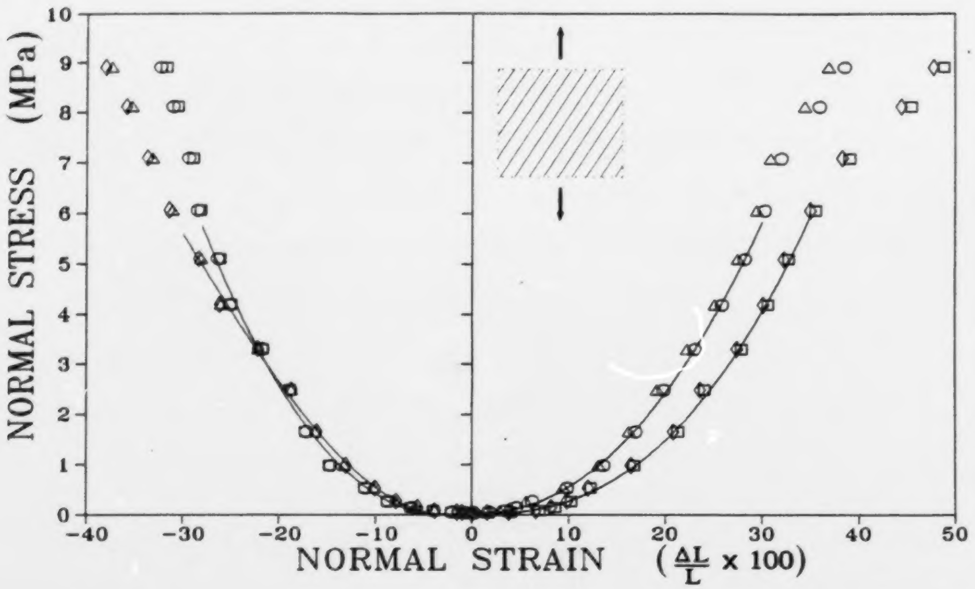

**Figure 7-16:** Stress-strain response for the off-axis fiber specimen showing both longitudinal and lateral normal strain. Coordinate system is aligned with the tensile loading axis.

## 7.7 DISCUSSION OF MENISCUS TEST RESULTS

The meniscus tests shown in the preceding sections are not meant to provide experimental data for meniscus material properties but they are to illustrate results that can be obtained with the test apparatus. Several aspects of the results should be considered.

Meniscus tissue is 70-75% fluid by weight. During a test, fluid is exuded through the specimen surface contributing to the volume loss. When evaluating change in volume, one must consider the change in volume that results from fluid loss as well as that due to the deformation. Fluid loss must also be considered when interpreting Poisson's ratio characteristics. Roth and Mow (1980) point out that Poisson's ratio is defined for a material of constant mass. Therefore, the lateral contraction measured may not be indicative of the solid phase of the meniscus.

Tensile tests have shown that the meniscus tissue exhibits nonhomogeneous deformation on the scale of the marker region. The specimens used in the example tests have a relatively large cross-sectional area (1.5 mm by 1.5 mm) compared with other published meniscus tests ($\approx$1.2 mm by 0.4 mm). The larger cross-sectional area was used in order to obtain a measurement of two lateral strains simultaneously. For this larger cross-section, the surface deformation may not reflect the average specimen deformation, just as two markers on a surface may not be representative of the average deformation on that surface. This can be seen from Figure 7-6a. The stiffness of the specimen determined from the two markers on the left side is quite different than the stiffness determined from the two right side markers. Would this surface deformation look the same if the specimen was 0.4 mm thick instead of 1.4 mm or would the absence of some interior fiber bundles change the surface deformation?

This leads to an important fundamental question regarding tensile tests with prepared specimens. What is the specimen cross-section that best represents the tissue properties? The diameter of the collagen fiber bundles should be considered. Kelly et al (1990) report a collagen fiber bundle diameter of 0.050 - 0.150 mm and Fithian et al (1989) report fiber bundles of 0.2 - 0.4 mm. What thickness should the specimen be in relation to the average bundle diameter to assume a continuum?

The effect of a larger cross-sectional area may be that the specimen contains a greater variation in fiber bundle sizes and orientations. Noyes and Grood (1976) proposed a higher tensile stiffness with smaller cross-sectional areas because the fiber bundles are loaded more uniformly. Nonuniform fiber orientations including the presence of tie fibers perpendicular to the main fiber orientation would likely cause uneven deformation and premature failure of some fibers before the ultimate stress is reached. Thin samples may provide a more uniform deformation but then measurement of deformation on the side surface is difficult. A possibility may be to use thin samples and only measure 2-dimensional deformation on the front surface. Four different specimens would be required for this case. Thin samples would have fiber orientations shown in Figures 7-6, 7-9a and 7-9b and 7-12.

The specimen size may also be related to the presence of positive lateral strains that occur during the parallel fiber test (Figure 7-7a). Possibilities contributing to this phenomenon may include uneven longitudinal strain distribution (Figure 7-7a), shearing of the parallel fiber specimen during tensile testing (Figure 7-6b), specimen shape and/or the presence of randomly oriented fibers in the tissue.

The off-axis tensile test is proposed as an alternative method to study the shear behaviour of the meniscus. Results from this test would also be affected by the presence of random fibers. Skaggs and Mow (1990) showed that a radial tie fiber increased the tensile stiffness of a perpendicular fiber test by a factor of ten. A radial tie fiber perpendicular to the plane of shearing would likely increase the shear resistance of the specimen.

Previous studies on meniscus shear properties have utilized dynamic loading in pure shear by means of torsion (Chern et al 1989) and a shear generator (Anderson et al 1991a). With the off-axis method, tensile stress components are present both perpendicular and parallel to the fiber direction, in addition to the shear stress. The effect of this stress condition should be considered. Chern et al (1989) showed that compression perpendicular to the shear planes increased the shear stiffness. It is not known if tension would lower the shear stiffness. Changing the fiber angle will affect the tensile component and this introduces another question: What is the optimum fiber angle for the off-axis test? The maximum shear stress occurs at 45° but the maximum shear strain occurs at an angle less than 45°.

The above discussion has shown that there are many questions to be considered before a large study is undertaken. Each of the questions could comprise an investigation of its own and present many possibilities for further work.

## 7.8 CHAPTER SUMMARY

Each of the three tests presented for meniscus tissue represent a single example of that particular test. Two dimensional and regional deformation of meniscus specimens has not been reported in literature before and would be a useful addition to the existing information. Some fundamental considerations regarding tests using prepared specimen should also be examined such as the effect of specimen size and shape on the measured material properties. Results obtained from the tests could be improved upon by the recommendations outlined in the next chapter.

# CHAPTER 8

# CONCLUSIONS AND RECOMMENDATIONS

In Chapter Two a linear transversely isotropic model was presented as a starting point for the solid phase of the meniscus. This provides a feasible model because in practice, material constants are determined without difficulty. Three tensile tests, each using a specimen with a distinct fiber orientation, were shown to be sufficient to determine a set of five material constants. Developing a nonlinear model would significantly escalate the problem, both theoretically and experimentally. Applying a linear model to the nonlinear response of the tissue would be more acceptable over a smaller range of strain, for example, the toe part of the stress strain curve (Figure 1-7). In linear finite element models reported to date, a stiffness based on the linear section of the stress-strain curve (Figure 1-7) has been used. A more representative value may be a secant to the curve passing through the origin. The viscoelastic nature of the tissue should also be incorporated in a model to provide a more realistic response. This has been accomplished to date using a biphasic model (Spilker et al 1989,1991) or quasilinear viscoelastic model (Anderson al 1991). Both of these models require the "elastic" properties of the tissue as a parameter in addition to information on the viscoelastic response.

The test machine developed in Chapter Four has possibilities for refinement. The first recommendation would be to replace the existing electric motor with a stepper motor. This would permit computer control of the crosshead motion permitting cyclic loading and feedback to the load sensing device. This would increase the versatility of the apparatus.

The test environment of the specimen is controlled by means of a ultrasonic humidifier producing a high humidity airstream. This was shown to be an effective method for preventing specimen moisture loss. Specimen environment should also include a means of temperature control. This could be accomplished by incorporating temperature control of the humidifier water tank and determining a tank temperature that will provide the required mist temperature.

The method of measuring specimen surface deformation was outlined in Chapter Five. An immediate recommendation before a detailed study is undertaken is to have the image capture board sampling directly from the cameras. Currently the test is recorded on video tape and later replayed into the image capture hardware. Direct sampling from the camera would eliminate any noise introduced by the tape recording and also eliminate the need for manual selection of images noted by the LED light source (Section 5.4.2). Another possibility for facilitating data collection would be to incorporate computer recognition of each marker and subsequent calculation of the marker centroid. This approach has been reported by Hoffman and Grigg (1984) and Humphrey (1987) and provides a large area for further study. Immediate strain calculation during a test would provide feedback for a programmable system and also eliminate the manual process now necessary.

Two charge coupled device (CCD) cameras were used as part of the measurement system, each with an image device containing a 694 x 491 array of sensing elements. A camera with a greater concentration of image elements would provide the possibility for higher resolution measurements. This would also require an image capture board with increased resolution. Benefits from higher resolution equipment would rely on the ability to identify the specimen markers. This in turn depends on specimen marker selection, lighting, lens configurations and magnification method. There are numerus possibilities for improvement in this area with the goal of reducing the uncertainty associated with the marker position. A noncontacting measurement device with improved performance has great potential.

The test results presented in Chapter Seven are not meant to provide values for meniscus material properties or assess the validity of a transversely isotropic model. Rather they represent an example of the types of proposed tests that could be conducted in a study. The off-axis tensile test is an alternative method to look at shear properties utilizing a tensile test. The deformation measurement method provides two dimensional strains and enables the calculation of shear strain along the fibers. This results in calculation of shear response along the fibers up to the point of failure, a case that has not been reported before.

The example tests do raise some important questions regarding tests using prepared tensile specimens. The cross-sectional area and relative dimensions of the test specimen and their effect on material properties should be considered before extensive testing is carried out. What specimen size relative to fiber bundle size best represents the tissue response? For an irregular shaped structure like the meniscus, are there alternative testing methods to determine material response rather than prepared tensile specimens?

Before a study of material properties is undertaken, one should keep in mind what the results will be used for. If numerical modelling is a goal then how sensitive are the results of the model to material properties? Maybe the effect of shape, boundary constraints and loading conditions have a far greater effect on the response of the model than material properties do and these should be areas of focus. If the properties from a healed (sutured, allograph, autograph) meniscus are to be compared to those of normal meniscus, then how does one account for variability in properties due to location, donor etc?

This thesis could be considered a first iteration in a soft tissue testing system. Recommendations and improvements are numerous, but initial ideas and equipment are in place and many possibilities exist. With many unanswered questions by all researchers, continued work in the area the area of soft tissues will be a challenging and interesting field for some time.

# REFERENCES

Adams A (1980): *The Camera.* Boston, New York Graphic Society.

Ahmed AM, Burke DL (1983): In-vitro measurement of static pressure distribution in synovial joints-Part 1: Tibial surface of the knee. *J Biomech Eng* 105:216-225.

Anderson DR, Kwan MK, Woo SL-Y, Akeson, Danzig LA, Gershuni DH (1990): Viscoelastic shear properties of equine meniscal cartilage. *Trans Orthop Res Soc* 15:247.

Anderson DR, Woo SL-Y, Kwan MK, Gershuni DH (1991a): Viscoelastic shear properties of the equine medial meniscus *J Orthop Res* 9:550-558.

Anderson DR, Gershuni DH, Nakhostine M, Melideo M, Petras S, Danzig LA (1991b): The effects of non-weight bearing and limited motion om the tensile behavior of the meniscus. *Trans Orthop Res Soc* 16:372.

Arms S, Boyle J, Johnson R, Pope M (1983): Strain measurement in the medial collateral ligament: An autopsy study. *J Biomech* 16:491-496.

Arnoczky SP, McDevitt CA, Schmidt MB, Mow VC, Warren RK (1988): The effect of cryopreservation on canine menisci. A biochemical, morphological and biomechanical evaluation. *J Orthop Res* 6:1-12.

Aspden RM (1985): A model for the function and failure of the meniscus. *Eng Med* 14:119-122.

Aspden RM, Larsson T, Svensson, Heinegård D (1991): Computer-controlled mechanical testing machine for small samples of biological viscoelastic materials. *J Biomed Eng* 13:521-525.

Aspden RM, Yarker YE, Hukins DWL (1985): Collagen orientations in the meniscus of the knee joint. *J Anat* 140:371-381.

Aspden RM, Gleave BD, Hukins DWL (1988): Dimensional measurements on images from video camera or cassette recorder using a BBC microcomputer. *J Biomed Eng* 10:291-292.

Athanasiou KA, Rosenwasser MP, Buckwalter JA, Malinin TI, Mow VC (1991): Interspecies comparisons of in situ intrinsic mechanical properties of distal femoral cartilage. *J Orthop Res* 9:330-340.

Beynnon BD, Pope MH, Fleming BC, Howe JG, Johnson RJ, Erickson AR, Wertheimer CM, Nichols C (1989): An in-vivo study of ACL strain biomechanics in the normal knee. *Trans Orthop Res Soc* 14:324.

Brown GA, Jevsevar DS, Rowell D (1991): X-ray stereophotogrammetric measurement of meniscal circumferential strains. *Trans Orthop Res Soc* 16:295.

Bullough PG, Munuera L, Murphy J, Weinstein AM (1970): The strength of the menisci of the knee as it relates to their fine structure. *J Bone Joint Surg* 52B:564-570.

Butler DL, Sheh MY, Stouffer DC, Samaranayake VA, Levy MS (1990): Surface strain variation in human patellar tendon and knee cruciate ligaments. *J Biomech Eng* 112:38-45.

Butler DL, Grood ES, Noyes FR, Zernicke RF, Brackett K (1984): Effects of structure and strain measurement technique on the material properties of young human tendons and fascia. *J Biomech* 17:579-596.

Butler DL, Noyes FR, Grood ES (1978): Measurement of the mechanical properties of ligaments. In: *CRC Handbook of Bioengineering and Biology. Section B, Vol I*, Feinberg BN, Fleming DG (eds), Clevland, CRC Press pp 279-314.

Chern KY, Zhu WB, Mow VC (1989): Anisotropic viscoelastic shear properties of meniscus. *Adv Bioeng WAM ASME* 15:105

Chern KY, Zhu WB, Kelly MA, Mow VC (1990): Anisotropic shear properties of bovine meniscus. *Trans Orthop Res Soc* 15:246.

Cox JS, Nye CE, Schaefer WW, Woodstien IJ (1975): The degenerative effects of partial and total resection of the medial meniscus in dog knees. *Clin Orthop Rel Res* 109;178-183.

Edwards RG, Lafferty JF, Lange KO (1970): Ligament strain in human knee joint. *J Basic Eng* 92:131-136.

Fairbank TJ (1948): Knee joint changes after meniscectomy. *J Bone Joint Surg* 30B:664-670.

Favenesi JA, Schaffer JC, Mow VC (1983): Biphasic mechanical properties of knee meniscus. *Trans Orthop Res Soc* 8:57.

Fithian DC, Schmidt MB, Ratcliffe A, Mow VC (1989): Human meniscus tensile properties: Regional variation and biochemical correlation. *Trans Orthop Res Soc* 14:205.

Fuchshuber P (1987): *An experimental and numerical analysis of orthodontic T springs.* M Sc thesis, Dept of Mech Eng, Uni of Alberta.

Fukubayashi T, Kurosawa H (1980): The contact area and pressure distribution pattern of the knee. A study of normal and osteoarthritic knee joints. *Acta Orthop Scand* 51:871-879.

Fung YC (1981): *Biomechanics: Mechanical Properties of Living Tissues*. New York, Springer-Verlag.

Fung YC (1967): Elasticity of soft tissues in simple elongation. *Am J Physiol* 213:1532-1544.

Fung YC (1990): *Biomechanics: motion, flow, stress, growth.* New York, Springer-Verlag.

Galante JO (1967): Tensile properties of the human annulus fibrosus. *Acta Orthop Scand*, Supplement 100.

Ghosh P, Taylor TKF (1987): The knee joint meniscus. A fibrocartilage of some distinction. *Clin Orthop Rel Res* 224:52-63.

Goertzen D, Budney D, Cinats J, Steigmann D (1991): An apparatus for in vitro testing of soft tissue. *Proc 17th Canadian Medical and Biological Engineering Society Conference*. pp 29-30.

Hasberry S, Pearcy MJ (1986): Temperature dependence of the tensile properties of interspinous ligaments of sheep. *J Biomed Eng* 8:62-66.

Haut RC (1983): Age dependent influence of strain rate on the tensile failure of rat-tail tendon. *J Biomech Eng* 105:236-299.

Hefzy MS, Grood ES, Zoghi M (1987): An axisymmetric finite element model of the meniscus. *Adv Bioeng WAM ASME* 13:51-52

Hoffman AH, Grigg P (1984): A method for measuring strains in soft tissue. *J Biomech* 17:795-800.

Hoffman AH, Grigg P, Fogarty KE, Burgess SM (1981): Development of a finite element based method for directly determining strains in soft tissue. In: *Bioengineering Proceedings of the 9th NE Conference*. Welkowitz W (ed), New York, Pergamon Press pp 329-332.

Humphrey JD, Strumpf RK, Yin FCP (1990): Determination of a constitutive relation for passive myocardium:II. Parameter estimation. *J Biomech Eng* 112:340-346

Humphrey JD, Vawter DL, Yito RP (1987): Quantification of strains in biaxially tested soft tissues. *J Biomech* 20:59-65.

Iaconis F, Steindler R, Marinozzi G (1987): Measurement of cross-sectional area of collagen structures (knee ligaments) by means of an optical method. *J Biomech* 20:1003-1010.

Jaunzemis W (1967): *Continuum Mechanics.*, New York, Macmillan.

Johnson RJ, Kettlekamp DB Clark W, Leaverton P (1974): Factors affecting late results after meniscectomy. *J Bone Joint Surg* 56A:719-729.

Kapandji IA (1987): *The Physiology of the Joints. Volume 2: Lower Limb* (5th ed), Edinburgh, Churchill Livingstone.

Kelly MA, Fithian DC, Chern KY, Mow VC (1990): Structure and function of the meniscus: Basic and clinical implications. In: *Biomechanics of Diarthrodial Joints. Volume I*, Mow VC, Ratcliffe A, Woo SL-Y (eds), New York, Springer-Verlag, pp 191-211.

Ker RF (1980): Small scale tensile tests. *Symp Soc Exp Biol* 34:487-488.

Knauss WG, Kenner VH (1981): A technique to measure lateral contraction in small biological specimens. *J Biomech* 14:569-575.

Krause WR, Pope MH, Johnson RJ, Wilder DG (1976): Mechanical changes in the knee after meniscectomy. *J Bone Joint Surg* 58A:599-604

Krause WR, Burdette WA, Loughran TP (1989): Properties of the normal and repaired canine meniscus. *Trans Orthop Res Soc* 14:207.

Lam TC, Thomas CG, Shrive NG, Frank CD, Sabiston CP (1990): The effects of temperature on the viscoelastic properties of the rabbit medial collateral ligament. *J Biomech Eng* 112:147-152.

Lanir Y, Fung YC (1974): Two dimensional properties of rabbit skin - I. Experimental system. *J Biomech* 7:29-34.

Lee TQ, Woo SL-Y (1988): A new method for determining cross-sectional shape and area of soft tissues. *J Biomech Eng* 110:110-114.

Levy IM, Torzilli PA, Warren RF (1982): The effect of medial meniscectomy on anterior - posterior motion of the knee. *J Bone Joint Surg* 64A:883-888.

Mabuchi K, Hayatsuk K, Fujie H (1991): Stiffness of canine stifle joint ligaments at relatively high rates of elongation. *J Biomech Eng* 113:404-409.

Manak JJ (1980): The two-dimensional in vitro passive stress-strain elasticity relationships for the steer thoracic aorta blood vessel tissue. *J Biomech* 13:637-646.

Markolf KL, Mensch JS, Amstutz HC (1976): Stiffness and laxity of the knee - Contributions of the supporting structures. A quantitative in vitro study. *J Bone Joint Surg* 58A:583-594.

Mathur PD, McDonald JR, Ghormley RK (1949): A study of the tensile strength of the menisci of the knee. *J Bone Joint Surg* 31A:650-654.

Meglan D, Berme N, Zuelzer W (1988): On construction circuitry and properties of liquid metal strain gauges. *J Biomech* 21:681-685.

Mow VC, Kuei SC, Lai WM, Armstrong CG (1980): Biphasic creep and stress relaxation of articular cartilage in compression: Theory and experiments. *J Biomech Eng* 102:73-84.

Mow VC, Hou JS, Owens JM, Ratcliffe A (1990): Biphasic and quasilinear viscoelastic theories for hydrated soft tissues. In: *Biomechanics of Diarthrodial Joints. Volume I*, Mow VC, Ratcliffe A, Woo SL-Y (eds), New York, Springer-Verlag, pp 215-260.

Neumann P, Keller T, Ekström L, Perry L Hansson T (1991): Vertebral bone mineral content - A predictor of tensile strain properties of lumbar anterior longitudinal ligament. *Trans Orthop Res Soc* 16:20.

Noyes FR, Grood ES (1976): The strength of the anterior cruciate ligament in humans and rhesus monkeys. Age and species related changes. *J Bone Joint Surg* 58A:1074-1082.

Omens JH, Fung YC (1990): Residual strain in the rat left ventricle. *Circul Res* 66:37-45.

Proctor CS, Schmidt MB, Whipple RR, Kelly MA, Mow VC (1989): Material properties of the normal medial bovine meniscus. *J Orthop Res* 7:771-782.

Riemersa DJ, Schamhardt HC (1982): The cyro-jaw, a clamp designed for in vitro rheology studies of horse digital flexor tendons. *J Biomech* 15:619-620.

Rivlin RS, Saunders DW (1951): Large elastic deformations of isotropic materials. VII Experiments on the deformation of rubber. *Phil Trans R Soc Lond* A243:251-288.

Roth V, Mow VC (1980): The intrinsic tensile behavior of the matrix of bovine articular cartilage and its variation with age. *J Bone Joint Surg* 62A:1102-1116.

Sabiston P, Frank C, Lam T, Shrive N (1990): Transplantation of the rabbit medial collateral ligament. I. Biomechanical evaluation of fresh autografts. *J Orthop Res* 8:35-45.

Sauren AAHJ, Huson A, Schouten RY (1984): An axisymmetric finite element analysis of the mechanical function of the meniscus. *Int J Sports Med* 5:93-95.

Schwerdt H, Constantinesco A, Chambron J (1980): Dynamic viscoelastic behaviour of the human tendon in vitro. *J Biomech* 13:913-922.

Seedhom BB, Hargreaves DJ (1979): Transmission of load in the knee joint with special reference to the role of the menisci. Part II. Experimental results, discussion and conclusions. *Eng Med* 8:220-228.

Shrive NG, O'Connor JJ, Goodfellow JW (1978): Load bearing in the knee joint. *Clin Orthop Rel Res* 131:279-287.

Shrive NG, Lam TC, Damson E, Frank CB (1988): A new method for measuring the cross-sectional area of connective tissue structures. *J Biomech Eng* 110;104-108.

Shrive NG (1991): Measuring strain in soft tissues. In: *The Workshop for Strain Measurement in Biomechanics*. Canadian Medical and Biological Engineering Society Conference pp 87-96.

Sikoryn TA, Aspden RM, Hukins DWL (1988) Simple computer controlled apparatus for in vitro mechanical testing of connective tissues. *J Biomed Eng* 10:357-359.

Skaggs DL, Mow Vc (1990): Function of radial tie fibers in the meniscus. *Trans Orthop Res Soc* 15:248.

Smillie IS (1970): *Injuries of the Knee Joint (4th ed)*. Edinburgh, Livingstone.

Sommerlath K, Gillquist J (1992): The effect of a meniscal prosthesis on knee biomechanics and cartilage. An experimental study in rabbits. *Am J Sports Med* 20:73-81.

Spencer AJM (1980): *Continuum Mechanics*. London, Longman.

Spencer AJM (1984): Constitutive theory for strongly anisotropic solids. In: *Continuum Theory of the Mechanics of Fibre-Reinforced Composite Materials*. Spencer AJM (ed), Wien, Springer-Verlag.

Spilker RL, Maxian TA, Mow VC (1989): A fibrous biphasic anisotropic finite element model of the meniscus. *Trans Orthop Res Soc* 15:244.

Spilker RL, Donzelli PS, Mow VC (1991): A finite element model of meniscus response to a sudden overload. *Trans Orthop Res Soc* 17:293.

Stokes I, Greenapple DM (1985): Measurement of surface deformation of soft tissue. *J Biomech* 18:1-7.

Talman E, Smith W, Boughner D. (1991): A device for measurement of heart valve tissue shear modulus. *Proc 17th Canadian Medical and Biological Engineering Society Conference*. pp 15-16.

Tapper EM, Hoover NW (1969): Late results after meniscectomy. *J Bone Joint Surg* 51A:517-526.

Taylor JR (1982): *An introduction to error analysis: The study of uncertainties in physical measurements.* Mill Valley, United Science Books.

Thompson WO, Fu FH, Thaete FL, Dye SF (1990): Assessment of tibial meniscal kinematics by 3D magnetic resonance imaging. *Trans Orthop Res Soc* 15:245.

Tissakht M, Ahmed AM (1990): Effect of tibial axial rotation on knee meniscal stress: A finite element study. *Trans Orthop Res Soc* 16:243.

Tissakht M, Farinaccio R, Ahmed AM (1989): Effect of ligament attachments on the response of the knee menisci in compression & torsion: A finite element study. *Trans Orthop Res Soc* 15:203.

Tissakht M, Marchand F, Ahmed AH (1991): Non-linear finite element analysis of the knee menisci: A composite fiber-reinforced model. *Trans Orthop Res Soc* 17:294.

Tkaczuk H. (1968): Tensile properties of human lumbar longitudinal ligaments. *Acta Orthop Scand*, Supplement 115

To SYC, Kwan MK, Woo SL-Y (1988) Simultaneous measurements of strains on two surfaces of tendons and ligaments. *J Biomech* 21:511-514.

Uezaki N, Kobayashi A, Matsushige K (1979): The viscoelastic properties of the human semilunar cartilage. *J Biomech* 12:65-73.

Vesely I, Boughner DR (1985): A multipurpose tissue bending machine. *J Biomech* 18:511-513.

Viidik A (1990): Structure and function of normal and healing tendons and ligaments. In: *Biomechanics of Diarthrodial Joints. Volume I*, Mow VC, Ratcliffe A, Woo SL-Y (eds), New York, Springer-Verlag, pp 3-38.

Viidik A (1979): Biomechanical behaviour of soft connective tissues. In: *Progress in Biomechanics*. Akkas N (ed), Alphen aan den Rijn, Sijthoff & Nordhoff, pp 75-113.

Viidik A (1987): Biomechanics of tendons and other soft tissues - testing methods and structure-function interdependence. In: *Biomechanics: Basic and Applied Research*. Dordrecht, Martinus Nijhoff, pp 59-72.

Vito RP (1980): The mechanical properties of soft tissues - I: A mechanical system for biaxial testing. *J Biomech* 13:947-950.

Vogel S, Papanicolaou MN (1983): A constant stress creep testing machine. *J Biomech* 16:153-156.

Voloshin AS, Wosk J (1983): Shock absorbtion of meniscectomized and painful knees. A comparative in vivo study. *J Biomed Eng* 5:157-161.

Vossoughi J, Vaishnav RN (1980) A uniaxial test system to study mechanical properties of the vascular tissue. *Adv Bioeng WAM ASME* pp 313-316.

Waldman IK (1986): In-vivo measurement of strains in myocardium. In: *Frontiers in Biomechanics*. Schmid-Schönbein GW, Woo SL-Y, Zweifach BW (eds), New York, Springer-Verlag.

Walker LB, Harris EH, Benedict JV (1964): Stress-strain relationship in Human Cadaveric plantaris tendon: A preliminary study. *Med Elect Biol Eng* 2:31-38.

Walker PS, Erkman MJ (1975): The role of the menisci in force transmission across the knee. *Clin Orthop Rel Res* 109:184-192.

Whipple R, Wirth CR, Mow VC (1984): Mechanical properties of the meniscus. *Adv Bioeng WAM ASME* 10:32-33.

Whipple RR, Wirth CR, Mow VC (1985): Anisotropic and zonal variations in the tensile properties of the meniscus. *Trans Orthop Res Soc* 10:367.

Woo SL-Y, Weiss JA, MacKenna DA (1990): Biomechanics and morphology of the medial collateral and anterior cruciate ligaments. In: *Biomechanics of Diarthrodial Joints. Volume I*, Mow VC, Ratcliffe A, Woo SL-Y (eds), New York, Springer-Verlag, pp 63-104.

Woo SL-Y, Orlando CA, Camp JF, Akeson WH (1986): Effects of post-mortem storage on ligament tensile behavior. *J Biomech* 19:399-404.

Woo SL-Y, Gomez MA, Endo CM, Akeson WH (1981): On the measurement of ligament strains and strain distribution. *Biorheology* 18:139-140.

Woo SL-Y, Gomez MA, Amiel D, Ritter MA, Gelberman RH, Akeson WH (1981): The effects of exercise on the biomechanical and biochemical properties of swine digital flexor tendons. *J Biomech Eng* 103:51-56.

Woo SL-Y, Lee TQ, Gomez MA, Sato S, Field FP (1987): Temperature dependent behavior of the canine medial collateral ligament. *J Biomech Eng* 109:68-71.

Woo SL-Y, Lubock P, Gomez MA, Jemmot GF, Kuei SC, Akeson WH (1979): Large deformational nonhomogeneous and directional properties of articular cartilage in uniaxial tension. *J Biomech* 12:437-446.

Wu H-C, Yao R-F (1976): Mechanical behaviour of the human annulus fibrosus. *J Biomech* 9:1-7.

Yin FCP, Tompkins WR, Peterson KL, Intaglietta M (1972): A video-dimension analyzer. *IEEE Trans Biomed Eng* 19:376-381.

Zernicke RF, Butler DL, Grood ES, Hefzy MS (1984): Strain topography of human tendon and fascia. *J Biomech Eng* 106:177-180.

# APPENDIX A

# MATRIX REPRESENTATION OF STIFFNESS TENSOR COMPONENTS

Representation of the fourth order stiffness tensor by a 6x6 matrix format is shown in this appendix. The general constitutive relation for a linearly elastic solid is

$$\sigma_{ij} = C_{ijkl} e_{kl} \qquad \text{A-1}$$

Expanding Equation A-1 by summing on k and l yields

$$\begin{aligned} \sigma_{ij} &= C_{ijk1} e_{k1} + C_{ijk2} e_{k2} + C_{ijk3} e_{k3} \\ &= C_{ij11} e_{11} + C_{ij21} e_{21} + C_{ij31} e_{31} + C_{ij12} e_{12} + C_{ij22} e_{22} + C_{ij32} e_{32} + \\ &\quad C_{ij13} e_{13} + C_{ij23} e_{23} + C_{ij33} e_{33} \end{aligned} \qquad \text{A-2}$$

Symmetry of both the stiffness tensor and the strain tensor with respect to the k and l indices ($C_{ijkl} = C_{ijlk}$ and $e_{kl} = e_{lk}$) allow terms to be combined

$$C_{ij21} e_{21} + C_{ij12} e_{12} = 2 C_{ij12} e_{12} \qquad \text{A-3}$$

The other two shear terms are combined in this manner and Equation A-2 is written as

$$\sigma_{ij} = C_{ij11} e_{11} + C_{ij22} e_{22} + C_{ij33} e_{33} + 2C_{ij12} e_{12} + 2C_{ij13} e_{13} + 2C_{ij23} e_{23} \qquad \text{A-4}$$

Each stress component can be evaluated from Equation A-4. The most general case of Equation A-1 is represented in matrix format as shown in A-5.

$$\begin{pmatrix} \sigma_{11} \\ \sigma_{22} \\ \sigma_{33} \\ \sigma_{12} \\ \sigma_{13} \\ \sigma_{23} \end{pmatrix} = \begin{pmatrix} C_{1111} & C_{1122} & C_{1133} & C_{1112} & C_{1113} & C_{1123} \\ & C_{2222} & C_{2233} & C_{2212} & C_{2213} & C_{2223} \\ & & C_{3333} & C_{3312} & C_{3313} & C_{3323} \\ & & & C_{1212} & C_{1213} & C_{1223} \\ & \text{symmetric} & & & C_{1313} & C_{1323} \\ & & & & & C_{2323} \end{pmatrix} \begin{pmatrix} e_{11} \\ e_{22} \\ e_{33} \\ 2e_{12} \\ 2e_{13} \\ 2e_{23} \end{pmatrix} \qquad \text{A-5}$$

# APPENDIX B
# TRANSFORMING ELASTIC CONSTANTS

In order to obtain engineering parameters from another set of constants, $\lambda$, $\mu_T$, $\alpha$, $\mu_L$ and $\beta$, transformation formulas are developed. The easiest way to express engineering parameters E and $\nu$ in terms of the five constants $\lambda$, $\mu_T$, $\alpha$, $\mu_L$ and $\beta$, is first to express strains in terms of stresses with compliance coefficients. From Equation 2-20, the relation between normal stresses in terms of normal strains for a fiber orientation in the 2-direction ($\theta = 0°$) can be written as

$$\begin{pmatrix} \sigma_{11} \\ \sigma_{22} \\ \sigma_{33} \end{pmatrix} = \begin{pmatrix} c_{11} & c_{12} & c_{13} \\ c_{12} & c_{22} & c_{12} \\ c_{13} & c_{12} & c_{11} \end{pmatrix} \begin{pmatrix} e_{11} \\ e_{22} \\ e_{33} \end{pmatrix} \tag{B-1}$$

where

$$c_{11} = \lambda + 2\mu_T \tag{B-2}$$

$$c_{12} = \lambda + \alpha \tag{B-3}$$

$$c_{13} = \lambda \tag{B-4}$$

$$c_{22} = \lambda + 2\alpha + 4\mu_L - 2\mu_T + \beta \tag{B-5}$$

Inverting the set of equations given by B-1, strains in terms of stresses are

$$\begin{pmatrix} e_{11} \\ e_{22} \\ e_{33} \end{pmatrix} = \begin{pmatrix} s_{11} & s_{12} & s_{13} \\ s_{12} & s_{22} & s_{12} \\ s_{13} & s_{12} & s_{11} \end{pmatrix} \begin{pmatrix} \sigma_{11} \\ \sigma_{22} \\ \sigma_{33} \end{pmatrix} \tag{B-6}$$

where

$$s_{11} = \frac{c_{22}c_{11} - c_{12}^2}{(c_{22}(c_{11} + c_{13}) - 2c_{12}^2)(c_{11} - c_{13})} \tag{B-7}$$

$$s_{12} = \frac{-c_{12}}{c_{22}(c_{11} + c_{13}) - 2c_{12}^2} \tag{B-8}$$

$$s_{13} = \frac{-c_{22}c_{13} + c_{12}^2}{(c_{22}(c_{11} + c_{13}) - 2c_{12}^2)(c_{11} - c_{13})} \tag{B-9}$$

$$s_{22} = \frac{c_{11} + c_{13}}{c_{22}(c_{11} + c_{13}) - 2c_{12}^2} \tag{B-10}$$

Extension moduli and Poison's ratios are readily obtained from these equations. The two extension moduli are

$$E_L = \frac{\sigma_{22}}{e_{22}} = \frac{1}{s_{22}} = \lambda + 2\alpha + 4\mu_L - 2\mu_T + \beta - \frac{(\lambda + \alpha)^2}{\lambda + \mu_T} \tag{B-11}$$

$$E_T = \frac{\sigma_{11}}{e_{11}} = \frac{\sigma_{33}}{e_{33}} = \frac{1}{s_{11}} = \frac{4\mu_T(\lambda + 2\alpha + 4\mu_L - 2\mu_T + \beta)(\lambda + \mu_T) - (\lambda + \alpha)^2}{(\lambda + 2\alpha + 4\mu_L - 2\mu_T + \beta)(\lambda + 2\mu_T) - (\lambda + \alpha)^2} \tag{B-12}$$

Three Poisson's ratios are possible:

$$\nu_{LT} = \frac{-s_{12}}{s_{22}} = \frac{\lambda + \alpha}{2(\lambda + \mu_T)} \tag{B-13}$$

$$\nu_{TL} = \frac{-s_{12}}{s_{11}} = \frac{2\mu_T(\lambda+\alpha)}{(\lambda+2\mu_T)(\lambda+2\alpha+4\mu_L-2\mu_T+\beta) - (\lambda+\alpha)^2} \tag{B-14}$$

$$\nu_{TT} = \frac{-s_{13}}{s_{11}} = \frac{\lambda(\lambda+2\alpha+4\mu_L-2\mu_T+\beta) - (\lambda+\alpha)^2}{(\lambda+2\mu_T)(\lambda+2\alpha+4\mu_L-2\mu_T+\beta) - (\lambda+\alpha)^2} \tag{B-15}$$

This allows calculation of engineering parameters in terms of the original set of constants.

# APPENDIX C

## RELATIONSHIP BETWEEN ENGINEERING MODULI $E_L$, $E_T$, $\nu_{LT}$ AND $\nu_{TL}$

The relationship given in Equation C-1 is given in this appendix.

$$\frac{E_L}{E_T} = \frac{\nu_{LT}}{\nu_{TL}} \qquad \text{C-1}$$

The elastic moduli are referred to directions in a material coordinate system aligned with the fiber direction. Subscripts L and T refer to directions longitudinal and transverse to the fiber direction, respectively. Equation C-1 can be derived using symmetry considerations for normal strains in terms of normal stresses. Referring to Figure C-1, normal stress $\sigma_{22}$, parallel to the fiber direction, results in three normal strains. With only $\sigma_{22}$ acting on the specimen, strain in the 1-direction is

$$e_{11} = -\frac{\nu_{LT}}{E_L}\sigma_{22} \qquad \text{C-2}$$

where $\nu_{LT}$ is Poisson's ratio for an applied load along the fibers and the resulting contractile strain in the transverse direction.

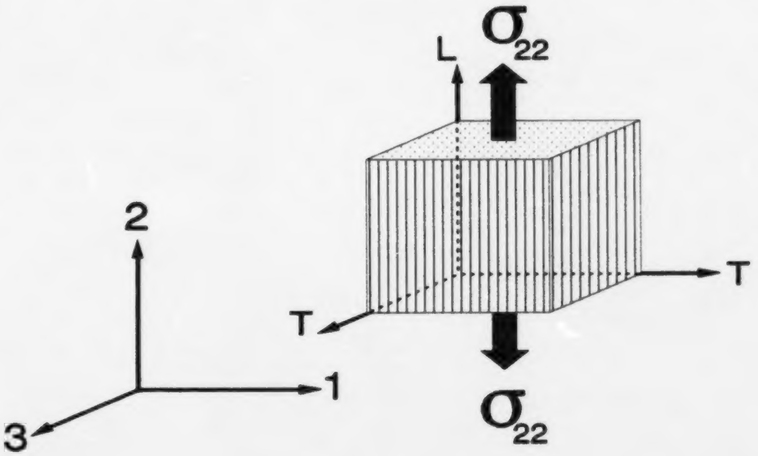

**Figure C-1:** $\sigma_{22}$ loading

The strain in the 2-direction is

$$e_{22} = \frac{1}{E_L}\sigma_{22} \qquad \text{C-3}$$

and the strain in the 3-direction for $\sigma_{22}$ acting alone is

$$e_{33} = -\frac{\nu_{LT}}{E_L}\sigma_3 \qquad \text{C-4}$$

For the same fiber orientation as Figure C-1, strains caused by $\sigma_{11}$ and $\sigma_{33}$ are assessed. These two cases are shown in Figure C-2 and C-3.

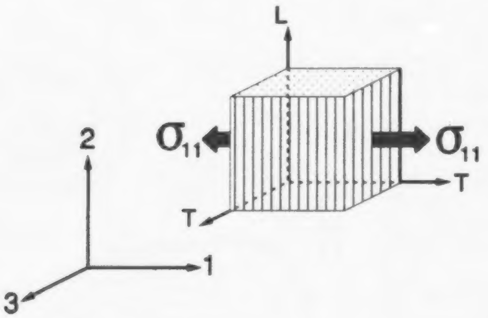

**Figure C-2:** $\sigma_{11}$ loading

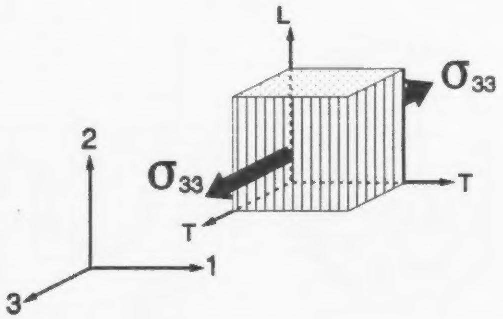

**Figure C-3:** $\sigma_{33}$ loading

With $\sigma_{11}$ applied to the specimen (Figure C-2), resulting strains are

$$e_{11} = \frac{1}{E_T}\sigma_{11} \qquad \text{C-5}$$

$$e_{22} = -\frac{\nu_{TL}}{E_T}\sigma_{11} \qquad \text{C-6}$$

$$e_{33} = -\frac{\nu_{TT}}{E_T}\sigma_{11} \qquad \text{C-7}$$

Similarly with $\sigma_{33}$ applied to the specimen (Figure C-3).

Strains in terms of stresses for these three loading cases are combined to yield

$$\begin{pmatrix} e_{11} \\ e_{22} \\ e_{33} \end{pmatrix} = \begin{bmatrix} \frac{1}{E_T} & -\frac{\nu_{LT}}{E_L} & -\frac{\nu_{TT}}{E_T} \\ -\frac{\nu_{TL}}{E_T} & \frac{1}{E_L} & -\frac{\nu_{TL}}{E_T} \\ -\frac{\nu_{TT}}{E_T} & -\frac{\nu_{LT}}{E_L} & \frac{1}{E_T} \end{bmatrix} \begin{pmatrix} \sigma_{11} \\ \sigma_{22} \\ \sigma_{33} \end{pmatrix} \qquad \text{C-8}$$

Symmetry considerations for the stiffness coefficients of Equations C-8 manifests the relationship between moduli given in Equation C-1.

# APPENDIX D
# LOAD CELL DESIGN

The load cell shown in Figure D-1 was fabricated from 6061-T6 aluminum. Nominal strain at a strain gauge location is calculated by a strength of materials method. Referring to Figure D-1, nominal strain ($e_n$) per unit load is given by

$$\frac{e_n}{F} = \frac{6Lh}{Eb(h^3-d^3)} \tag{D-1}$$

where E is Young's modulus for aluminum (70 000 MPa). The ratio of actual strain ($e_a$) to nominal strain ($e_n$) strain is expressed in terms of a concentration factor k,

$$k = \frac{\text{actual strain}}{\text{nominal strain}} = \frac{e_a}{e_n} \tag{D-2}$$

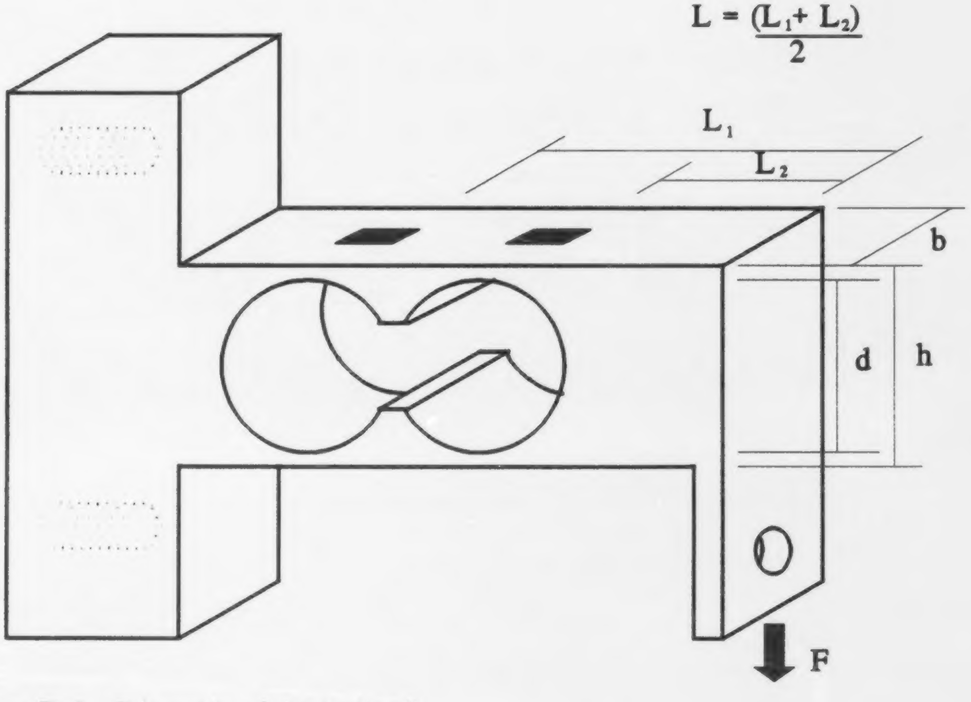

**Figure D-1:** Schematic of the load cell

The value of k was determined based on data obtained from Fuchshuber (1987). A concentration factor of k = 10 was determined for a d/h ratio of 0.86.

At a maximum load of 60 N, an allowable strain of 1500 μs was used based on a yield strain of 3400 μs, providing a load cell sensitivity of 30 μs per Newton. Dimensions of the load cell where selected to satisfy the sensitivity requirement with a concentration factor of 10 relating actual strain to nominal strain defined in Equation D-1. The load cell dimensions as shown in Figure D-1 are: d = 12.7 mm, h = 14.7 mm, b = 9.5 mm, $L_1$ = 19 mm, $L_2$ = 12.7 mm.

Actual strain gauge readings were made with a strain indicator (P-350, Automation Industries Inc.). Sensitivity determined as the average of the four strain gauge outputs was 25 μs per Newton. Linearity and hysteresis were assessed by recording the indicated strain gauge output for known loads (dead weights). A maximum load of 50.2 N was applied and then unloaded back to zero load. The results of the dead weight test are shown in Figure D-2. For a maximum applied load of 50.2 N, the maximum departure from the best fit line was 0.2% of the maximum load tested.

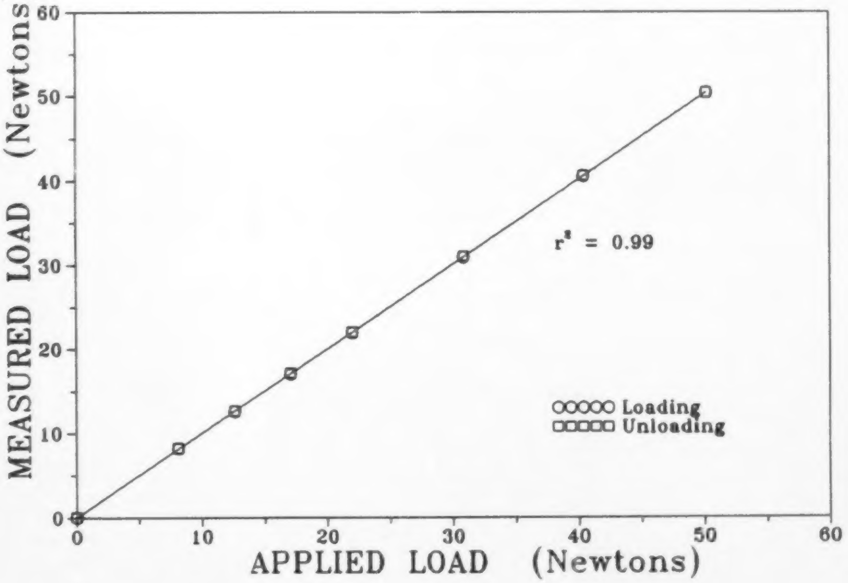

**Figure D-2:** Load cell linearity

# APPENDIX E

# CAMERA LENS AND LENS EXTENDER SELECTION

This appendix shows the selection of a lens and lens extender combination that will provide the magnification required for the small test specimens.

A fundamental equation in optics for a simple lens arrangement is (Adams 1980)

$$\frac{1}{u} + \frac{1}{v} = \frac{1}{f} \qquad \textbf{(E-1)}$$

where : u is the distance from the object to the lens plane,
v is the distance from the lens plane to the image and
f is the lens focal length.

Magnification of the image in relation to the object size is

$$M = \frac{v}{u} = \frac{I}{O} \qquad \textbf{(E-2)}$$

where O is the object size and I is the image size.

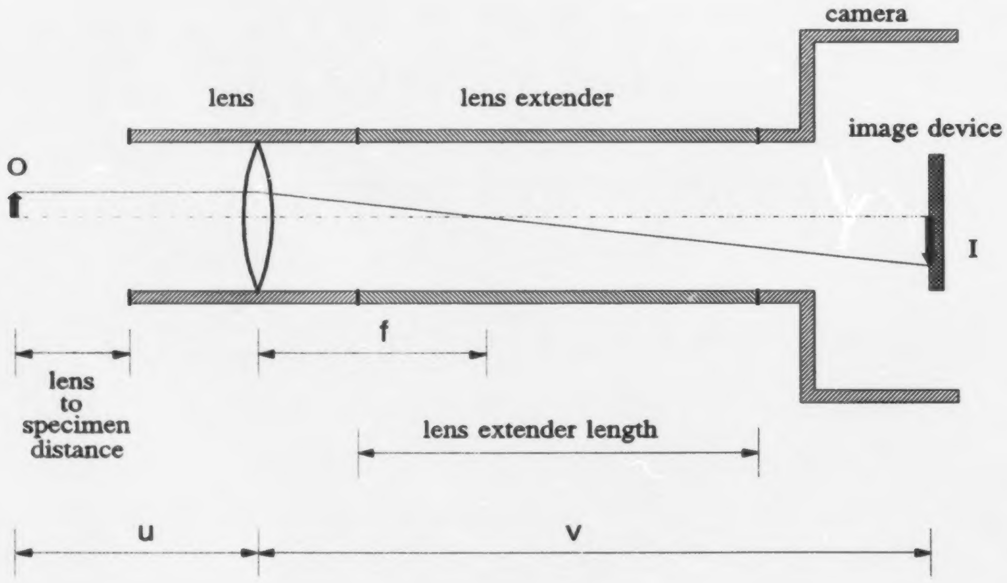
camera
lens
lens extender
image device
O
I
f
lens to specimen distance
lens extender length
u
v

**Figure E-1:** Camera lens and lens extender configuration

To determine a lens and lens extender combination that will provide the required magnification, Equations E-1 and E-2 are combined to yield

$$v = f(M+1) \tag{E-3}$$

The image device in the camera is 8.8 mm wide by 6.6 mm high. A test requirement is that 2 mm is to fill the screen height. This requires a magnification from object to image sensor of approximately 3 times. Selection of the lens focal length will determine the lens extender length.

A lens with a small focal length will minimize the lens extender length, but from Equation E-2, the lens to specimen distance is also reduced. The lens to specimen distance is less than the distance u, as can be seen from Figure E-1. The lens to specimen distance is limited by two factors. The first involves contact between the lens from the other camera which is oriented perpendicularly. The second factor is the requirement that the lens is far enough away from the specimen to allow for proper illumination of the specimen.

The lens extender length is always less than distance v. The length v is made up of the lens extender length as well as the additional lengths on each end as shown in Figure E-1.

A 50 mm lens was found to provide the optimum configuration: maintain a workable specimen to lens distance and yet minimize the lens extender length. A 50 mm lens with a 170 mm lens extender (v ≈ 200 mm) will provide a magnification of 3 and a lens to specimen distance of approximately 35 mm (u ≈ 67 mm). A 200 mm lens extender resulted in a lens to specimen distance of ≈25 mm.